6-1-2008

Optimal Control of Electrodynamic Tethers

Robert E. Stevens

OPTIMAL CONTROL OF ELECTRODYNAMIC TETHER SATELLITES

DISSERTATION

Robert E. Stevens, Commander, USN

AFIT/DS/ENY/08-13

DEPARTMENT OF THE AIR FORCE
AIR UNIVERSITY
AIR FORCE INSTITUTE OF TECHNOLOGY

Wright-Patterson Air Force Base, Ohio

The views expressed in this dissertation are those of the author and do not reflect the official policy or position of the United States Air Force, Department of Defense, or the United States Government.

AFIT/DS/ENY/08-13

OPTIMAL CONTROL OF ELECTRODYNAMIC TETHER SATELLITES

DISSERTATION

Presented to the Faculty

Graduate School of Engineering and Management

Air Force Institute of Technology

Air University

Air Education and Training Command

in Partial Fulfillment of the Requirements for the

Degree of Doctor of Philosophy

Robert E. Stevens, BS, MS

Commander, USN

June 2008

AFIT/DS/ENY/08-13

OPTIMAL CONTROL OF ELECTRODYNAMIC TETHER SATELLITES

Robert E. Stevens, BS, MS
Commander, USN

Approved:

	Date
_____	_____
William E. Wiesel (Chairman)	
_____	_____
William P. Baker (Member)	
_____	_____
I.M. Ross (Member)	
_____	_____
Richard G. Cobb (Member)	

Accepted:

_____	_____
M. U. Thomas	Date
Dean, Graduate School of Engineering and Management	

Abstract

Low thrust propulsion systems such as electrodynamic tethers offer a fuel-efficient means to maneuver satellites to new orbits, however they can only perform such maneuvers when they are continuously operated for a long time. Such long-term maneuvers occur over many orbits often rendering short time scale trajectory optimization methods ineffective. An approach to multi-revolution, long time scale optimal control of an electrodynamic tether is investigated for a tethered satellite system in Low Earth Orbit with atmospheric drag. Control is assumed to be periodic over several orbits since under the assumptions of a nearly circular orbit, periodic control yields the only solution that significantly contributes to secular changes in the orbital parameters. The optimal control problem is constructed in such a way as to maneuver the satellite to a new orbit while minimizing a cost function subject to the constraints of the time-averaged equations of motion by controlling current in the tether. To accurately capture the tether orbital dynamics, libration is modeled and controlled over long time scales in a similar manner to the orbital states. Libration is addressed in two parts; equilibrium and stability analysis, and control. Libration equations of motion are derived and analyzed to provide equilibrium and stability criteria that define the constraints of the design. A new libration mean square state is introduced and constrained to maintain libration within an acceptable envelope throughout a given maneuver. A multiple time scale approach is used to capture the effects of the Earth's rotating tilted magnetic field. Optimal control solutions are achieved using a pseudospectral method to maneuver an electrodynamic tether to new orbits over long time scales while managing librational motion using only the current in the tether wire.

To my wife for her steadfast support

Acknowledgments

I thank Mike Ross for his assistance in efficiently transforming math problems into numerical ones that are well-conditioned for numerical optimization and Joe Carroll for providing insights into tether design and controls that helped form the basis for using long time scales in optimal control problems. I also appreciate the guidance of my research advisor and committee chair Bill Wiesel. I am especially indebted to Bill Baker for the many hours he spent helping me apply the mathematical method of averaging to optimal control problems.

Robert E Stevens

Table of Contents

List of Figures

List of Symbols

$\mathbf{A}$	= Jacobian of $\mathbf{f}$
A_i	= area of component i
$\mathbf{B}$	= local magnetic flux density vector
B^*	= ballistic coefficient
C_d	= coefficient of drag
$\mathbf{D}$	= drag force vector
$\mathbf{F}_i$	= force vector on component i
I	= instantaneous control current in electrodynamic tether
I_m	= maximum allowable rms control current in tether
$\mathbf{J}$	= specific moment of inertia
$\mathbf{L}, L$	= straight tether length vector and magnitude
$\mathcal{L}$	= Lagrangian function
M_i, M	= effective mass of end-body i and total system mass
Q_i	= generalized force i
$R_\oplus$	= radius of the Earth
T	= kinetic energy or slow time scale variable (context dependent)
V	= potential energy
a	= semimajor axis of the orbit
d_t	= tether diameter
e	= orbit eccentricity
$\mathbf{f}$	= state vector time derivative
h	= altitude of system center of mass (COM); vertical rectangular eccentricity vector coord
h^*	= atmospheric scale height
i	= orbit inclination
k	= horizontal rectangular eccentricity vector coordinate in the perifocal frame
m_i	= mass of component i
n	= orbital mean motion
P	= orbital period
$\mathbf{r}, r$	= position vector and magnitude from Earth center to system COM
t	= time
$\mathbf{u}$	= control vector
v_i	= velocity of component i
v_a	= velocity of air with respect to system COM
$\mathbf{x}$	= state vector
δ_t	= tether linear density [mass/length]
ε	= ratio of maximum Lorenz torque to gravity gradient torque; scaling parameter
ϕ	= out-of-plane libration angle
γ	= flight path angle
γ_m	= Earth magnetic dipole moment
μ_e	= effective reduced system mass
μ_g	= Earth-satellite gravitational reduced mass
μ_m	= system reduced mass
ν	= orbit true anomaly

θ	= in-plane libration angle
ρ	= atmospheric density
$\hat{\boldsymbol{\rho}}, \boldsymbol{\rho}_{\mathbf{i}}$	= straight tether unit position vector from m_1 to m_2, position of component i w.r.t. COM
τ	= tether tension
ω	= argument of perigee
ω_e, ω_o	= angular velocity in rotating frame and inertial frame respectively
Ω	= right ascension of the ascending node
$\boldsymbol{\psi}$	= basis in Fourier space
ψ	= tether curve angle
$(\dot{})$	= time derivative unless otherwise specified
$(')$	= time derivative with respect to rotating frame

I. Introduction

With increasing dependence of government missions, scientific exploration, and commercial ventures on spaceborne payloads, it is critical to have the right satellite over the right place at the right time. Currently, most satellites are confined to Keplarian orbits that reside above the "reasonable" atmosphere. Conventional rockets do not permit a satellite to orbit at lower altitudes where atmospheric drag is non-negligible nor do they usually allow large orbit adjustments over a long lifetime since these scenarios would require a prohibitive amount of propellant. However, a low thrust propulsion system requiring little or no propellant could permit station-keeping at lower altitudes and even provide some limited orbital maneuvering capabilities. Electrodynamic tethers (EDTs) in low Earth orbit offer an attractive alternative to conventional satellites that use propellant-based propulsion systems because the thrusting forces are derived using the Earth's geomagnetic potential. Electrodynamic tethers are electrically conductive wires extending between two or more subsatellites and when a current is passed through the wire in the Earth's magnetic field, a Lorenz force is generated perpendicular to both the current direction and the direction of the local Earth magnetic field lines. A two-ball EDT, defined as two subsatellites joined by a conducting tether, is depicted in Figure 1 showing how the Lorenz force generated by running current through the wire may be used to overcome drag and maneuver the satellite pair.

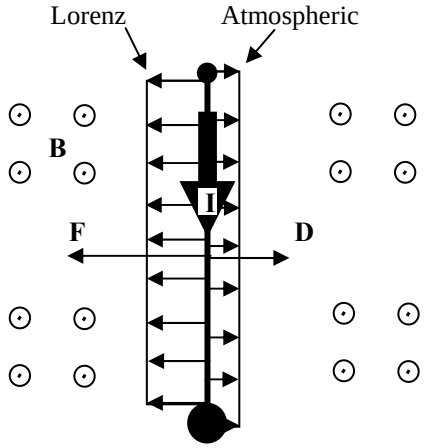

Figure 1. Electrodynamic Tether Force Model

The force magnitude depends on the current I, length of wire and the wire orientation with respect to the local magnetic field according to Lorenz's law, $\mathbf{F} = I\mathbf{L} \times \mathbf{B}$, where $\mathbf{L}$ represents the length vector between the satellite pair and $\mathbf{B}$ represents the local Earth magnetic flux density vector. Controlling the current in the wire through variable resistance, the satellite system would be capable of maneuvering to new orbits without propellant, albeit at a slower rate than traditional maneuvering rockets. A capability such as this would enable space missions requiring orbiting sensors at extremely low altitudes or those requiring frequent repositioning of satellites by way of orbit transfers.

Because of the low thrust provided by an EDT system, an orbit transfer requires a long time to reach a desired orbit. Obtaining optimal control solutions for satellites that maneuver for a long time can be challenging and computationally intensive when instantaneous state dynamics and controls use dynamics expressed using short time scales. Williams demonstrates an approach to optimal control using non-linear perturbation equations of motion as dynamic constraints and solves an optimal control problem by direct transcription using Non-linear Programming (NLP) software. This method is shown to be effective in determining controls that execute a modest orbital maneuver using an electrodynamic tether for thrust; however the optimization solver required hundreds of collocation node points to capture all the small state variations that occur for a maneuver that only takes a single day. Many nodes were required to fully depict the instantaneous states and control that exhibit periodic behavior. Hundreds of collocation nodes correspond to thousands of optimization variables and constraints for the NLP solver to compute. The number of nodes and computation time required to perform the optimization over long periods of time can be difficult or impossible to achieve using the short time scale model and are highly susceptible to round-off errors. In many low-thrust maneuvering situations the instantaneous orbit state will vary only slightly from Keplarian motion within an orbital period due to small perturbations, but the variations tend to be periodic in the short term and cancel out over the long term leaving only slow secular state changes. Addressing long term behavior, Carroll[8] and Tragesser and San present a technique of non-optimal periodic tether control that uses the method of averaging derived from perturbation theory enabling control of the average states thus avoiding the computational burden associated with controlling the rapidly changing

instantaneous states. They demonstrate that this approach is good for determining control for longer time periods, however the results are not optimal and the periodic control is considered to be unchanging throughout the trajectory. Furthermore, determining the control requires constraining the maximum current which is less straightforward using the method of averaging than constraining instantaneous current using the short time scale model. The problem, therefore, is that it is difficult or impossible to determine optimal controls for an EDT performing a long term orbit transfer using the methods of control currently presented in the literature. The aim of this dissertation is to take advantage of both control methods to achieve optimal control of an electrodynamic tether over long time periods. We seek to modify the optimal control problem of a low thrust orbit transfer considering that we already know something about the dynamics of the system, namely that it is nearly periodic when the EDT is continuously thrusting. Bearing this in mind, we may dispose of the dynamic model describing the rapidly changing instantaneous behavior in favor of a dynamic model that only describes the secular behavior of the average state over large time scales.

The research objective is to maneuver an electrodynamic tether to a new orbit over many revolutions by posing an optimal control problem in the context of large time scales since we are mainly interested in the secular behavior and not the periodic behavior occurring during each revolution. Although this research focuses on optimal control of electrodynamic tethers, this approach to optimal controls over large time scales could, in principle, apply to any continuous low-thrust system.

In the relevant EDT orbit control literature, the dynamic models used are limited to non-atmospheric environments over short periods of time[1] or they ignore attitude dynamics (libration) and long term optimal control[2]. In order to develop a real system that will operate in a low Earth orbit, drag effects and libration must be addressed and either included in the controller model or justifiably ignored. Because the source of thrust is derived from the Earth's tilted magnetic field, it is also important to include the effects of the Earth's rotation on the satellite motion. To achieve the primary objective of determining optimal EDT orbit transfers spanning many orbits, the following outline describes the approach taken in this dissertation.

- Determine optimal long term maneuvers for nadir-pointing tethers ignoring Earth's tilted magnetic dipole (Chapter III)
    - Develop set of suitable dynamic equations and path constraints

    - Pose and solve optimal control problems, first ignoring drag and then including drag
    - Validate optimal control solutions by propagating with a “truth” model
- Introduce the effects of the Earth’s tilted magnetic dipole into the dynamic model (Chapter IV)
    - Modify the dynamic model and path constraints to include the effects of a tilted Earth magnetic field that rotates once per day
    - Pose and solve optimal control problems with and without drag
    - Validate optimal control solutions by propagating with a “truth” model
- Introduce tether libration into the dynamic model (Chapter V)
    - Perform stability analysis of tether libration
    - Modify the dynamic model and path constraints to include the effects of tether libration
    - Pose and solve optimal control problems with and without drag
    - Validate optimal control solutions by propagating with a “truth” model

II. Literature Review

The main body of spacecraft tether literature as it relates to this research may be divided into several categories. In the area of tether dynamic analysis and control, the chief motions studied are orbital, librational and vibrational. Models used for these motions depend on the application, but will sometimes include either electrodynamic forces [Refs 1-2, 6-15] or aerodynamic drag [Refs 3,4 and 5], but very few include both. Researchers have investigated tether control strategies using tether length variation, end-body drag, thrusters, and in the case of electrodynamic tethers (EDTs), wire current (references provided in forthcoming discussion). This research will focus on the unexplored area of long term optimal control of an EDT.

The first category of relevant literature addresses orbital maneuvering using EDTs. Most of these papers discuss system design issues but do not detail controller design. Tragesser and San describe various EDT current controllers, but they are non-optimal and librational motion is ignored.[6] In the area of optimal control, the published works are very limited. The most relevant paper discussing the optimal control of electrodynamic thrusting tethers is one from Williams.[7] The dynamic model in this paper ignores the atmosphere and the librations are not explicitly bounded, however the paper showcases an example optimal orbital maneuver useful for comparison. In other related orbital maneuvering works, long term EDT thrusting strategies were published first by Carroll[8] and then Tragesser and San for no-drag orbits, however optimal control over large time scales is not addressed.

There is a large body of work addressing the second category, EDT libration analysis and control. In the case of electrodynamic tether models, Pelaez et. al. explore the stability of these systems assuming a constant tether current for inclined [9,10] and elliptical orbits. In more elaborate analyses, two bar tether models were employed.[11] Although many of these papers do not address control, they do provide insights into the behavior of unthrottled active electrodynamic tethers in a non-atmospheric environment. Reference 12 shows the librational instability that occurs with a constant current EDT, thus control is necessary to compensate for drag while simultaneously maintaining stability.. Without control, an EDT

system would need a “self-balanced” design to maintain stable attitude dynamics according to Ref 13. Ref 14 concludes that EDT control can be employed to manage instabilities for orbits with eccentricity less than 0.35. Hoyt presents a method to stabilize using feedback control.[15] There are other methods of attitude control for hanging EDTs besides using torques due to Lorenz forces about the center of mass (COM). Williams describes a method of libration stability control using tether length variation[16], as does Yu for orbits with e<0.3, however only in-plane motion is considered.[17] Thrusters have also been proposed for libration control,[18] however by using propellant, this method defeats the stated purpose of using EDTs in the first place. Most controller designs used one of the linear techniques like Ref 19 which describes thruster and tension control using LQR methods. Some papers, such as Refs 20 and 21, present nonlinear control methods (feedback linearization) to maneuver between equilibrium points. A combination of control methods is presented in Ref 22 where both electromagnetic forces and length rate are used to manage librations.

De Matteis and De Socio caution against instabilities due to atmospheric density gradients in very long tethers (>75 km) that could lead to a destabilizing libration resonance at altitudes lower than 240 km.[23] The culprit in this case was that a long librating tether would be subject to very different drag forces throughout large pendular swings. However for the tether lengths, operational altitudes and allowable librations considered in this work, the density variations are relatively minor and this effect is ignored.

Another category of tether literature is devoted to vibration and mode shapes. Von Flotow shows that a tether under the uniform loading of an electrodynamic and aerodynamic force will tend to sag in the middle with a slow first lateral mode of vibration (slow relative to the longitudinal vibration). Using the fact that the period of the first lateral mode of vibration is long, he approximates the tether to be in a state of quasi-static equilibrium in the shape of a section of a circular arc.[24] This shape and vibration approximation is used in determining the maximum current limits for the system (Appendix D). Other vibration-related work includes control of an electrodynamic tether through input shaping to reduce vibrations and librations[25] and vibrations due to a constant Lorenz force load.[26] Watanabe suggests a bang-bang current control providing input shaping to reduce vibrations and librations while thrusting with an EDT.[27] Williams investigates control of flexible tethers using electromagnetic forces and a movable

attachment.[28] These analyses, however, do not include atmospheric effects. De Matteis[29] presents equations of motion that include aerodynamic effects in modeling vibrational behavior of non-electrodynamic tethers. There are several authors who develop controllers for non-electrodynamic tethers using tension control or reels for length variation.[30] Others focus on the deployment and retrieval phases.[31]

The remainder of the tether literature is largely aimed at specific design studies or missions. Many authors have addressed designing tethers to operate efficiently and safely in the space environment. Bare wires efficiently collect electrons to produce the current used for thrust.[32,33] Porous tapes have been proposed and investigated to increase the survivability where micrometeors can sever a thin wire and end a mission.[34,35] Several other papers were written to support SEDS (Small Expendable Deployer System) and other specific space demonstrations.[36,37,38] Estes et. al. document lessons learned from the various missions that have deployed in space.[39] A good reference covering all the general topics reviewed is the book *Dynamics of Space Tether Systems* by Beletsky and Levin.[40]

In the area of optimal control of low thrust multirevolution transfers, Ross, Gong and Sekavat propose a technique that manages the high frequency content of optimal solutions. Solutions are achieved by solving a large time scale optimal control problem using a small number of nodes. Applying Bellman's principle, they then iteratively solve the problem and propagate the control solution along smaller sections of the original optimal path, thus capturing all its detailed high frequency components. This general method has the advantage of solving large time scale optimal control problems while still avoiding the aliasing common when there are not enough collocation node points to resolve the high frequency content. A more exhaustive list of the literature reviewed along with a brief synopsis of their pertinent contents is included in Appendix I.

The electrodynamic tether literature provides ample coverage of libration stability analysis and control, however only a few papers address orbital maneuvering. Williams paper on optimal orbit transfer and Tragesser and San's maneuvering approach using periodic control stood out as the two works most relevant to the research presented in this dissertation. Starting with key concepts extracted from these two papers, a new approach to optimal orbital maneuvering is presented.

III. Optimal Orbital Maneuvering

In this chapter, we examine optimal maneuvers using a two-ball EDT as defined in the introduction (Figure 1). Because of the low altitudes considered, the trajectories account for atmospheric drag and are nearly circular therefore the orbital equations of motion may be expanded about the very small eccentricity. This assumption is good for orbits with small eccentricities as long as errors remain within the tolerance of the spectral algorithm used for optimization.[41,42] Furthermore, the maneuvers are known to occur over many orbital revolutions, so the small oscillatory changes in the orbital parameters that are evident over short time scales (within each revolution) are averaged out leaving only the secular changes that occur over long time durations (many revolutions). See Appendix F for a full discussion on different time scales. The only control we have at our disposal to perform the desired maneuvers is the current in the wire using variable resistance. The dynamic behavior of the EDT in its slowly changing orbit is predictably periodic, consisting of a linear combination of sinusoidal functions of true anomaly, or equivalently, time. Because motion of a constantly thrusting EDT deviates from Keplarian motion in a periodic manner over each orbit, a controller that is also periodic over the orbit will contribute to secular changes in the orbital parameters over a long time as shown in Appendix G. Other contributions of the controller are averaged out in the long-term. Therefore we assume periodic control current, I , modeled using the relevant terms of a Fourier series.

$$I\left(\nu,\mathbf{u}\left(T\right)\right)=I_m\left(u_1\left(T\right)+u_2\left(T\right)\cos\nu+u_3\left(T\right)\sin\nu+u_4\left(T\right)\cos 2\nu+u_5\left(T\right)\sin 2\nu\right) \tag{1}$$

where ν is the true anomaly and I_m is the maximum allowable rms control current. To highlight the fact that the controlled Fourier coefficients vary only over large time scales, we write them as functions of T . The slow time scale variable T is a scaled version of the clock time, t , which is itself proportional to the true anomaly. All state variables and controls that are functions of T change very slowly and are considered constant over short time intervals. For a more complete discussion on time scaling, see Chapter V and Appendix F. The control in Fourier space with bases $\mathbf{\Psi}\left(\nu\right)=[1,\cos\nu,\sin\nu,\cos 2\nu,\sin 2\nu]^T$ is therefore completely defined by

$$\mathbf{u}\left(T\right)=\left[u_1,u_2,u_3,u_4,u_5\right]^T \tag{2}$$

such that the current in the clock time domain is given in Eq. (1) by $I = I_m \boldsymbol{\Psi}^T(\nu)\mathbf{u}(T)$. With the control written in this form, the approach to optimal control is viewed in the Fourier space where the goal is to determine the time dependent Fourier coefficients, $\mathbf{u}(T)$, that minimize a given cost function for a trajectory subject to the time-averaged dynamic equations of motion. A pseudospectral method of dynamic

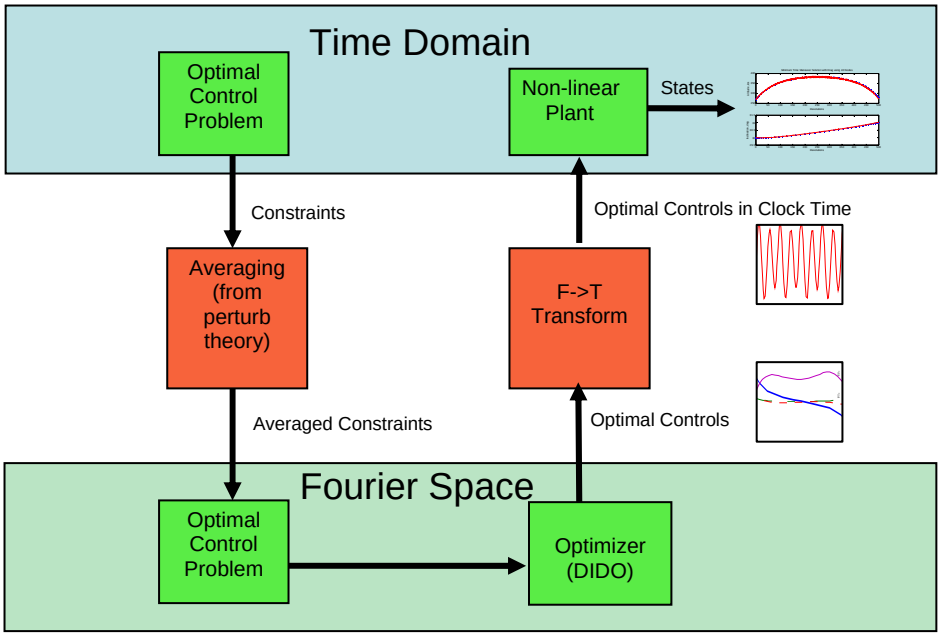

Figure 2. Optimal Control in Fourier Space

optimization is employed using DIDO software[41,42] to solve the subject optimal control problems yielding the optimal control coefficients and path discretized over large periods of time. The diagram in Figure 2 shows that optimal control problems exhibiting periodic behavior may be transformed into a Fourier space using the method of averaging. This eliminates dependence on fast time variables (ν, t) and the resulting averaged states and controls will only depend on the slow time variable (T). The problem posed in this Fourier space may now be solved by an optimizer producing average states and controls that change slowly over time.

If it is desired to capture the instantaneous states for subsections of the averaged trajectory, then the general method of multirevolution optimal control proposed by Gong, Ross and Sekhavat would be suitable. In this way, instantaneous optimal controls could be determined for sections of the optimal

averaged path. This method was tested over a shorter time span, where an optimal control problem was posed and solved using this antialiasing algorithm that applies Bellman's principle to capture high frequency content of an optimal trajectory. The algorithm was used to solve a fixed time (6 orbits), maximum inclination problem (constrained to use positive current only) initially using 32 nodes. Then the algorithm iteratively solved subsections of the optimal path using 32 nodes, propagated the resulting optimal control which provided a new initial condition for the optimizer until the desired end conditions were reached. The final solution used 16 iterations and was able to capture fast time periodic behavior of some of the states (θ, ϕ, a), but the secular behavior was difficult to observe due to the few number of revolutions. Longer term maneuvers were not attempted due to the number of iterations required to capture all the fast time dynamics of the instantaneous states. The method did demonstrate, however, that it could potentially be used to solve for sections of the optimal averaged path without placing any assumptions on the controller (i.e. not required to be periodic) perhaps taking advantage of some of the higher order effects availed by using instantaneous state dynamics. The remainder of this dissertation will focus on the construction of and solution to optimal EDT control problems in Fourier space, and will begin by deriving a dynamic model.

Dynamic Model

Orbital changes due to the relatively weak Lorenz forces generated along the electrodynamic tether occur over many orbital revolutions. The EDT is modeled as a "dumbbell" consisting of two end bodies tethered together with a taut (i.e. positive tension) 4 km copper wire. The Lorenz force generated along the wire containing electric current is given by

$$\mathbf{F} = I\mathbf{L} \times \mathbf{B} \tag{3}$$

where I represents tether current (the control), $\mathbf{B}$ represents the Earth's local magnetic flux density vector, and $\mathbf{L}$ is the tether length vector pointing in the direction from the upper end mass to the lower one (see Appendix A). The tether geometry and current direction that yields a positive transverse thrust is shown in Figure 1.

The local magnetic flux density for an Earth-orbiting satellite is modeled as

$$\mathbf{B} = \frac{\gamma_m}{r^3}\begin{bmatrix} -2\sin(\omega+\nu)\sin i \\ \cos(\omega+\nu)\sin i \\ \cos i \end{bmatrix}_e = \begin{bmatrix} B_r \\ B_t \\ B_n \end{bmatrix}_e \tag{4}$$

where γ_m represents the Earth's magnetic dipole moment, i is the inclination relative to the magnetic equator and B_r, B_t, and B_n represent the magnetic flux density vector components in the radial, transverse and orbit normal directions respectively (i.e. $\hat{e}_r$, $\hat{e}_t$ and $\hat{e}_n$ directions). At the equator, a force of 0.1 N distributed along a one amp, 4 km EDT is achievable at an altitude of 270 km, which can be the same order of magnitude as the atmospheric drag at that altitude depending on the physical characteristics of the tether and end bodies. To ensure the satellite orbits longer than a few days, the control system will need to apply a constant average current in order to provide constant in-track thrust that will compensate for drag forces acting in the opposite direction. The problem of drag compensation is exacerbated when the EDT orbits at a higher inclination since the out-of-plane component of the magnetic field which produces the required in-track thrust is reduced (see Eq. (4)). Drag magnitude depends on the physical properties and dimensions of the EDT, the atmospheric density and satellite velocity. For a near circular orbit, the drag force on the entire tether system is given by

$$\mathbf{D} = -\frac{1}{2}B^*\rho(r)\frac{\mu}{r}\hat{\mathbf{e}}_\mathbf{t} \tag{5}$$

where $\rho(r)$ represents the average air density at radial distance r, and B^* is the average ballistic coefficient of the entire tether. Here the ballistic coefficient is defined as $B^* = \frac{C_d A}{m}$ where C_d is the average coefficient of drag, A is the average cross-sectional area perpendicular to the velocity vector, and m is the system mass. Modeling the atmosphere as an exponentially decaying density using a scale height h^*, we can expand about the small eccentricity and approximate the average density through first order as[43]

$$\rho(r) = \rho_0 e^{-\frac{r-R_\oplus}{h^*}} \approx \rho(a)\left(1+\frac{ae\cos\nu}{h^*}\right) \tag{6}$$

where the radial distance has been approximated as $r \approx a(1-e\cos\nu)$.

Gravity gradient torque tends to keep the tether nadir-pointing with libration that is assumed to be small (libration is addressed in Chapter V), so the acceleration due to the Lorenz force in Eq. (3) is given by

$$\mathbf{F} = \frac{IL\gamma_m}{mr^3}\left(\cos i\hat{\mathbf{e}}_\mathbf{t} - \cos(\nu+\omega)\sin i\hat{\mathbf{e}}_\mathbf{n}\right) \tag{7}$$

Recognizing that the orbits of interest at this low altitude are nearly circular, we ignore $O(e^2)$ and higher order terms and write the equations of variation for the five classical orbital elements as

$$\begin{aligned}
\frac{da}{dt} &= \frac{2a}{nr}(\mathbf{F}+\mathbf{D})\cdot\hat{\mathbf{e}}_\mathbf{t} \\
\frac{de}{dt} &= \frac{1}{na^2e}\left(\frac{a^2}{r}-r\right)(\mathbf{F}+\mathbf{D})\cdot\hat{\mathbf{e}}_\mathbf{t} \\
\frac{d\omega}{dt} &= \frac{1}{nae}\left(1+\frac{1}{1+e\cos\nu}\right)\sin\nu(\mathbf{F}+\mathbf{D})\cdot\hat{\mathbf{e}}_\mathbf{t} - \frac{r\cot i\sin(\nu+\omega)}{na^2}\mathbf{F}\cdot\hat{\mathbf{e}}_\mathbf{n} \\
\frac{di}{dt} &= \frac{r\cos(\nu+\omega)}{na^2}\mathbf{F}\cdot\hat{\mathbf{e}}_\mathbf{n} \\
\frac{d\Omega}{dt} &= \frac{r\sin(\nu+\omega)}{na^2\sin i}\mathbf{F}\cdot\hat{\mathbf{e}}_\mathbf{n}
\end{aligned} \tag{8}$$

where n is the mean motion of the satellite (Ref 43 pp. 84-85). Expanding these equations of motion about the small eccentricity using $r^{-k} \approx a^{-k}(1+ke\cos\nu)$ and ignoring second and higher order terms, we write the general perturbation equations of motion for a nadir pointing tether in terms of the true anomaly. This is the only variable that changes significantly on a short time scale.

$$\begin{aligned}
\frac{da}{dt} &\approx 2Ca\cos iI(\nu)(1+4e\cos\nu) - 2D\left(1+\left(2+\frac{a}{h^*}\right)e\cos\nu\right) \\
\frac{de}{dt} &\approx C\cos iI(\nu)\left(2\cos\nu+5e\cos^2\nu+e\right) - \frac{2D}{a}\left(\cos\nu+e+\left(1+\frac{a}{h^*}\right)e\cos^2\nu\right) \\
\frac{d\omega}{dt} &\approx \frac{C\cos i\sin(2\omega+2\nu)}{2}I(\nu)(1+2e\cos\nu) + \sin\nu\left[\frac{C\cos i}{e}I(\nu)(2+5e\cos\nu) - \frac{D}{ae}\left(2+\left(1+\frac{2a}{h^*}\right)e\cos\nu\right)\right] \\
\frac{di}{dt} &\approx -C\sin iI(\nu)\cos^2(\nu+\omega)(1+2e\cos\nu) \\
\frac{d\Omega}{dt} &\approx -\frac{CI(\nu)}{2}\sin(2\nu+2\omega)(1+2e\cos\nu)
\end{aligned} \tag{9}$$

We have let $C = \frac{L\gamma_m}{nma^4}$ represent the term resulting from thrust, and $D = \frac{B^*\mu\rho(a)}{2na}$ represent the drag term. In this form, these equations could serve as dynamic constraints in posing our optimal control problems,

however due to the rapid variation of true anomaly with each revolution we would need to discretize the problem with enough node points for the solver to capture the motion of each varying element with each revolution. This is the approach Williams used (Ref. 1) to achieve optimal control solutions for short time scale problems. Since we are only interested in the secular state changes of the EDT orbit over long time scales, we use the method of averaging to eliminate the small oscillations that occur within each revolution which effectively approximates the nonautonomous system in Eq. (9) as an autonomous averaged one.[44] This is achieved by recognizing that

$$dt = \frac{1}{n}\left[1 - 2e\cos\nu + O\left(e^2\right)\right]d\nu \tag{10}$$

and then integrating over $2\pi N$ (N =1,2,…). Because the average states vary slowly with time, they are considered constant over the short time periods of integration and are removed from the integrand. The fast-time variable, ν, always appears in the argument of a sine or a cosine function, therefore integrating Eq. (9) with respect to ν will yield non-zero results only when the control current, I, is itself periodic (i.e. it is a combination of sine and cosine functions of ν). A current that is purely dc will produce secular motion in semi-major axis and inclination since the first two derivatives in Eq. (9) would yield non-zero values after integration. Because an EDT depends on the Earth's magnetic field for propulsion, the orbits of interest remain very close to the Earth and are therefore nearly circular. To avoid singularity near $e = 0$, we will substitute two equinoctial coordinates for the eccentricity and argument of perigee in Eq. (9). The new coordinates are the eccentricity vector components defined as $h = e\sin\omega$ and $k = e\cos\omega$. The average state equations of motion are derived in Appendix G using the periodic current defined in Eq. (1), and are written as

$$
\begin{aligned}
\frac{\Delta a}{\Delta T} &\approx 2CI_m a\cos i\left(u_1+u_2 e\right)-2D \\
\frac{\Delta h}{\Delta T} &\approx CI_m\cos i\left[\left(\frac{3h}{2}\right)u_1+\left(\frac{h}{e}\right)u_2+\left(\frac{k}{e}\right)u_3+\left(\frac{h}{4}+\frac{hk^2}{2e^2}\right)u_4+\left(\frac{k}{4}+\frac{\left(k^2-h^2\right)k}{4e^2}\right)u_5\right]-\frac{D}{a}\left(1+\frac{a}{h^*}\right)h \\
\frac{\Delta k}{\Delta T} &\approx CI_m\cos i\left[\left(\frac{3k}{2}\right)u_1+\left(\frac{k}{e}\right)u_2-\left(\frac{h}{e}\right)u_3+\left(\frac{k}{4}-\frac{h^2k}{2e^2}\right)u_4+\left(-\frac{h}{4}+\frac{\left(h^2-k^2\right)h}{4e^2}\right)u_5\right]-\frac{D}{a}\left(1+\frac{a}{h^*}\right)k \quad (11) \\
\frac{\Delta i}{\Delta T} &\approx -CI_m\sin i\left(\left(\frac{1}{2}\right)u_1+\left(\frac{k^2-h^2}{4e^2}\right)u_4-\left(\frac{hk}{2e^2}\right)u_5\right) \\
\frac{\Delta\Omega}{\Delta T} &\approx -CI_m\left(\left(\frac{hk}{2e^2}\right)u_4+\left(\frac{k^2-h^2}{4e^2}\right)u_5\right)
\end{aligned}
$$

Secular changes to the orbit state are now expressed over a large time scale, $\Delta T=\frac{2\pi N}{n}$. The state vector $\mathbf{x}$ now represents the average orbital state values rather than the instantaneous values and is written using a quasi equinoctial element set, i.e. $\mathbf{x}\left(T\right)=\left[a,h,k,i,\Omega\right]^T$. Notice that these average states vary slowly over long time scales (indicated by T) and are considered constant "within" each revolution. The average state equations of motion are thus devoid of the short time scale variable, true anomaly. From the first equation in (11) we see that the average drag effect due to the air density (in the drag term, D) primarily affects the average change in semi-major axis. To a lesser extent drag decreases the h and k states and has a circularizing effect since $e=\sqrt{h^2+k^2}$. With the secular equations of motion in hand, we now turn to constraining the allowable tether current to values that are within the system power limitations.

Constraints

To determine the optimal controls for the system described by Eq. (11), we need to solve for the periodic control coefficients, $\mathbf{u}\left(T\right)$. Besides enforcing the initial state conditions as event constraints, the control current must also be bound to remain within an available power limit which is itself defined by the electron collection capabilities, ohmic losses, voltage current and other factors. For a description of electron collection in the ionosphere and the associated limitations see Ref 45. Because the control in Eq. (1) is defined using the rapidly changing true anomaly we cannot simply bound the instantaneous periodic current between a minimum and maximum value since we need to keep our averaged equations of motion

devoid of short time scale variables. To properly bound the control then, we need to define a path constraint that is a function of the slowly varying Fourier control coefficients, $\mathbf{u}(T)$. The approach used herein limits the average power available for thrust which in turn places bounds the on the rms current. For a given constant wire resistance R and average power limit, P_{avgMax}, the maximum allowable rms current is defined by Joule's law combined with Ohm's law

$$I_m^2 = \frac{P_{avgMax}}{R} \tag{12}$$

The actual electric current rms value over one orbit (period) is defined by

$$I_{rms}^2 = \frac{1}{2\pi}\int_0^{2\pi} I^2(\mathbf{u},\nu)d\nu \tag{13}$$

For the periodic current, this value is (using Eq. (1))

$$I_{rms}^2 = I_m^2\left(u_1^2 + \frac{1}{2}\left(u_2^2 + u_3^2 + u_4^2 + u_5^2\right)\right) \tag{14}$$

Using Eq. (14) we may express the path constraints in terms of the controls. The path constraint for the control is written as

$$g_1\left(\mathbf{u}(T)\right) = I_{rms}^2 - \frac{P_{avgMax}}{R} \le 0 \tag{15}$$

which places an upper bound on the rms control current throughout the transfer. Choosing a proper value for the maximum allowable rms control current is addressed in Appendix D.

This path constraint approach has the double advantage of averaging out any parameters periodic with the orbit that affect the available thrust current, such as diurnally varying ionospheric electron density, as well as eliminating the short-time variable, the true anomaly. The event constraints (constraints on states at specific times during the trajectory) are comprised only of the initial conditions and are written as

$$\mathbf{e}\left(\mathbf{x}(T_0)\right) = \left[a(T_0), h(T_0), k(T_0), i(T_0)\right]^T \tag{16}$$

Finally, states, controls and time are bounded by upper and lower limits (denoted using subscripts 'u' and 'l' respectively). These box constraints are written as

$$\begin{aligned} \mathbf{x}_l &\le \mathbf{x}(T) \le \mathbf{x}_u \\ \mathbf{u}_l &\le \mathbf{u}(T) \le \mathbf{u}_u \\ T_{0l} &\le T_0 \le T_{0u} \\ T_{fl} &\le T_f \le T_{fu} \end{aligned} \tag{17}$$

Now all the pieces are in place to construct and solve optimal control problems that will maneuver an EDT to a new orbit over many revolutions while overcoming drag by controlling nothing but current in a wire.

Three Optimal Control Problems and Their Solutions

Three sample maneuvers were chosen to demonstrate large time scale optimal control because of their slow secular orbital changes that occur over many revolutions. The tether modeled in all three problems is 4 km long and 2 mm in diameter (based on TiPs, a nonconducting tether system deployed in 1996). The system mass and average cross-sectional area is 500 kg and 8 m^2 respectively. The first two problems outline the optimal control problem setup, solution and results for maximizing the average altitude and inclination, and serve as benchmark problems since other authors have investigated similar non-optimal problems.[1,2] The third problem provides an example optimal control problem and solution that achieves a minimum time orbit change occurring over 500 revolutions using only 40 nodes in the discretized optimization problem. All problems were solved using DIDO, an optimization software package that discretizes and solves general optimization problems using a pseudospectral method.[46] Even though the derivation that produced Eq. (11) required integration over a hypothetical integer number of revolutions, the optimizer does not need to discretize the trajectory over the same integer multiples since the dynamic equations of motion are established for the continuous average state, not the instantaneous state. This average state, however, is meaningless unless the total maneuver time is long enough to span several periods. This akin to ensuring a sample interval is big enough to capture all the desired frequencies in signal analysis.

Verification of the optimal control solution was achieved by evaluating the Hamiltonian output by DIDO. To demonstrate the accuracy of the model used as the dynamic constraint in these problems, the output Fourier coefficient controls were converted into the time domain and then used to propagate instantaneous states using Eq. (8).

Maximum Final Altitude

Consider the scenario where there is a need to tow an object (spacecraft, debris, etc.) to a higher orbit in the same orbital plane using an EDT. For the sake of testing the algorithm against a known solution we seek the maximum altitude an EDT can reach in 50 orbital revolutions with no drag. In this case we expect that a direct current in the nadir-pointing tether will provide maximum thrust in the direction of the velocity to spiral the spacecraft out to a higher orbit.[2,8] Although we may actually want to control the other orbital elements to a desired end state, we seek only this known solution for this benchmark problem. The optimal control problem is written as the following.

Minimize Cost: $J = -a_f$

Subject to:

Dynamic Constraints $\dot{\mathbf{x}}(T) = \mathbf{f}\left(\mathbf{x}(T), \mathbf{u}(T)\right)$

Event Constraints $\mathbf{e}\left(\mathbf{x}(T_0)\right) = [6648 \text{ km}, 0, 0.001, 30^\circ]^T$

Path Constraints $g_1\left(\mathbf{u}(T)\right) = I_{rms}^2 - 2.25 \le 0 \text{ Amps}^2$

where $\dot{\mathbf{x}}(T)$ is the average state change and $\mathbf{f}\left(\mathbf{x}(T), \mathbf{u}(T)\right) = \Delta\mathbf{x}/\Delta T$. Box constraints in Eq. (17) are also enforced where we have chosen the bounds to be

$$\begin{aligned} \mathbf{x}_u &= \left[16000 \text{ km}, 0.4, 0.4, 80^\circ, 180^\circ\right]^T \\ \mathbf{x}_l &= \left[6638 \text{ km}, -0.4, -0.4, 15^\circ, -180^\circ\right]^T \\ \mathbf{u}_u &= \left[1, \sqrt{2}, \sqrt{2}, \sqrt{2}, \sqrt{2}\right]^T \\ \mathbf{u}_l &= -\mathbf{u}_u \\ T_0 &= 0 \\ T_f &= 50P \end{aligned} \tag{18}$$

where P is the orbital period at $T = 0$. The initial states h and k correspond to an eccentricity of 0.001 and an initial argument of perigee of zero. Before using the optimization solver, the states and time were scaled to span values of order 1 to make the problem numerically well-conditioned.[41,47] Solving the problem using DIDO yields the control history shown at the top of Figure 3, and the bottom of the figure shows the control transformed into the short time scale domain, in this case just a direct current. The

average altitude and inclination trajectories are shown in Figure 5, where the stars indicate the DIDO solution at distinct times (spanning large time scale steps) and the lines indicate the propagation of the instantaneous state values using DIDO derived controls and a Matlab® ode solver. As expected, in order to perform a maximum climb maneuver the solution indicates that the controller should drive a maximum allowable direct current through the wire to accomplish the large transverse thrust needed to boost the orbit. Starting at an altitude of 270 km, this EDT can climb about 130 km in about 3 days without drag. Introducing drag into the dynamic constraints does not affect the control profile, but reduces the achievable altitude change in the given number of orbit periods (50) to about 117 km. In reality we would need to contend with libration control and, at times, adverse battery conditions that could limit power available for tether thrusting. However, in principle, modest maneuvers can be accomplished if they are not time critical. Because there is no explicit time dependence in the Lagrangian of the Hamiltonian of this optimal control problem (Eq. (19)), the resulting Hamiltonian should be constant, i.e. $\dot{H} = 0$. The Lagrangian of the Hamiltonian is

$$\overline{H} = H + \mu_g g_1 + \boldsymbol{\mu}_x^T \mathbf{x} + \boldsymbol{\mu}_u^T \mathbf{u} \tag{19}$$

where the Hamiltonian is given by $H = \boldsymbol{\lambda}^T \mathbf{f}$ and $\boldsymbol{\lambda}$ represents the costates. The covector functions associated with the path constraint, state-variable box constraints and control-variable constraints are represented by μ_g, $\boldsymbol{\mu}_x$ and $\boldsymbol{\mu}_u$ respectively. DIDO uses the Covector Mapping Principle[48] to produce adjoints and the Hamiltonian as part of the solution. To check optimality the output Hamiltonian was plotted and it was revealed that it was indeed constant as shown in Figure 4.

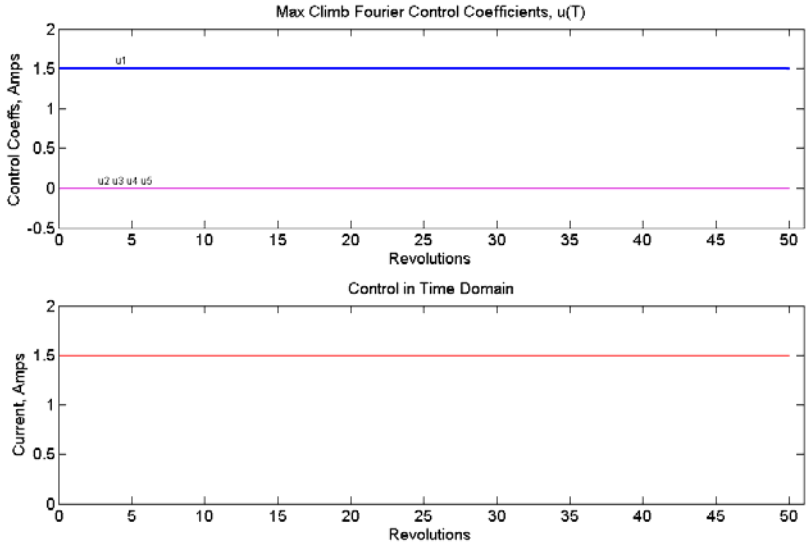

Figure 3. Control Solution for Maximum Altitude Maneuver Using 32 Nodes

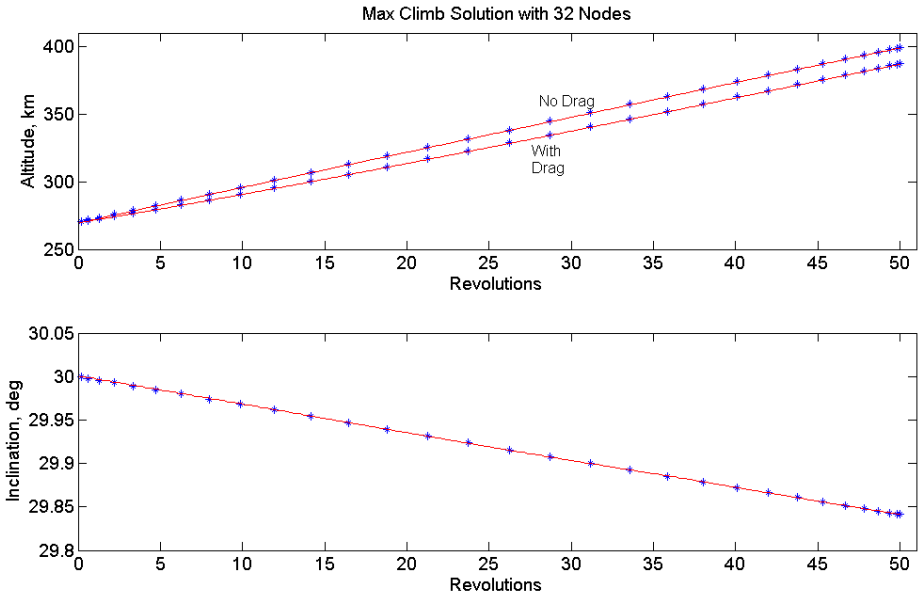

Figure 4. Maximum Altitude Maneuver Trajectories. Stars indicate DIDO solution; lines indicate instantaneous state propagation using the optimal control.

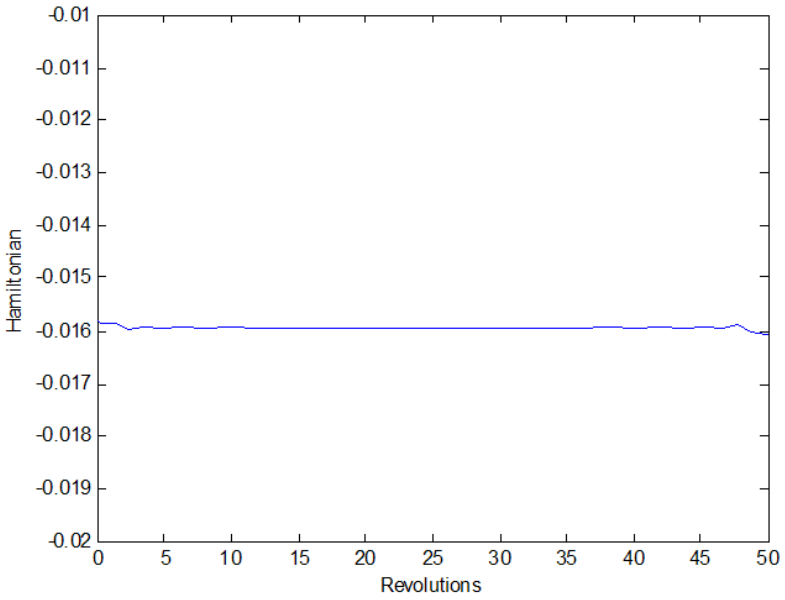

Figure 5. Hamiltonian Profile for Maximum Altitude with Drag

Maximum Final Inclination

From Eq. (11) it is evident that a carefully and constantly applied dc control current could indeed compensate precisely for drag to maintain altitude, however it would come at the expense of a secular decay of the inclination after a long time, which may be undesirable. To maximize the final inclination achievable in a fixed time (now for 500 revolutions), we write the same optimal control problem as in the previous example with the following exceptions.

Minimize cost: $J = -i_f$

Subject to:

$$T_f = 500P$$
$$\mathbf{e}\left(\mathbf{x}\left(T_0\right)\right) = [6648 \text{ km}, 0, 0.01, 30^\circ]^T$$
$$g_2\left(\mathbf{x}\left(T\right)\right) = h^2 + k^2 - e_0{}^2 = 0$$

where the new path constraint, $g_2\left(\mathbf{x}\left(T\right)\right)$, ensures a constant eccentricity transfer.

As a test case, we first look for the no drag solution (i.e. atmospheric density terms in Eq. (11) are zero), then compare it with the solution that accounts for drag. The 32-node DIDO control solution to the no drag problem is depicted in Figure 6.

The contrast between the two plots of the same control in Figure 6 clearly shows the advantage of solving the optimal control problem using Fourier coefficients over a large time scale. Attempts to discretize and optimize this control problem using instantaneous states and their respective dynamic equations of motion (Eq. (8)) for this long term trajectory would require thousands of nodes and run the risk of round-off errors and long solution times. Propagating the instantaneous states using the optimal control output produces the trajectory shown in Figure 7 where the magnified inserts clearly show the instantaneous fast time dynamic behavior.

Because there is no drag to contend with, the optimal solution indicates that it is best to mainly use an ac current that has double the orbital frequency, i.e. a combination of u_4 and u_5 within constraints. This result is consistent with Refs 2 and 8 which indicate that to achieve maximum inclination change the control strategy is to drive a current such that $I = -\sqrt{2} I_m \cos 2(\nu + \omega)$. Here, it is assumed that the path constraint in Eq. (15) is active which bounds the peak amplitude of this ac input to $\sqrt{2} I_m$. Transforming this result into the Fourier coefficient controller described in Eq. (1) we see that the control solution is the

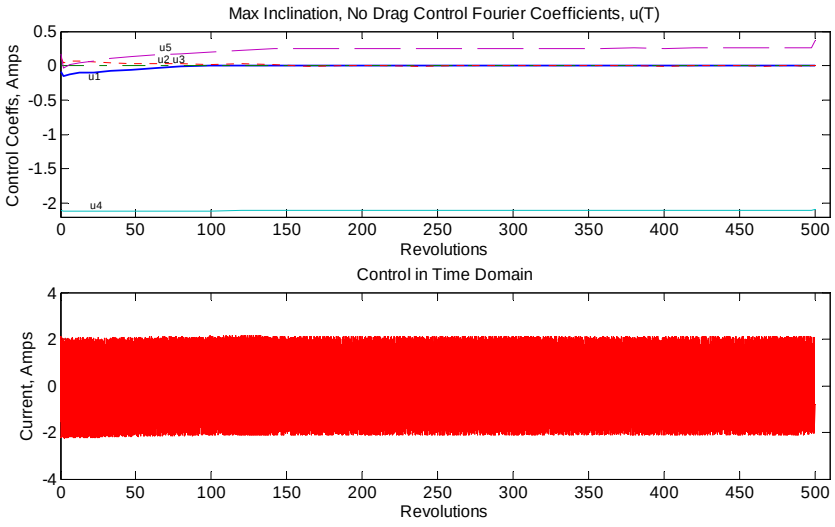

Figure 6. Maximum Inclination Control Solution with No Drag

same, only expressed in the context of the partial equinoctial set. To achieve a maximum final inclination, the control may be written

$$\begin{aligned} I &= -\sqrt{2}I_m \cos(2\nu + 2\omega) = -\sqrt{2}I_m (\cos 2\omega \cos 2\nu - \sin 2\omega \sin 2\nu) \\ &= -\sqrt{2}I_m \left(\frac{k^2 - h^2}{e^2} \cos 2\nu - \frac{2kh}{e^2} \sin 2\nu \right) \end{aligned} \tag{20}$$

In this form we recognize the Fourier coefficients for the second mode cosine and sine functions as

$$\begin{aligned} u_4 &= -\sqrt{2}I_m \left(\frac{k^2 - h^2}{e^2} \right) \\ u_5 &= \sqrt{2}I_m \left(\frac{2kh}{e^2} \right) \end{aligned} \tag{21}$$

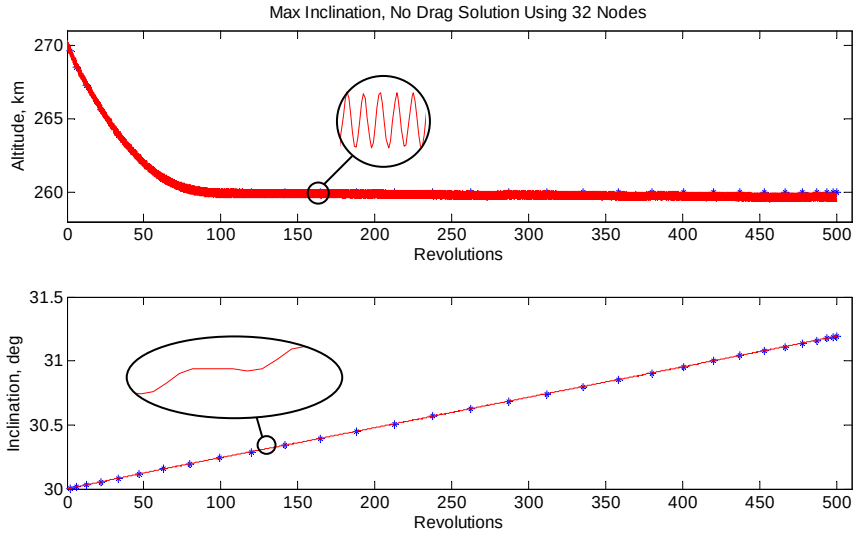

Figure 7. Maximum Inclination Maneuver Trajectory without Drag

The optimal controls calculated using Eq. (21) are consistent with the corresponding control Fourier coefficients determined by DIDO (within an error 2-norm of 0.04). This trajectory uses some negative dc thrust to decrease altitude while increasing the orbit's inclination. The Fourier control coefficients displayed in Figure 6 show that the tether current controller initially uses a small negative dc component to descend to the lowest allowable altitude in order to maximize the final inclination. Controlling the spacecraft in such a way increases the orbit inclination from 30° to 31.19° in about a month. This strategy outperforms a similar constant altitude maneuver by 0.04°. When drag is considered, the control strategy is altogether different because more of the limited available current must be constant dc in order to compensate for the increased drag as seen by comparing Figure 6 and Figure 8. We see from Eq. (11) that a large positive dc coefficient tends to reduce the inclination. There is a penalty for orbiting where the atmospheric density is higher because more power is expended simply to maintain altitude which causes inclination to decay and less power available to maximize the inclination. In this case, the strategy is to climb to a lower density altitude, level off to increase inclination then descend again to the minimum

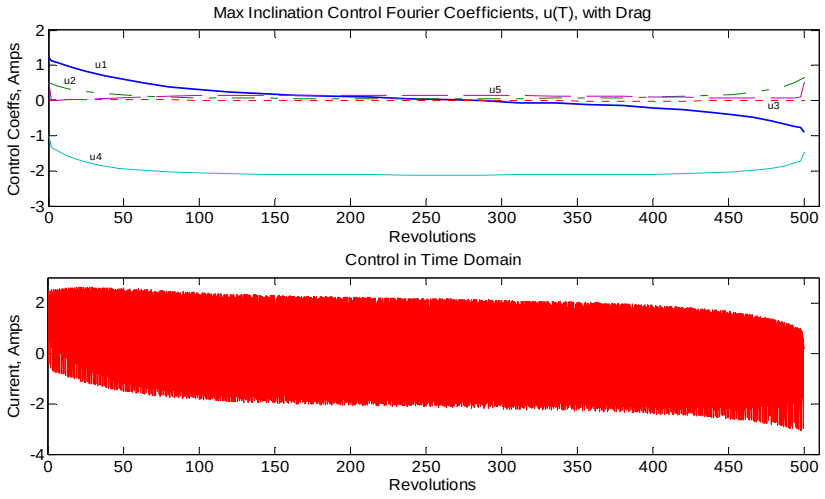

Figure 8. Maximum Inclination Control Solution with Drag

allowable altitude taking advantage of the largest possible inclination gain opportunities as shown in Figure 9. The initial climb comes at the expense of inclination gain, however overall the satellite achieves maximum inclination change because it operates in a lower average drag environment and does not need to

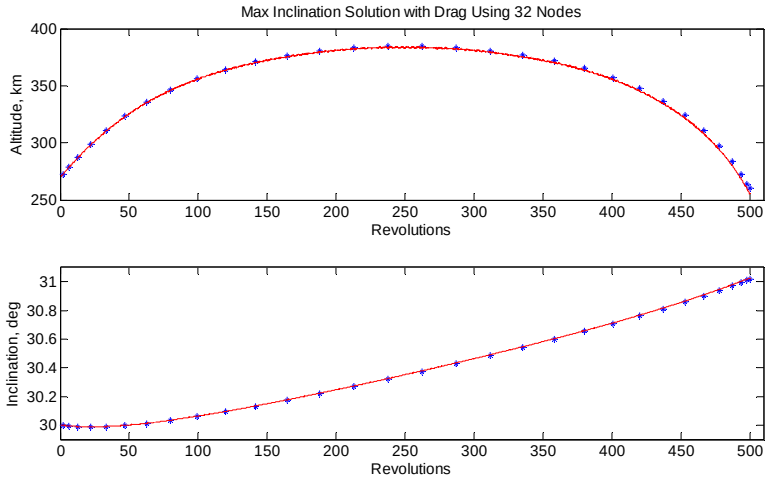

Figure 9. Maximum Inclination Maneuver Trajectory with Drag

expend as much power to maintain altitude. After a month of thrusting in a reduced average drag environment, the satellite achieves an inclination gain of 1.0° outperforming a constant altitude maneuver by 0.25°. Because this maneuver occurs over so many revolutions, it would be near impossible for short time scale optimization to yield a solution to this problem. The problem is complex when attempting to solve in the clock time domain but it is reduced to a simple Zermelo problem* in Fourier space. The next example problem will demonstrate how to apply this method to a more general orbit transfer.

* In 1923 German mathematician Ernst Zermelo posed the problem of navigating a boat from point A to point B in minimum time factoring in wind and current. The solution is not a straight line path. Ref. Jean van Heijenoort, 1967. From *Frege to Godel: A Source Book in Mathematical Logic, 1879-1931*. Harvard Univ. Press.

Minimum Time Orbit Change

Having looked at the baseline orbital maneuvers, we now turn our attention to determining the controls for a minimum time orbit change involving a desired final altitude and inclination while maintaining a constant eccentricity. In this example we start by using our initial states from the first example and then construct the optimal control problem to achieve a 10 km climb and a one degree inclination increase, while maintaining a constant eccentricity of 0.005, in the quickest time. We write the problem as

Minimize Cost: $J = t_f$

Subject to:

$$\dot{\mathbf{x}}(T) = \mathbf{f}\left(\mathbf{x}(T), \mathbf{u}(T)\right)$$
$$\mathbf{e_0}\left(\mathbf{x}(T_0)\right) = [6648 \text{ km}, 0, 0.005, 30^\circ]^T$$
$$\mathbf{e_f}\left(\mathbf{x}(T_f)\right) = \left[a_f, i_f\right]^T = [6658 \text{ km}, 31^\circ]^T$$
$$g_1\left(\mathbf{u}(T)\right) = I_{rms}^2 - 2.25 \le 0 \text{ Amps}^2$$
$$g_2\left(\mathbf{x}(T)\right) = h^2 + k^2 - e_0^2 = 0$$

Box constraints are still those listed in relations (17) and Eqs. (18), but since this problem has a free final time, we write

$$T_0 + \delta \le T_f \le 5\times 10^4 P$$

The control solution without drag, depicted in Figure 10, indicates that the strategy is to initially apply a negative dc control current, indicated by u_1, to descend. The controller needs to apply large ac control components cycling at twice the orbital frequency to reach the desired inclination (i.e. large u_4 and u_5 components), all while avoiding large components cycling at the orbital frequency, namely u_2 and u_3, which are large contributors to eccentricity change. The dc component is nearly zero for the majority of the trajectory and then reverts to positive flow at the end of the trajectory to climb to the final desired orbital altitude (Figure 11). When drag is considered, the dc component of the control current is

throttled (see Figure 12) such that the satellite initially climbs and then descends to the final orbit minimizing the cost due to increased drag at lower altitudes as much as possible as shown in Figure 13. Contending with drag, this EDT takes an additional four days to complete the maneuver.

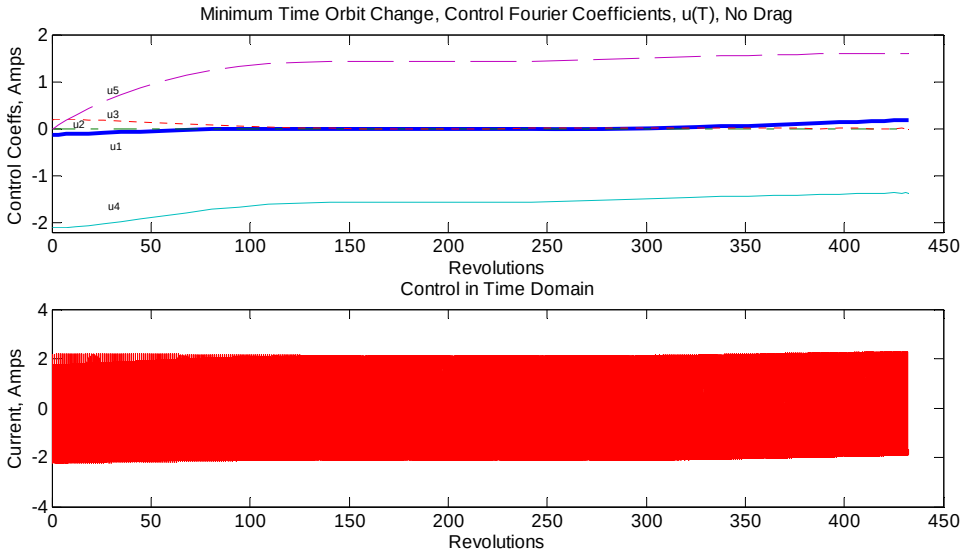

Figure 10. Minimum Time Orbit Change Control Solution without Drag

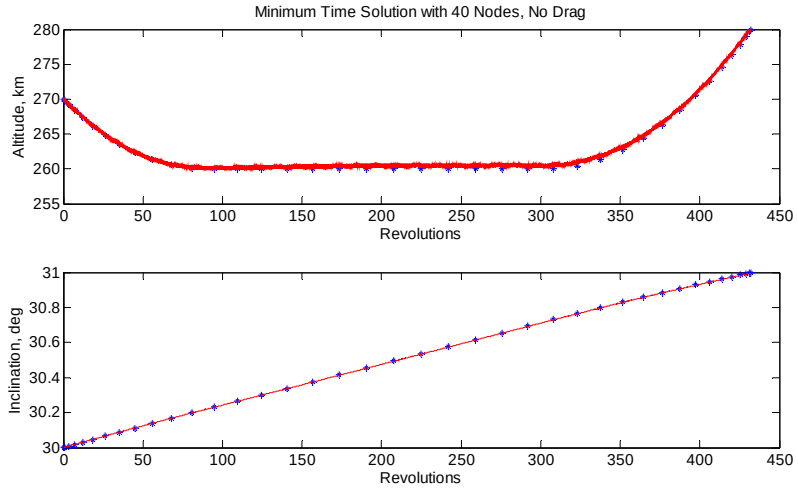

Figure 11. Minimum Time Orbit Change Trajectory without Drag

Controlling the slowly varying current Fourier coefficients over many revolutions has the advantage of solving long-term problems with relatively few nodes in the optimization algorithm. A similar problem solved using a small time scale and exact equations of motion would yield the instantaneous states during

each revolution, however it would require an exorbitant number of nodes over the same time frame to arrive at a meaningful solution. The periodic current would require at least four nodes per orbit revolution in the short time scale domain to establish a control current that avoids the node points aliasing undesired harmonics. The first day alone in this example consists of 32 control current cycles (Figure 14) which would require at least 64 nodes to adequately capture all the cycles. Using large time scales and averaged states, we have solved a multirevolution orbital maneuvering problem using 40 optimization nodes contrasted to the two thousand nodes that would have been required using a short time scale and instantaneous states. These examples demonstrate that solving optimal control problems in Fourier space

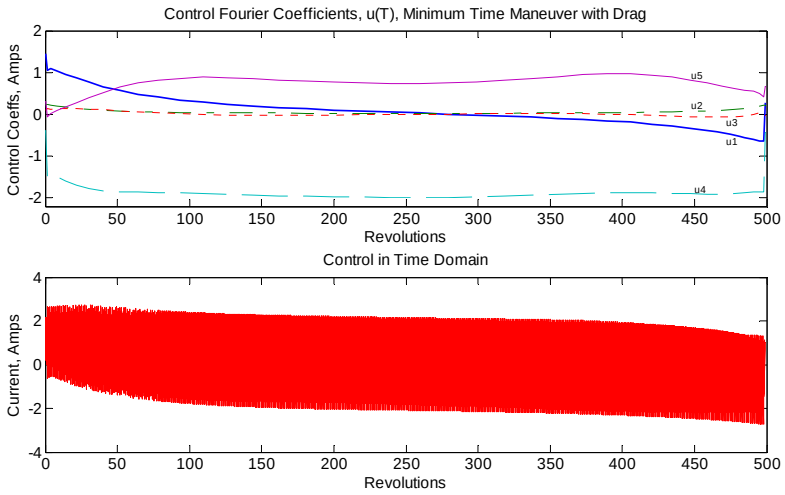

Figure 12. Minimum Time Orbit Change Control Solution with Drag

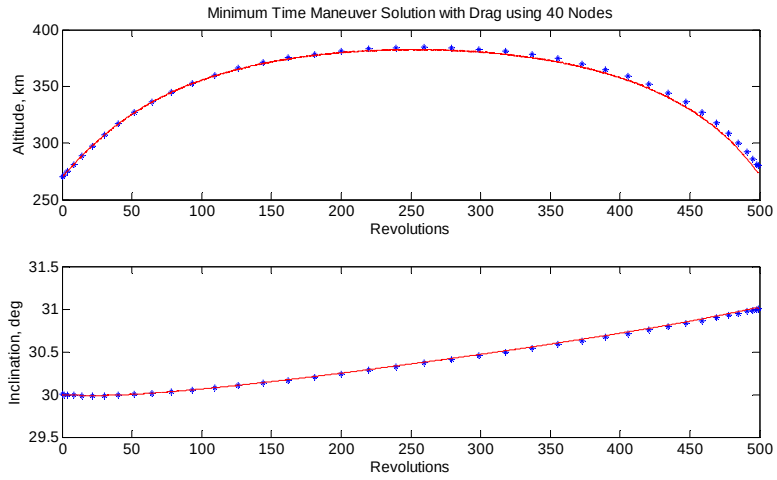

Figure 13. Minimum Time Orbit Change Trajectory with Drag

using large time scales and time-averaged orbital states has significant advantages when the desire is to control the secular behavior of a continuously operating, low thrust satellite system over a long time rather than the instantaneous periodic behavior. In satellite control, a rapidly changing periodic variable may be averaged out leaving only the dynamics of the slowly changing variables. In this dissertation, a method of constructing and solving a large time scale optimal control problem using an electrodynamic tether to maneuver to a desired orbit has been investigated. Optimal controls for three sample maneuvers spanning up to 500 orbital revolutions were determined using 30 to 40 optimization nodes instead of the hundreds or thousands of nodes required using the instantaneous clock time dynamics. The remainder of this dissertation will use the concepts introduced here to improve the controller dynamic model by including the effects of the Earth's rotating tilted magnetic dipole (Chapter IV) and tether libration (Chapter V).

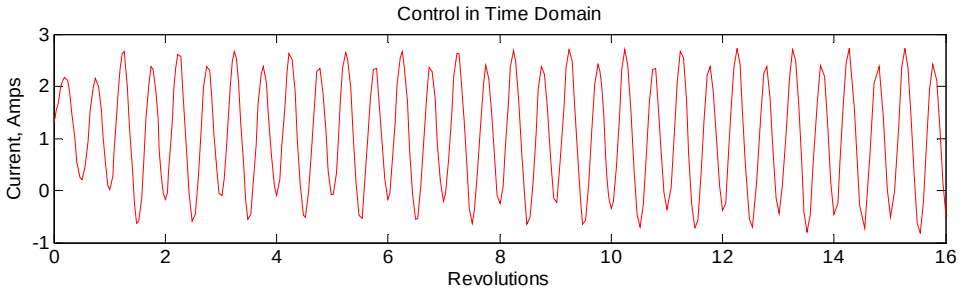

Figure 14. Current Control in Time Clock Time Domain for the First 16 Revolutions for Minimum Time Maneuver with Drag

Table 1. Summary of Results

Maneuver Type	No Drag	With Drag
Maximum Final Altitude	$\Delta a = 130$ km	$\Delta a = 117$ km
Maximum Final Inclination	$\Delta i = 1.19^{\circ}$	$\Delta i = 1.0^{\circ}$
Minimum Time Orbit Transfer	$\Delta \nu = 432$ revs	$\Delta \nu = 499$ revs

IV. Multiple Time Scales - Modeling Earth's Tilted Magnetic Dipole

Because electrodynamic tethers depend on the Earth's magnetic field to generate a thrusting force, an accurate model of this field is required to accurately control the spacecraft. The models used so far have assumed that the Earth's magnetic dipole moment vector is aligned with the Earth's poles and the magnetic field remains constant as the EDT orbits through it. In reality the Earth's magnetic dipole moment vector is tilted with respect to the North Pole by about 11.5 degrees (according to NASA) and rotates with the Earth once per day. Since the local magnetic field vector at any given point in the EDT's orbit cycles with a period of one sidereal day, the controller must account for this effect in the model. Fortunately this effect is predictably periodic and may be included in our existing model of averaged state dynamics. The diagram in Figure 15 depicts the planes containing the geographic equator, magnetic equator, and the EDT orbit where the magnetic equatorial plane rotates about the North geographic pole vector (**N**).

The inclination and argument of latitude at epoch of the satellite with respect to the magnetic equatorial plane are represented by i_m and α_m respectively for a dipole that is tilted by δ. The argument of latitude at

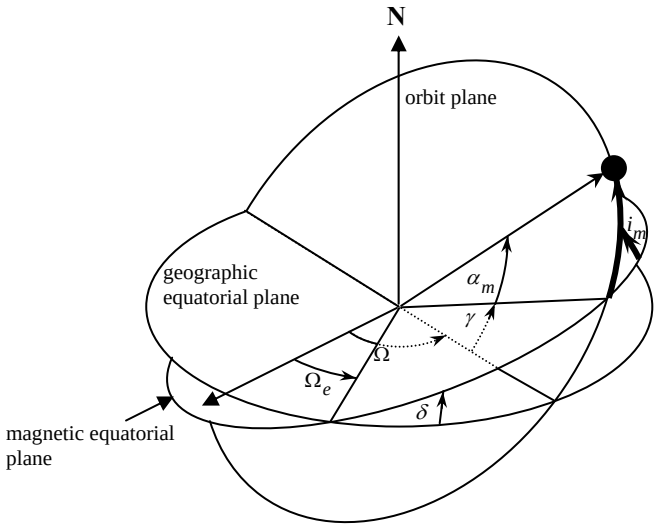

Figure 15. Earth's Tilted Magnetic Dipole Geometry

epoch of the satellite with respect to the geographic and equatorial planes are given respectively by

$$\alpha = \omega + \nu$$
$$\alpha_m = \alpha - \gamma$$

The inclinations with respect to the two equatorial reference planes are related using the law of cosines of spherical trigonometry.

$$\cos i_m = \cos\delta\cos i + \sin\delta\sin i\cos\left(\Omega - \Omega_e\right)$$
$$\sin i_m = \sqrt{1-\cos^2 i_m}$$

where we assume the satellite to be in an orbit such that $0 \le i_m \le 90^o \ \forall t > 0$ and Ω_e is the angle from an inertial reference direction to the intersection of the two equatorial planes in the direction of the longitude of the ascending node in the geographic equatorial plane. This angle varies with time over a medium time scale (i.e. a day) and is related to the true anomaly by

$$\Omega_e = \frac{1}{\eta}\nu$$

where η is a scaling factor. Applying the spherical trigonometric laws of sines and cosines once again, we obtain the relationships between the arguments of latitude in both reference equatorial planes.

$$\sin\gamma\sin i_m = \sin\delta\sin\left(\Omega - \Omega_e\right)$$
$$\cos\gamma\sin i\sin i_m = \left(\cos\delta - \cos i\cos i_m\right)$$

The argument of latitude at epoch in the magnetic equatorial plane is then written

$$\sin\alpha_m = \sin\left(\alpha - \gamma\right) = \sin\alpha\cos\gamma - \cos\alpha\sin\gamma$$
$$\cos\alpha_m = \cos\left(\alpha - \gamma\right) = \cos\alpha\cos\gamma + \sin\alpha\sin\gamma$$

The local magnetic field vector direction is a function of the inclination and argument of latitude at epoch with respect to the magnetic equator may now be expressed in terms of a time varying function that depends on the same orbital parameters referenced to the geographic equator. In the satellite frame (Figure 33 in Appendix A), the magnetic field vector is

$$\mathbf{B} = \frac{\gamma_m}{r^3}\begin{bmatrix} -2\sin\alpha_m \sin i_m \\ \cos\alpha_m \sin i_m \\ \cos i_m \end{bmatrix} = \frac{\gamma_m}{r^3}\begin{bmatrix} -2\left[\dfrac{\sin\alpha}{\sin i}\left(\cos\delta - \cos i \cos i_m\right) - \cos\alpha \sin\delta \sin\left(\Omega - \Omega_e\right)\right] \\ \dfrac{\cos\alpha}{\sin i}\left(\cos\delta - \cos i \cos i_m\right) + \sin\alpha \sin\delta \sin\left(\Omega - \Omega_e\right) \\ \cos i_m \end{bmatrix}$$

After making the appropriate substitutions and grouping terms, a form for the magnetic field in terms of the orbital elements referenced to the geographic equatorial plane is derived as

$$\mathbf{B} = \mathbf{B}_\mathbf{I} \cos\delta + \mathbf{B}_\boldsymbol{\eta} \sin\delta \tag{22}$$

where

$$\begin{aligned} \mathbf{B}_\mathbf{I} &= \frac{\gamma_m}{r^3}\begin{bmatrix} -2\sin\alpha \sin i \\ \cos\alpha \sin i \\ \cos i \end{bmatrix} \\ \mathbf{B}_\boldsymbol{\eta} &= \frac{\gamma_m}{r^3}\begin{bmatrix} 2\left[\sin\alpha \cos i \cos\left(\Omega - \Omega_e\right) + \cos\alpha \sin\left(\Omega - \Omega_e\right)\right] \\ -\cos\alpha \cos i \cos\left(\Omega - \Omega_e\right) + \sin\alpha \sin\left(\Omega - \Omega_e\right) \\ \sin i \cos\left(\Omega - \Omega_e\right) \end{bmatrix} \end{aligned} \tag{23}$$

The dynamic model of the local magnetic flux density vector may be decoupled into two terms, each affecting the motion of the EDT over a different time scale. The first magnetic field term $\mathbf{B}_\mathbf{I}$ is derived from the same non-tilted dipole moment model used in Eq. (4) and it is periodic on a short time scale of one orbit, but does not change with respect to the medium time scale (i.e. a day). It may be averaged over a single period. The second magnetic field term $\mathbf{B}_\boldsymbol{\eta}$, however, is periodic on a medium time scale of η orbits $(\eta > 1)$ since it contains Ω_e terms. For optimal control problems spanning times such that $\nu \gg 2\pi\eta$ this magnetic field term may be averaged over η orbits. As expected, when the model assumes that there is no tilted dipole moment, then Eq. (22) reduces to the standard model used in Eq. (4) that is periodic over one period.

The Lorenz force due to a control current driven through the tether is given as

$$\mathbf{F} = I\mathbf{L} \times \mathbf{B} = I\mathbf{L} \times \left(\mathbf{B}_\mathbf{I} \cos\delta + \mathbf{B}_\boldsymbol{\eta} \sin\delta\right) = \mathbf{F}_\mathbf{I} \cos\delta + \mathbf{F}_\boldsymbol{\eta} \sin\delta$$

where $\mathbf{F}_1$ represents the contribution to the electrodynamic force that is periodic over a single orbit and $\mathbf{F}_\eta$ represents the contribution that is periodic only over η orbits, i.e.

$$\mathbf{F}_1 = I\mathbf{L}\times\mathbf{B}_1$$
$$\mathbf{F}_\eta = I\mathbf{L}\times\mathbf{B}_\eta$$

The $\mathbf{F}_1$ contribution is the same as that derived in Eq. (7) and may be averaged over one orbit as shown in the example problems in the previous section using the non-tilted dipole model. The $\mathbf{F}_\eta$ term contributes to the total Lorenz force when there is a non-zero tilt in the Earth's magnetic dipole moment and the vector direction cycles with period $2\pi\eta$. For a nadir-pointing EDT using the satellite frame defined in Figure 33, this force contribution is

$$\mathbf{F}_\eta = IL\left(\left(\mathbf{B}_\eta\cdot\hat{\mathbf{e}}_\mathbf{n}\right)\hat{\mathbf{e}}_\mathbf{t} - \left(\mathbf{B}_\eta\cdot\hat{\mathbf{e}}_\mathbf{t}\right)\hat{\mathbf{e}}_\mathbf{n}\right)$$

with components

$$\begin{aligned}
\mathbf{F}_\eta\cdot\hat{\mathbf{e}}_\mathbf{r} &= 0\\
\mathbf{F}_\eta\cdot\hat{\mathbf{e}}_\mathbf{t} &= CI\sin i\left(\cos\Omega\cos\Omega_e + \sin\Omega\sin\Omega_e\right)\\
\mathbf{F}_\eta\cdot\hat{\mathbf{e}}_\mathbf{n} &= CI\left[\cos\alpha\cos i\left(\cos\Omega\cos\Omega_e + \sin\Omega\sin\Omega_e\right) - \sin\alpha\left(\sin\Omega\cos\Omega_e - \cos\Omega\sin\Omega_e\right)\right]
\end{aligned} \tag{24}$$

where $C = \dfrac{L\gamma_m}{nma^4}$. Assuming that states and controls change very slowly over η orbits, the average states change due to this force contribution only when there is a control current that is resonant with $\Omega_e = \dfrac{\nu}{\eta}$. We will therefore define a control current as in Eq.(1) that now includes Fourier control coefficients u_6 and u_7 that correspond with this harmonic as

$$I\left(\nu,\mathbf{u}(T),\eta(T)\right) = I_m\left(u_1 + u_2\cos\nu + u_3\sin\nu + u_4\cos 2\nu + u_5\sin 2\nu + u_6\cos\frac{\nu}{\eta} + u_7\sin\frac{\nu}{\eta}\right) \tag{25}$$

Substituting Eqs. (24) and (25) into the perturbation equations of motion (Eq.(8)) and changing the independent variable to the true anomaly using the approximation $dt \approx \dfrac{1}{n}\left(1-2e\cos\nu\right)d\nu$ we write the averaged perturbation equation for the semi-major axis as

$$\Delta a = \Delta a_1\cos\delta + \Delta a_\eta\sin\delta$$

where Δa_1 is the same averaged perturbation equation for the non-tilted dipole given in Eq.(75) and

$$\Delta a_\eta = \frac{2C}{n} a \sin i \int_0^{2\pi\eta} I(\nu)(1+2e\cos\nu)\left(c\Omega\cos\frac{\nu}{\eta} + s\Omega\sin\frac{\nu}{\eta}\right) d\nu \tag{26}$$

The sine and cosine functions of the longitude of ascending nodes do not change much over the $2\pi\eta$ interval and may be considered constants for the integration (they are abbreviated as $\sin\Omega = s\Omega$ and $\cos\Omega = c\Omega$ for clarity). When η is an integer, the only terms in the current (Eq.(25)) that will resonate with the lower frequency harmonic and survive the integration are the u_6 and u_7 terms. Therefore, in this case the contribution to the change in the average semi-major axis due to the rotating tilted dipole is

$$\Delta a_\eta = CI_m a \sin i\left(c\Omega u_6 + s\Omega u_7 \right)\frac{2\pi\eta}{n} \tag{27}$$

where we have assumed that frequencies of the $\mathbf{F}_1$ and $\mathbf{F}_\eta$ contributions are commensurate and that terms with incommensurate frequencies drop out after integration in Eq. (26) yielding an exact solution shown in Eq. (27). For a satellite orbiting at an altitude of approximately 261 km, the scaling parameter corresponds to 16 orbital revolutions per sidereal day, i.e. $\eta = 16$. To consider an orbit transfer at altitudes that do not correspond to an integer number of revolutions per sidereal day where the multiple frequencies under consideration are not commensurate, we average the state over a larger integer number of revolutions to achieve an approximate model for the averaged state dynamics. This is accomplished by recognizing that for some tolerance $\tau > 0$, $\exists\, N \in \mathbb{Z}$ and $p \in \mathbb{Z}$ such that $|\eta N - p| < \tau$. Simply said, if we choose N such that an interval $2\pi\eta N$ is very close to an integer number of periods, then the commensurate frequency model in Eq. (27) will suffice to represent the averaged dynamics within a tolerance that is defined by τ. This means that the duration of the maneuver must be long enough to obtain an accurate average of instantaneous states that include contributions at lower frequencies. By choosing intervals that do not correspond to integer periods (i.e. $\eta N \notin \mathbb{Z}$), the maximum mean square error of our estimate for $\frac{\Delta a}{a}$ incurred by using Eq.(27) is of the same order as the nondimensional quantity $\frac{CI_m}{n}$ (~10^{-5} for the examples here). The error due to the approximation is itself periodic, free of secular growth, and is exactly zero

when $\eta N \in \mathbb{Z}$. Therefore, after integrating Eq. (26) over the interval from 0 to $2\pi\eta N$, Eq. (27) becomes (for $N \gg 1$)

$$\Delta a_\eta = \frac{CI_m aN}{n}\left[2\pi\eta \sin i\left(c\Omega u_6 + s\Omega u_7\right) + \mathcal{O}\left(\frac{1}{N}\right)\right]$$

Similarly the average inclination change due to the contributions of the rotating tilted dipole is derived using the method of averaging.

$$\begin{aligned}\Delta i_\eta &= -\frac{C}{n}\int_0^{2\pi\eta N} I(\nu)\cos\alpha\left[\cos\alpha\cos i\left(c\Omega\cos\frac{\nu}{\eta}+s\Omega\sin\frac{\nu}{\eta}\right)-\sin\alpha\left(s\Omega\cos\frac{\nu}{\eta}-c\Omega\sin\frac{\nu}{\eta}\right)\right]d\nu \\ &\approx -\frac{CI_m}{n}\cos i\int_0^{2\pi\eta N}\cos^2\alpha\left(c\Omega\cos\frac{\nu}{\eta}+s\Omega\sin\frac{\nu}{\eta}\right)\left(u_6\cos\frac{\nu}{\eta}+u_7\sin\frac{\nu}{\eta}\right)d\nu\end{aligned}$$

Integrating yields

$$\Delta i_\eta \approx -\frac{CI_m}{4}\cos i\left(c\Omega u_6 + s\Omega u_7\right)\frac{2\pi\eta N}{n}$$

For the longitude of the ascending node, the change due to this contribution is

$$\begin{aligned}\Delta\Omega_\eta &= -\frac{C}{n}\int_0^{2\pi\eta N} I(\nu)\sin\alpha\left[\cos\alpha\cos i\left(c\Omega\cos\frac{\nu}{\eta}+s\Omega\sin\frac{\nu}{\eta}\right)-\sin\alpha\left(s\Omega\cos\frac{\nu}{\eta}-c\Omega\sin\frac{\nu}{\eta}\right)\right]d\nu \\ &\approx \frac{CI_m}{n}\int_0^{2\pi\eta N}\sin^2\alpha\left(s\Omega\cos\frac{\nu}{\eta}-c\Omega\sin\frac{\nu}{\eta}\right)\left(u_6\cos\frac{\nu}{\eta}+u_7\sin\frac{\nu}{\eta}\right)d\nu \\ &\approx \frac{CI_m}{4}\left(s\Omega u_6 - c\Omega u_7\right)\frac{2\pi\eta N}{n}\end{aligned}$$

The eccentricity vector components are derived as follows.

$$\begin{aligned}\Delta h_\eta &= \int_0^{2\pi\eta N}\left\{k\left[\frac{1}{nae}\left(1+\frac{1}{1+e\cos\nu}\right)\sin\nu\left(\mathbf{F}_\eta\cdot\hat{\mathbf{e}}_t\right)-\frac{r\cot i\sin\alpha}{na^2}\left(\mathbf{F}_\eta\cdot\hat{\mathbf{e}}_n\right)\right]+\tilde{h}\frac{1}{na^2e}\left(\frac{a^2}{r}-r\right)\left(\mathbf{F}_\eta\cdot\hat{\mathbf{e}}_t\right)\right\}\frac{(1-2e\cos\nu)}{n}d\nu \\ &\approx \frac{C}{n}\int_0^{2\pi\eta N}\tilde{k}\left\{(2+e\cos\nu)\sin\nu\sin i\left(c\Omega\cos\frac{\nu}{\eta}+s\Omega\sin\frac{\nu}{\eta}\right)\right. \\ &\qquad \left.-\sin\alpha\left[\cos\alpha\cos i\left(c\Omega\cos\frac{\nu}{\eta}+s\Omega\sin\frac{\nu}{\eta}\right)-\sin\alpha\left(s\Omega\cos\frac{\nu}{\eta}-c\Omega\sin\frac{\nu}{\eta}\right)\right]\right\}I(\nu) \\ &\qquad +\tilde{h}\sin i\left(2\cos\nu+e\left(\cos^2\nu+1\right)\right)\left(c\Omega\cos\frac{\nu}{\eta}+s\Omega\sin\frac{\nu}{\eta}\right)I(\nu)\,d\nu\end{aligned}$$

Integrating yields

$$\Delta h_\eta \approx \frac{CI_m}{4}\left(\tilde{k}\cot i\left(s\Omega u_6 - c\Omega u_7\right)+3h\sin i\left(c\Omega u_6 + s\Omega u_7\right)\right)\frac{2\pi\eta N}{n}$$

$$\Delta k_\eta = \frac{C}{n}\int_0^{2\pi\eta N} \tilde{h}\left\{(2+e\cos\nu)\sin\nu\sin i\left(c\Omega\cos\frac{\nu}{\eta}+s\Omega\sin\frac{\nu}{\eta}\right)\right.$$
$$\left.+\cot i\sin\alpha\left[\cos\alpha\cos i\left(c\Omega\cos\frac{\nu}{\eta}+s\Omega\sin\frac{\nu}{\eta}\right)-\sin\alpha\left(s\Omega\cos\frac{\nu}{\eta}-c\Omega\sin\frac{\nu}{\eta}\right)\right]\right\}I(\nu)$$
$$+\tilde{k}\sin i\left(2\cos\nu+e\left(\cos^2\nu+1\right)\right)\left(c\Omega\cos\frac{\nu}{\eta}+s\Omega\sin\frac{\nu}{\eta}\right)I(\nu)\,d\nu$$

which produces

$$\Delta k_\eta \approx \frac{CI_m}{4}\left(\tilde{h}\cot i\left(-s\Omega u_6+c\Omega u_7\right)+3k\sin i\left(c\Omega u_6+s\Omega u_7\right)\right)\frac{2\pi\eta N}{n}$$

For a given averaged state x, the total rate of change is approximated as

$$\Delta x \approx \Delta x_1\cos\delta+\Delta x_\eta\sin\delta$$

where the non-tilted dipole dynamics periodic over a single orbit, Δx_1, are given in Appendix G.

Recognizing that $\Delta T=\frac{2\pi\eta N}{n}$, the averaged dynamics $\frac{\Delta\mathbf{x}}{\Delta T}$ may be determined. For a sufficiently long orbit transfer using an electrodynamic tether, this averaging method will capture the averaged effects due to the lower frequency rotation of the tilted dipole. The following example will demonstrate this idea.

Solution to an Optimal Control Problem Using Multiple Time Scales

Using the tether model from the previous optimal maneuver example, a longer term optimal orbit change maneuver is investigated that includes the moderately varying effect of the Earth's rotating tilted dipole. For this model, we use the magnetic field described by Eq. (23) and a dipole tilt of 11.5 degrees. The example maneuver will increase the inclination of an EDT in a 261 km parking orbit (where $\eta\approx 16$) from 40 to 45 degrees ending at the same altitude while maintaining a constant eccentricity of 0.005 in a drag environment. The optimal control problem is therefore written as

Minimize Cost: $J=t_f$

Subject to:

$$\dot{\mathbf{x}}(T) = \mathbf{f}\left(\mathbf{x}(T), \mathbf{u}(T)\right)$$
$$\mathbf{e_0}\left(\mathbf{x}(T_0)\right) = [6639\text{ km}, 0, 0.005, 40^\circ, 0^\circ]^T$$
$$\mathbf{e_f}\left(\mathbf{x}(T_f)\right) = \left[a_f, i_f\right]^T = [6639\text{ km}, 45^\circ]^T$$
$$g_1\left(\mathbf{u}(T)\right) = I_{rms}^2 - 2.25 \le 0\ \text{Amps}^2$$
$$g_2\left(\mathbf{x}(T)\right) = h^2 + k^2 - e_0^2 = 0$$

where the mean square current is defined using Eq. (13) as

$$I_{rms}^2 = I_m^2\left[u_1^2 + \frac{1}{2}\left(u_2^2 + u_3^2 + u_4^2 + u_5^2 + u_6^2 + u_7^2\right)\right]$$

The dynamic constraints are given by $\mathbf{f}\left(\mathbf{x}(T), \mathbf{u}(T)\right) = d\mathbf{x}/dT \approx \Delta\mathbf{x}/\Delta T$ and box constraints given in Eq. (17) are also enforced. Solving the optimal control problem using DIDO yields the optimal control profile shown in Figure 16.

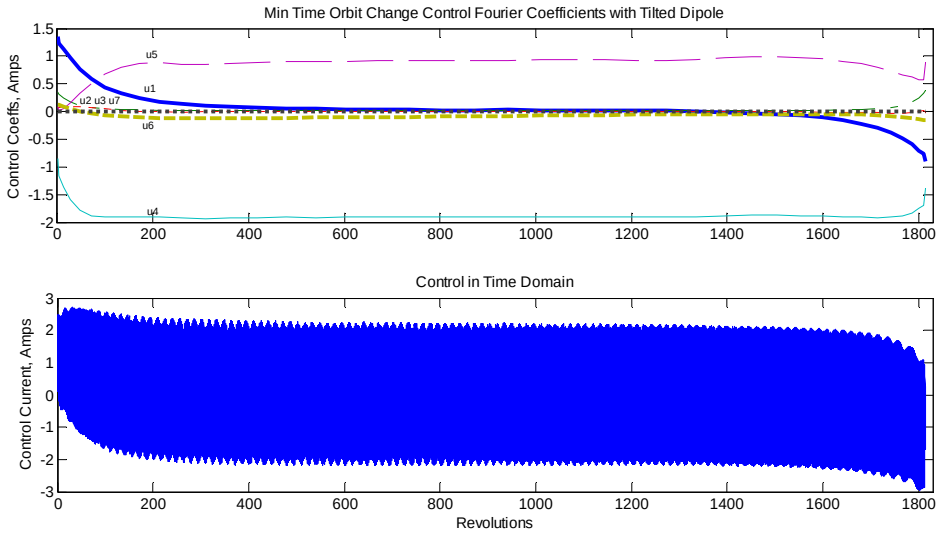

Figure 16. Control Profile Using Tilted Dipole Model

The controller dc component, u_1, and the Fourier coefficients corresponding with the higher frequencies (u_2 through u_5) look similar to the corresponding minimum time problem in the previous section (see Figure 12). Slightly more power is dedicated in the form of direct current, corresponding to u_1, to change the altitude because at this higher inclination orbit the local magnetic field is less effective for thrust. In the tilted dipole case, however, a small controller contribution at the lower frequency, u_6, is evident which

superimposes a lower frequency component on to the control signal (see bottom of Figure 16). The altitude and inclination trajectories shown in Figure 17 reveal a similar "climb and descend" strategy to that of the example in the previous section. This maneuver is more aggressive than the previous one taking 113 days to complete and close inspection of the propagated trajectory reveals the impact of a rotating tilted Earth magnetic dipole. The magnified inserts in Figure 17 show the effects of the 3 time scales; the fast time dynamics of the instantaneous altitude, the medium time attitude dynamics with daily oscillations, and the slow trend of the average altitude.

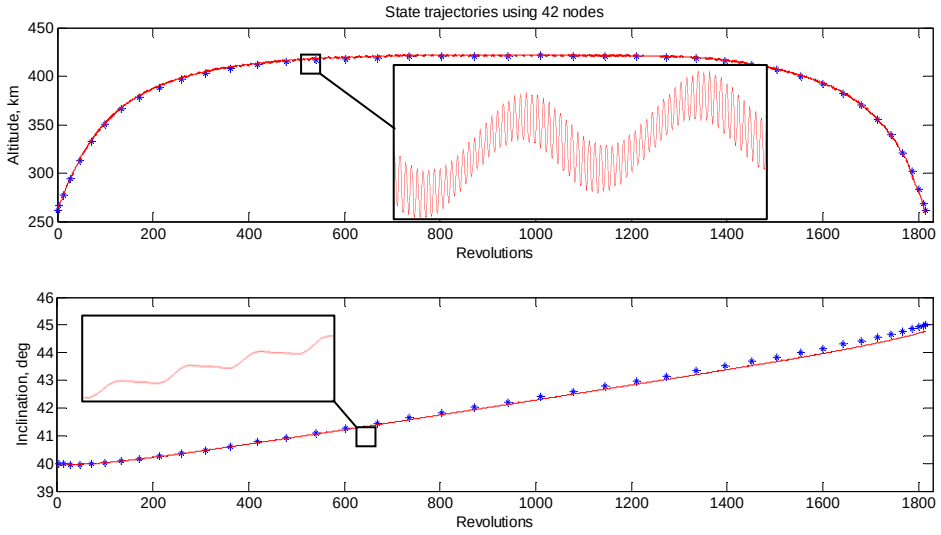

Figure 17. State Trajectories Using Tilted Dipole Model with Drag

For comparison, optimal controls were determined for the same problem using a model that does not include a tilted magnetic dipole. The controls (Figure 18) look similar to the previous ones, albeit without the medium time scale components. The maneuver appears to take two fewer days to complete when power is not directed to compensate for the magnetic dipole motion; however the propagation of the altitude does not match very closely with the output from the model (Figure 19) for such a long term maneuver. The propagation was performed in the same manner as the previous example for comparison, indicating that the errors are model errors and not numerical errors.

Summary

Because an EDT draws its thrusting capability from the Earth's magnetic field, it is important to use a magnetic field model with an appropriate amount of fidelity. Engineers may obtain control strategies using a less accurate model for maneuvers that do not span many revolutions (in this example, less than about 300 revolutions), however for transfers that take a very long time a tilted dipole model must be

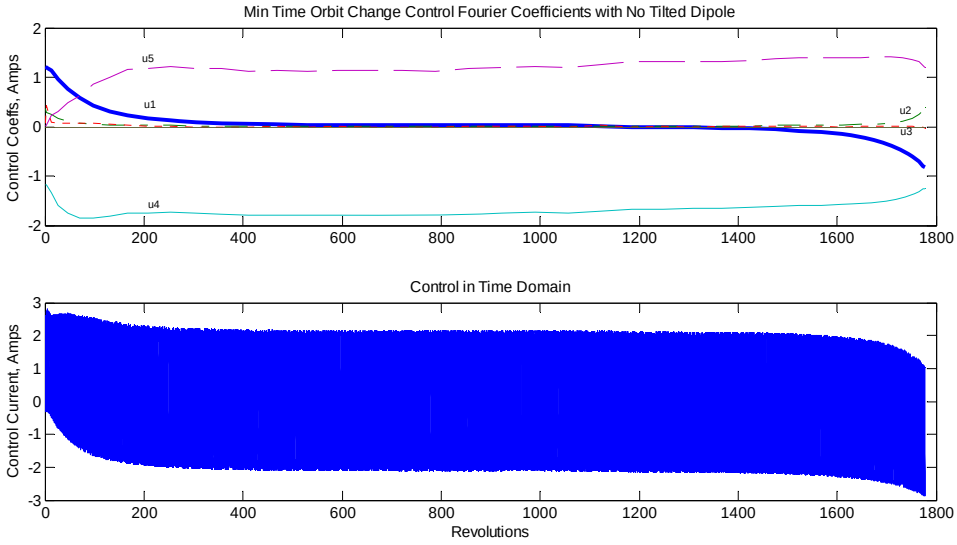

Figure 18. Optimal Control with Drag, but No Earth Dipole Tilt

considered. Using the multiple time scale approach and the method of averaging, one can include this low frequency effect in the model by introducing a new time scale variable in the controller. The next step to improving the controller is to include the librational motion of the EDT in the dynamic model, which is the subject of the next chapter.

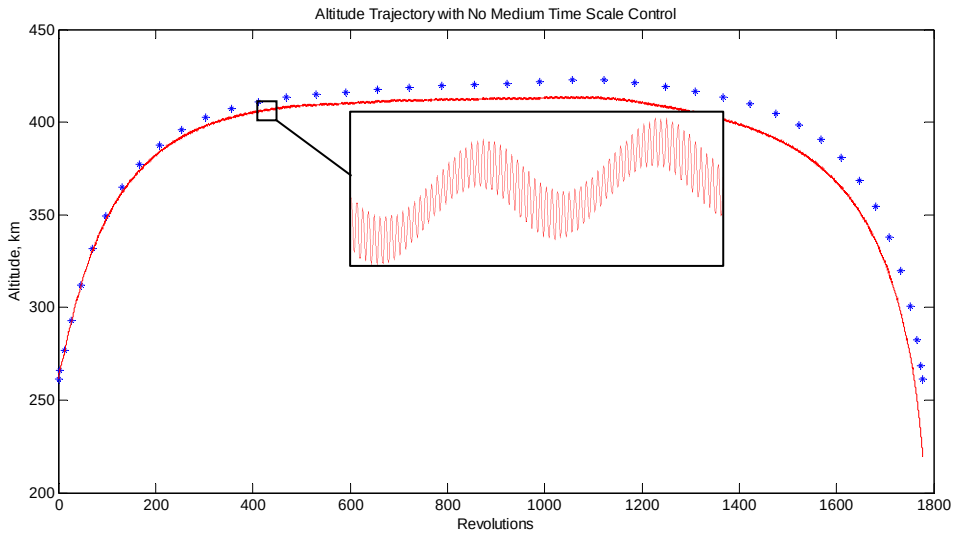

Figure 19. The controller model breaks down when Earth magnetic dipole tilt is excluded for a long term orbit transfer. Stars indicate the model-derived altitude trajectory; line indicates propagated altitude trajectory in a rotating tilted dipole magnetic field.

V. Tether Libration

When controlling an electrodynamic tether (EDT) to reach a new orbit as discussed in Chapters III and IV, it was assumed that the tether was nadir-pointing and non-librating. This was done to introduce the method of averaging for solving the optimal control problem in Fourier space. In reality, however, we would need to account for the librations of the long tether. It is well known that an unperturbed inert (unpowered) tether librates in and out of plane about an equilibrium point for circular orbits without growth or decay.[52,53] An uncontrolled EDT with a constant current running through it, however, will eventually go unstable as aptly pointed out in Ref 10. The purpose of this chapter is to analyze the stability of an EDT and to use the resulting stability criteria to define libration constraints. The objective will be to determine the optimal control that will maneuver an EDT to a new orbit while simultaneously driving libration amplitude to a desired end state within these specified libration bounds. To achieve this objective, this chapter will first provide an examination of the stability of the tether libration both with and without drag. Given that an EDT with a dc control current eventually goes unstable, it is shown that the system may be stabilized using a method of feedback linearization. This demonstration provides confidence that there is at least one feasible control solution, thereby allowing us to seek an optimal control solution. The remainder of the chapter is devoted to the derivation of dynamic model and path constraints and then determining optimal controls for a librating EDT in orbit transfer.

Equilibrium and Stability

The first step in stability analysis is to obtain the attitude dynamic equations of motion for the system. The attitude equations of motion will initially be based on the following assumptions for an EDT system of two subsatellites connected by a wire in tension. These assumptions and approximations may be relaxed as need arises, but the ones listed here are necessary to model the EDT system and clearly demonstrate the utility of multiple time scale optimal controls applied to libration control.

Rigid Rod in Tension – The tether is assumed to be perfectly straight between two subsatellites. This approximation is valid for certain ranges of maximum allowable wire control current (see Appendix D). Because the tether is straight, the center of mass (COM) is located along tether. The tether cannot undergo compression or go slack, but rather it remains in tension and does not stretch. The former condition is valid because tether attitudes will be constrained through active control to remain below libration angles that would permit a slack tether. The no-stretch condition is justified since the materials used will be such that the stretch dynamics is insignificant and may be ignored.

Medium Length Tether – The tether is long enough to consider gravity gradient and aerodynamic torques due to air density variations along the length of the tether to be significant. The latter assumption may be restricted to $L/h^* \ll 1$ when appropriate, but the term will be retained for generality in the derivation of the equations of motion. The characteristic (or scale) height of the atmosphere, h^*, is about 30 to 60 km for altitudes between 150 and 400 km [MSIS Standard Atmosphere]. See Figure 20 for MSIS standard atmosphere plots. The tether is considered short enough, however, the magnetic field is approximately constant along the tether length. Implicit in this assumption is the tether length is small compared to the distance to the center of the Earth, r, such that $r \gg L$.

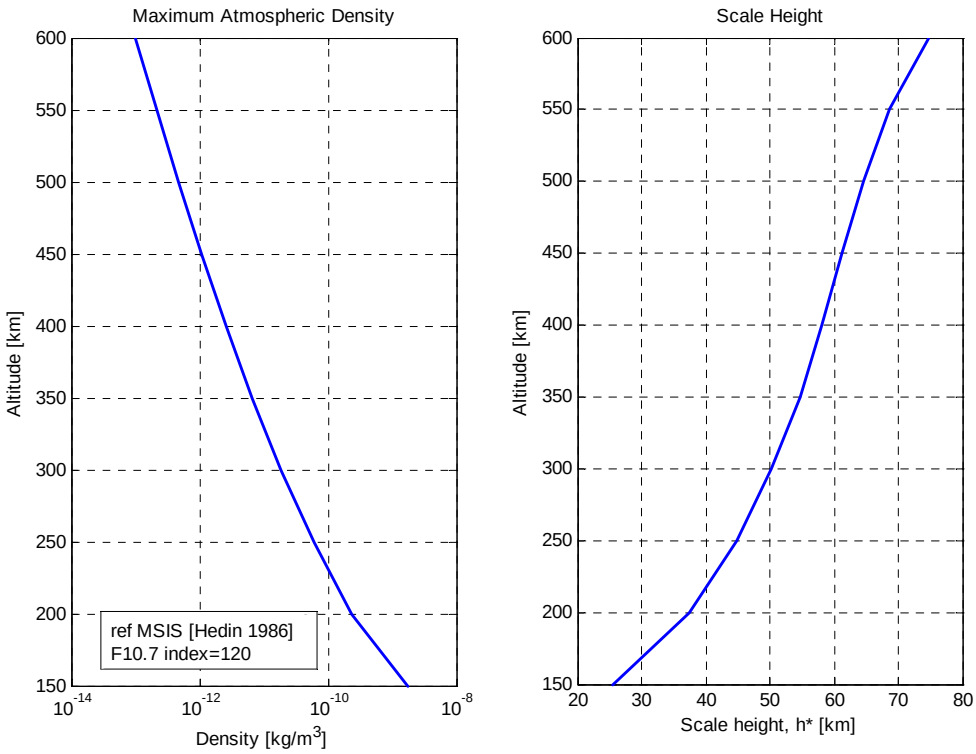

Figure 20. Standard MSIS Atmosphere

Spherical Earth with Non-tilted Magnetic Dipole – Although the magnetic dipole is actually tilted approximately 11.5 degrees from true north and rotates once per day, this effect is ignored without severe impact to the initial stability analysis and control design. Figure 21 depicts the coordinates used to describe the in-plane and out-of-plane librations respectively.

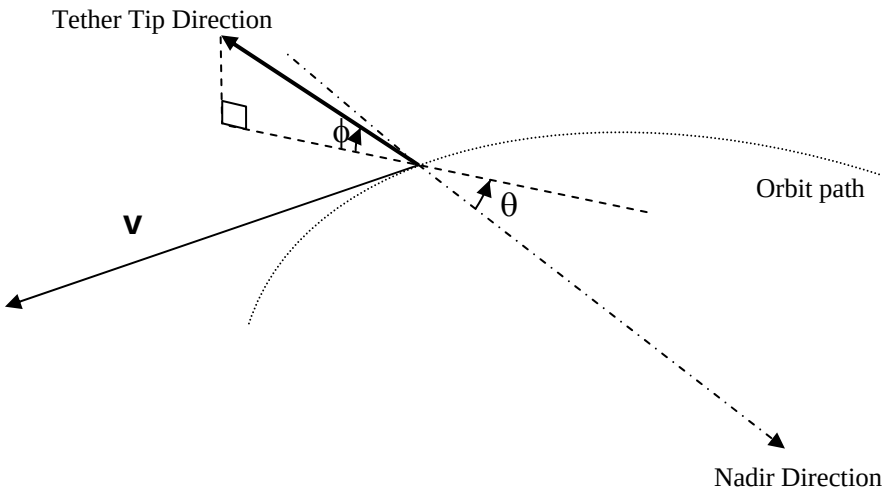

Figure 21. EDT Attitude Geometry defining the in-plane and out-of-plane libration angles θ and ϕ, respectively

It may be desirable to have the tether maintain certain attitudes (θ, ϕ) or operate within limits of acceptable attitudes. With the equations of motion we can proceed to determine the equilibrium points, their stability and the non-linear motion of the tether in the rotating frame of reference. The libration equations of motion were derived in Appendix A using Lagrange's method, shown here employing the rigid tether assumption.

$$\ddot{\theta} = -\ddot{\nu} + 2(\dot{\theta} + \dot{\nu})\dot{\phi}\tan\phi - 3\frac{\mu_g}{r^3}\sin\theta\cos\theta + \frac{Q_\theta}{\mu_e L^2\cos^2\phi} \tag{28}$$

$$\ddot{\phi} = -\{(\dot{\theta} + \dot{\nu})^2 + 3\frac{\mu_g}{r^3}\cos^2\theta\}\sin\phi\cos\phi + \frac{Q_\phi}{\mu_e L^2} \tag{29}$$

Variable ν is the true anomaly, L is the tether length and μ_e is the effective reduced mass (defined in Appendix B) that accounts for the end-masses and the tether mass. The scalars Q_θ and Q_ϕ are the generalized forces due to the combination of electromagnetic Lorenz and aerodynamic drag forces. These equations make no assumptions about the ellipticity of the orbit and may be related to the rate of change of the true anomaly by

$$\frac{\mu_g}{r^3} = \frac{\dot{\nu}^2}{1+e\cos\nu}$$

where e is the eccentricity of the orbit. We start by analyzing the unperturbed system and then later add some of the perturbing effects like atmospheric drag.

No Drag Model

Unperturbed tether system stability has been analyzed by others[9,10,52], but will be repeated here in a manner that serves the purposes of this research. Starting with the equations of motion we can readily observe the equilibrium points, θ_e and ϕ_e, where $\ddot{\theta} = \dot{\theta} = \ddot{\phi} = \dot{\phi} = \dot{L} = 0$.

$$c^2\phi\left(\ddot{\nu} + \frac{3\mu_g}{r^3}c\theta s\theta\right) = 0 \tag{30}$$

$$c\phi s\phi\left(\dot{\nu}^2 + \frac{3\mu_g}{r^3}c^2\theta\right) = 0 \tag{31}$$

Although the above equations allow for an equilibrium point at $\phi_e = \pm\frac{\pi}{2}$ when the tether is perpendicular to the orbital plane, we shall soon discover that the tether cannot maintain pure positive tension at this attitude thereby allowing the end bodies to orbit separately without constraint. In controlling space tethers, we will avoid this case since we desire to maintain tether tension to keep a valid dynamic model. Other equilibrium points are present when we consider a circular orbit. With a circular orbit, the true anomaly changes at a constant rate $\dot{\nu} = \omega_o = \sqrt{\frac{\mu_g}{r^3}}$ so $\ddot{\nu} = 0$. With this assumption, consider the in-plane libration case, $\phi_e = 0$ such that Eq. (30) reduces to $3\omega_o^2 c\theta s\theta = 0$ while the second is satisfied for all θ. The equilibrium points in this case occur when the tether is in a lead-trail co-orbital configuration, i.e. $\theta_e = \pm\frac{\pi}{2}$, or in a nadir/zenith-pointing configuration, i.e. $(\theta_e, \phi_e) = (0,0)$ or $(\pi, 0)$. It will be shown later that a tether can go slack in a lead-trail orientation, so we will instead avoid this configuration and only investigate the system stability of the nadir-pointing equilibrium point where positive tension can be maintained.

The unperturbed equations of motion for a tether in a circular orbit are first rearranged as explicit solutions for the libration accelerations.

$$\ddot{\theta} = 2\dot{\phi}t\phi\left(\dot{\theta}+\omega_o\right) - 3\omega_o^2 c\theta s\theta$$
$$\ddot{\phi} = -c\phi s\phi\left(\left(\dot{\theta}+\omega_o\right)^2 + 3\omega_o^2 c^2\theta\right)$$

Defining the state vector as $\mathbf{x} = \left[\theta, \phi, \dot{\theta}, \dot{\phi}\right]^T$ we can generate the state vector time derivative and its Jacobian.

$$\mathbf{f} = \dot{\mathbf{x}} = \begin{bmatrix} \dot{\theta} \\ \dot{\phi} \\ 2\dot{\phi}t\phi\left(\dot{\theta}+\omega_o\right) - 3\omega_o^2 c\theta s\theta \\ -c\phi s\phi\left(\left(\dot{\theta}+\omega_o\right)^2 + 3\omega_o^2 c^2\theta\right) \end{bmatrix} \tag{32}$$

$$\mathbf{A} = \frac{\partial \mathbf{f}}{\partial \mathbf{x}} = \begin{bmatrix} 0 & 0 & 1 & 0 \\ 0 & 0 & 0 & 1 \\ -3\omega_o^2(c^2\theta - s^2\theta) & 2\sec^2\phi\dot{\phi}(\dot{\theta}+\omega_o) & 2\dot{\phi}t\phi & 2t\phi(\dot{\theta}+\omega_o) \\ 6\omega_o^2 c\theta s\theta c\phi s\phi & -(c^2\phi - s^2\phi)\{(\dot{\theta}+\omega_o)^2 + 3\omega_o^2 c^2\theta\} & -2c\phi s\phi(\dot{\theta}+\omega_o) & 0 \end{bmatrix}$$

Linearizing $\mathbf{A}$ and evaluating it at equilibrium point $\left(\theta_e, \phi_e\right) = (0,0)$ yields

$$\mathbf{A}\big|_{\mathbf{x}_{eq}} = \begin{bmatrix} 0 & 0 & 1 & 0 \\ 0 & 0 & 0 & 1 \\ -3\omega_o^2 & 0 & 0 & 0 \\ 0 & -4\omega_o^2 & 0 & 0 \end{bmatrix} \tag{33}$$

Defining $a = -3\omega_o^2$ and $b = -4\omega_o^2$ the characteristic equation is

$$\left|\lambda I - A\right| = \begin{vmatrix} \lambda & 0 & 1 & 0 \\ 0 & \lambda & 0 & 1 \\ a & 0 & \lambda & 0 \\ 0 & b & 0 & \lambda \end{vmatrix} = \lambda^4 - \left(b + a\right)\lambda^2 + ab = 0 \tag{34}$$

$$\lambda_1^2 = b,\ \lambda_2^2 = a$$

The eigenvalues are therefore $\pm\sqrt{b}$ and $\pm\sqrt{a}$. Note that as long as $a < 0$ and $b < 0$ then the system will have marginal stability. When $a > 0$ or $b > 0$, then there will be a positive real eigenvalue which indicates an instability. In this case, the eigenvalues are $\pm\sqrt{3}\omega_o i$ and $\pm 2\omega_o i$, pure imaginary numbers. This means that in the vicinity of the nadir-pointing equilibrium position, the tether will have pendular motion with frequency $\sqrt{3}\omega_o$ in the orbital plane and $2\omega_o$ out of plane. Only circular orbits have been considered at this point. For non-circular orbits the true anomaly rate changes with respect to time, therefore the system would be non-autonomous. Floquet theory would be better suited to determine the stability of this system with a periodic solution. Palaez et. al offer a more thorough discussion of the stability in Refs 9 and 10 for a powered EDT not subject to drag.

Drag Model

For purposes of controlling tether libration in a circular orbit, the strategy requiring the least amount of energy would be one that controls about the equilibrium point. When atmospheric drag is considered, the equilibrium point may be slightly different than that of the tether in a pure vacuum. To determine this equilibrium point, we again write the equations of motion that include torque due to the drag.

$$\mu_e L^2 c^2\phi\left(\ddot{\theta} + 3\omega_o^2 c\theta s\theta - 2\dot{\phi}t\phi\left(\dot{\theta} + \omega_o\right)\right) = Q_{\theta a}$$
$$\mu_e L^2\left(\ddot{\phi} + c\phi s\phi\left(\left(\dot{\theta} + \omega_o\right)^2 + 3\omega_o^2 c^2\theta\right)\right) = Q_{\phi a}$$

The in- and out-of-plane torques for a tether are derived in Appendix A with the results shown here assuming a circular orbit.

$$Q_{\theta a} = \rho(h)v^2 c\phi c\theta\left\{\frac{\mu_m L}{2}\left(B_1^* e^{p_1} - B_2^* e^{-p_2}\right) - C\left(e^{-p_2}(-p_2 - 1) - e^{p_1}(p_1 - 1)\right)\right\} \quad (35)$$

$$Q_{\phi a} = \rho(h)v^2 s\phi s\theta\left\{\frac{\mu_m L}{2}\left(B_1^* e^{p_1} - B_2^* e^{-p_2}\right) - C\left(e^{-p_2}(-p_2 - 1) - e^{p_1}(p_1 - 1)\right)\right\} \quad (36)$$

where $C = d_t\left(1 - \cos^2\phi\sin^2(\theta+\gamma)\right)^{1/2}\left(\frac{h^*}{c\phi c\theta}\right)^2$ and the non-dimensional parameters p_1 and p_2 are given as $p_1 = \frac{\mu_m L c\phi c\theta}{h^* M_1}$ and $p_2 = \frac{\mu_m L c\phi c\theta}{h^* M_2}$. The other parameters in Eqs. (35) and (36) are the system velocity v, the atmospheric density $\rho(h)$ at altitude h, and B^* values representing the ballistic coefficients of the end-masses. The mass parameters M_1 and M_2 are defined as $M_1 = m_1 + \frac{m_t}{2}$ and $M_2 = m_2 + \frac{m_t}{2}$ where m_1 is the mass of end-body 1, m_2 is the mass of end-body 2, and m_t is the mass of the tether (see Appendix B for details).

To obtain equilibria of long tethers at various altitudes, no simplifying assumption on the size of L/h^* has been made yet. According to the equations of motion equilibrium is achieved when $\ddot{\phi} = \ddot{\theta} = 0$ which occurs when $\phi = 0$ and θ satisfies the following equation.

$$3\mu_e L^2\omega_o^2 s\theta_e = v^2\rho(h)\left\{\frac{\mu_m L}{2}\left(B_1^* e^{\frac{\mu_m Lc\theta_e}{M_1 h^*}} - B_2^* e^{\frac{-\mu_m Lc\theta_e}{M_2 h^*}}\right) - C\left(e^{\frac{-\mu_m Lc\theta_e}{M_2 h^*}}\left(\frac{-\mu_m Lc\theta_e}{M_2 h^*} - 1\right) - e^{\frac{\mu_m Lc\theta_e}{M_1 h^*}}\left(\frac{\mu_m Lc\theta_e}{M_1 h^*} - 1\right)\right)\right\} \quad (37)$$

Recall that $B_1^* = \frac{C_{d1}A_1}{M_1}$ and $B_2^* = \frac{C_{d1}A_2}{M_2}$ and when $\phi = 0$ in a circular orbit, then $C = d_t\frac{h^{*2}}{c\theta}$. This result is consistent with that of Beletsky and Levin [Ref 52, p 214 and 262].

This indicates that an equilibrium point resides in the plane of the circular orbit and is offset from nadir pointing by an angle θ_e that satisfies the transcendental Equation (37). Solutions to Eq. (37) are obtained numerically for given values of altitude, density and tether characteristics. Figure 22 and Figure

23 show the equilibrium points residing in the orbital plane for various tether characteristics and altitudes. These plots show three main trends. They are

- Increasing the altitude drives the equilibrium point to nadir. In the absence of drag, the equilibrium point is exactly zero.
- Increasing the disparity between the upper and lower endmasses drives the equilibrium point away from nadir. When one mass is more massive than the other, it is less susceptible to drag resulting in a more tipped orientation on average.
- Increasing the tether length beyond 3 or 4 km up to 10 km does not significantly affect the equilibrium point.

If we make the approximation that $\frac{L}{h^*} \ll 1$, then the equilibrium condition reduces to

$$3\mu_e L^2 \omega_o^2 s\theta_e = v^2 \rho(h)\left\{\frac{\mu_m L}{2}\left(B_1^* - B_2^*\right) - d_t \frac{\left(h^*\right)^2}{c\theta_e}\left(-\frac{c\theta_e L}{h^*}\right)\right\}$$

$$3\mu_e \omega_o^2 s\theta_e L = v^2 \rho(h)\left\{\frac{\mu_m}{2}\left(B_1^* - B_2^*\right) + d_t h^*\right\} \tag{38}$$

In this form, we may explicitly solve for θ_e. Caution must be exercised since $s\theta_e$ is bounded by $[-1,1]$ for real θ_e values, thus the quantity $\left(B_1^* - B_2^*\right)$ is also bounded to certain values for given tether dimensions and mass distribution. There is a nadir-pointing equilibrium condition where $(\theta_e, \phi_e) = (0,0)$ when the tether properties are such that $\left(B_1^* - B_2^*\right) \approx -2\frac{d_t h^*}{\mu_m}$.

Stability about the neighborhood of an arbitrary equilibrium point may be determined approximately using the same technique as was done in the case with no drag. When the in-plane angular acceleration due to aerodynamic drag torque (Eq. (62) in Appendix A) is included in the dynamics, the state vector's time derivative is given by

$$\mathbf{f} = \dot{\mathbf{x}} = \begin{bmatrix} \dot{\theta} \\ \dot{\phi} \\ 2\dot{\phi}t\phi\left(\dot{\theta}+\omega_o\right) - 3\omega_o^2 c\theta s\theta + \dfrac{v^2\rho(h)}{\mu_e L c^2\phi}\left\{\dfrac{\mu_m}{2}c\phi c\theta\left(B_1^* - B_2^*\right) + d_t h^*\left(1-c^2\phi s^2\theta\right)^{1/2}\right\} \\ -c\phi s\phi\left(\left(\dot{\theta}+\omega_o\right)^2 + 3\omega_o^2 c^2\theta\right) + \dfrac{v^2\rho(h)}{\mu_e L} s\phi s\theta\left\{\dfrac{\mu_m}{2}\left(B_2^* - B_1^*\right) - \dfrac{d_t h^*}{c\theta c\phi}\left(1-c^2\phi s^2\theta\right)^{1/2}\right\} \end{bmatrix}$$

In calculating the linearized **A** matrix about the in-plane equilibrium point $(\theta_e, 0)$ with $\dot{\theta}_e = \dot{\phi}_e = 0$, the only terms that will differ from those given in Eq. (33) are $A_{31} = \left.\dfrac{\partial f_3}{\partial\theta}\right|_{(\theta_e,0)}$ and $A_{42} = \left.\dfrac{\partial f_4}{\partial\phi}\right|_{(\theta_e,0)}$. Because of the structure of the linearized **A** matrix, the eigenvalues will have positive and negative real parts if these two elements of the matrix are positive and an instability would exist (see the characteristic Eq. (34)). If these elements remain negative, then there would be a pendular libration in the neighborhood of the equilibrium point, as we had with the no-drag case. The first element under investigation is given as

$$A_{31} = \left.\frac{\partial f_3}{\partial\theta}\right|_{(\theta_e,0)} = -3\omega_0^2(c^2\theta_e - s^2\theta_e) - \frac{v^2\rho(h)}{\mu_e L} s\theta_e\left\{\frac{\mu_m}{2}\left(B_1^* - B_2^*\right) + d_t h^*\right\}$$

We may substitute the equilibrium condition (38) into the second term on the right hand side of A_{31} to produce

$$A_{31} = -3\omega_0^2(c^2\theta_e - s^2\theta_e) - \frac{\left(3\mu_e\omega_0^2 s\theta_e L\right)s\theta_e}{\mu_e L} = -3\omega_0^2(c^2\theta_e - s^2\theta_e) - 3\omega_0^2 s^2\theta_e$$

$$A_{31} = -3\omega_0^2 c^2\theta_e$$

Likewise, the A_{42} term is calculated as

$$\frac{\partial f_4}{\partial\phi} = -4\omega_0^2 c^2\theta(c^2\phi - s^2\phi) + \frac{v^2\rho\left(h\right)c\phi s\theta}{\mu_e L}\left\{\frac{\mu_m}{2}\left(B_2^* - B_1^*\right) - \frac{d_t h^*}{c\theta c\phi}\left(1-c^2\phi s^2\theta\right)^{1/2}\right\}$$

$$A_{42} = \left.\frac{\partial f_4}{\partial\phi}\right|_{\left(\theta_e,0\right)} = -4\omega_0^2 c^2\theta_e - \frac{v^2\rho\left(h\right)s\theta_e}{\mu_e L}\left\{\frac{\mu_m}{2}\left(B_1^* - B_2^*\right) + d_t h^*\right\}$$

Once again, substituting the equilibrium condition (38) into the second term on the right side yields

$$A_{42} = -4\omega_0^2 c^2\theta_e - 3\omega_o^2 s^2\theta_e$$

$$A_{42} = -\omega_0^2\left(3 + c^2\theta_e\right)$$

Notice that both terms A_{31} and A_{42} remain negative, thus in the vicinity of the equilibrium point the tether librates with in-plane frequency $\sqrt{3}c\theta_e\omega_o$ and out-of-plane frequency $\sqrt{3+c^2\theta_e}\omega_o$. For the nadir-pointing case, we have the same solution as that of the no-drag case.

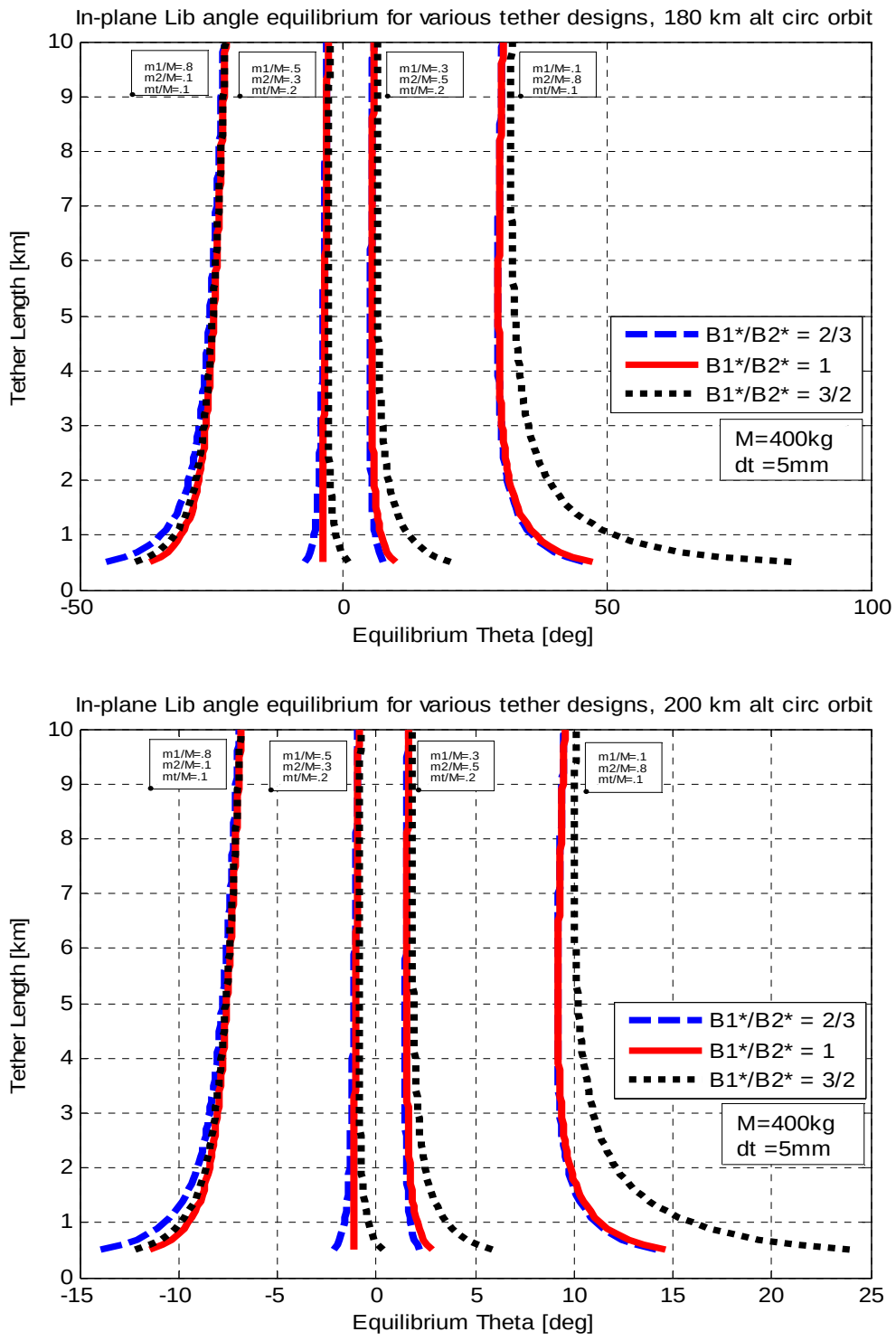

Figure 22. In-plane equilibrium points for 180 km and 200 km circular orbits

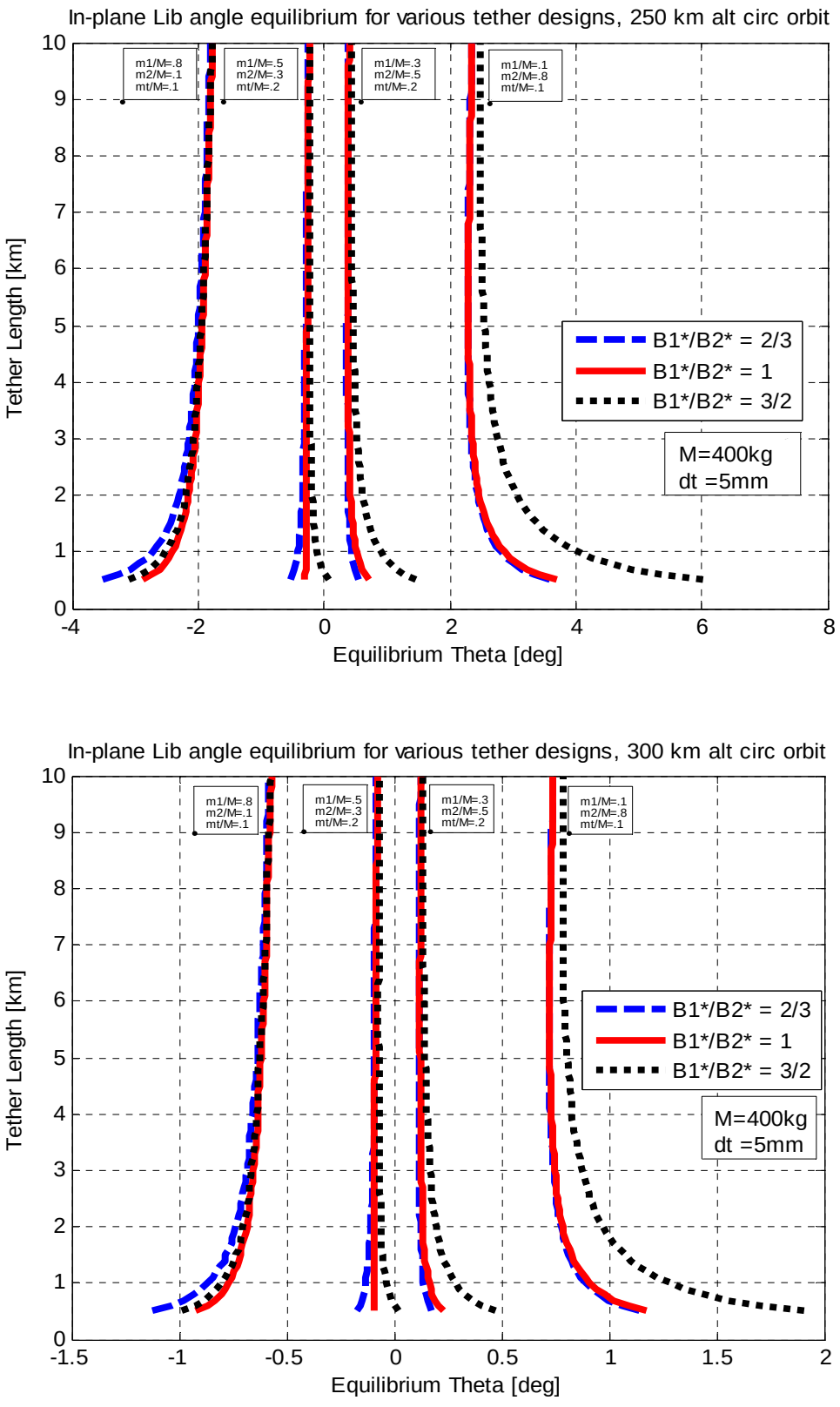

Figure 23. In-plane equilibrium points for 250 km and 300 km circular orbits

Tension

When determining the equilibrium point, we assumed that the tether was rigid, which is only a good approximation when the tether is in tension. In the case of a slack tether, we would have to unconstrain the equations of motion and retain the $\dot{L}$ term in the equations of motion. We can use the equations of motion to determine if the tether is in tension at the nadir pointing equilibrium point. The tension is depicted in Figure 24.

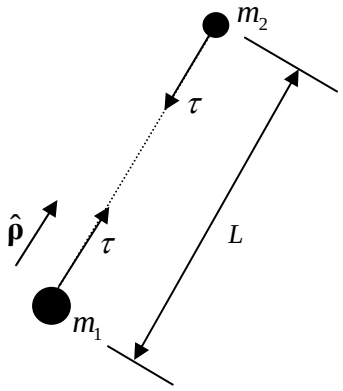

Figure 24. Tether Tension Diagram

The generalized force along the tether length is derived as follows.

$$Q_{Lt} = \boldsymbol{\tau} \cdot \frac{\partial \mathbf{v_1}}{\partial \dot{L}} - \boldsymbol{\tau} \cdot \frac{\partial \mathbf{v}_2}{\partial \dot{L}} \text{ where } \boldsymbol{\tau} = \tau \hat{\boldsymbol{\rho}}, \ \frac{\partial \mathbf{v_1}}{\partial \dot{L}} = \frac{-\mu_m}{M_1} \hat{\boldsymbol{\rho}}, \text{ and } \frac{\partial \mathbf{v}_2}{\partial \dot{L}} = \frac{\mu_m}{M_2} \hat{\boldsymbol{\rho}}$$

$$Q_{Lt} = -\left(\frac{\mu_m}{M_1} + \frac{\mu_m}{M_2} \right) \tau = -\tau$$

The force due to the atmospheric drag along the tether for $\phi = 0$ is

$$Q_{La} = \frac{\mu m}{2} \rho(h) v^2 s\theta \left(B_1^* e^{p_1} - B_2^* e^{-p_2} \right)$$

The electrodynamic force does not add any force along the tether since it acts perpendicular to the assumed straight tether. So from the equation of motion in L for a circular orbit (Eq. (59)), i.e. $\dot{\nu} = \sqrt{\frac{\mu_g}{r^3}} = \omega_o$, and a rigid rod $\left(\ddot{L} = \dot{L} = 0\right)$ in equilibrium we have

$$\mu_e L\left(\frac{\ddot{L}}{L} - \dot{\phi}^2 - c^2\phi\left(\dot{\theta}+\dot{\nu}\right)^2 - \frac{\mu_g}{r^3}\left(3c^2\phi c^2\theta - 1\right)\right) = -3\mu_e L\omega_o^2 c^2\theta = Q_{La} + Q_{Lt} \tag{39}$$

$$-3\mu_e L\omega_o^2 c^2\theta = \frac{\mu_m}{2}\rho(h)v^2 s\theta\left(B_1^* e^{p_1} - B_2^* e^{-p_2}\right) - \tau$$

$$\tau = 3\mu_e L\omega_o^2 c^2\theta + \frac{\mu_m}{2}\rho(h)v^2 s\theta\left(B_1^* e^{p_1} - B_2^* e^{-p_2}\right) \tag{40}$$

This result is consistent with Ref 45 p. 125. We defined τ to be in tension when it is positive as defined in Figure 24. The first term on the right hand side of Eq. (40) is always positive and dominates the second term near $\theta = 0, \pi$ except when the term in brackets is a very large value. This would occur in extreme cases where the design of the tether is such that the upper and lower masses have very different ballistic coefficients so that one end mass is subject to much more drag than the other. For example, if the in-plane libration angle θ is positive (i.e. the upper mass leads the lower one) and the upper mass undergoes so much drag that it falls behind faster than the gravity gradient can correct to the vertical position, then the tether could go slack. The graphs shown in Appendix E present numerical solutions for tension τ at different in-plane equilibrium points. The remaining graphs in Appendix E are θ_e solutions for the zero tension condition. Each of these angles will serve as an upper bound for in-plane libration so the tether does not go slack. For this design, the tether would need to be fairly close to 90 degrees (i.e. lead-trail configuration) for reasonable ballistic coefficients before losing tension. The tension in the nadir-pointing position is $\tau = 3\mu_e L\omega_o^2$. For a 2 km tether in a 250 km orbit, this force would be about 0.7 N.

The other singularity points mentioned were ruled out because the tether cannot maintain positive tension in those circumstances. For the singularity at $\phi = \pm\frac{\pi}{2}$ we have the equation of motion

$$\tau = -\frac{\mu_e \mu_g L}{r^3} + Q_{La} \text{ with } Q_{La} = 0 .$$

This indicates that the force along the tether wire would be in compression, which of course is physically impossible. For the circular orbit singularity at $\theta_e = \pm\frac{\pi}{2}$ (lead-trail orientation)

$$\tau = -\mu_e L \omega_c^2 s^2 \phi \pm \frac{\mu_m}{2} v^2 \rho(h) c\phi \left(B_1^* - B_2^* \right)$$

Tension in this case is only positive when $\phi_e = 0$ (or π), $\theta_e = +\pi/2 \left(\text{or } -\pi/2 \right)$ and $B_1^* > B_2^*$, i.e. the trailing end-mass in the lead-trail formation is subject to a greater drag force. Otherwise the tether goes slack. The stability of EDTs has been explored by other researchers who conclude that when driving a constant uncontrolled current through the tether wire, the system will eventually go unstable, tumbling end over end. Instead of reproducing the results here, we will explore an example of a controller that uses feedback linearization to drive down the libration. After gaining confidence that the system may be stabilized by employing active control, we will turn to posing and solving optimal control of a librating EDT.

Demonstration of Attitude Control Using Feedback Linearization

With the dynamic models presented in Chapters III and IV, we are positioned to explore electrodynamic tether libration control strategies. Before determining optimal control for a librating EDT, in this section we will first determine a feasible solution.

Libration control example using feedback linearization

There are two types of 2-ball tether system attitude control strategies, a hanging tether and a spinning tether. A hanging system will use active control to maintain pendular motion about equilibrium whereas a spinning system will allow the system to tumble end-over-end, thus avoiding the need for active attitude control. In this section we explore a possible attitude control strategy using torque resulting from the applied Lorenz force. Although not optimal, feedback linearization provides a quick way to see if

attitude control is achievable for a given system using nothing but the Lorenz force on the wire. We start with the dynamic equations of motion derived in Appendix A. They are repeated here for the state vector $\mathbf{x} = [\theta, \phi, \dot{\theta}, \dot{\phi}]^T$.

$$\mathbf{f} = \dot{\mathbf{x}} = \begin{bmatrix} \dot{\theta} \\ \dot{\phi} \\ 2\dot{\phi}t\phi\left(\dot{\theta} + \omega_o\right) - 3\omega_o^2 c\theta s\theta + \dfrac{Q_{\theta a} + Q_{\theta e}}{\mu_e L^2 c^2 \phi} \\ -c\phi s\phi\left(\left(\dot{\theta} + \omega_o\right)^2 + 3\omega_o^2 c^2\theta\right) + \dfrac{Q_{\phi a} + Q_{\phi e}}{\mu_e L^2} \end{bmatrix} = \begin{bmatrix} f_1 \\ f_2 \\ f_3 \\ f_4 \end{bmatrix}$$

We will take advantage of the assumption that the tether length is significantly shorter than the atmospheric scale height, $\frac{L}{h^*} << 1$ and write the generalized forces due to drag from Eq. (62) and Eq. (63) as the following.

$$Q_{\theta a} = v^2 \rho(h) L \left\{ \frac{\mu_m}{2} c\phi c\theta \left(B_1^* - B_2^*\right) + d_t h^* \left(1 - \mathrm{c}^2\,\phi\,\mathrm{s}^2\,\theta\right)^{1/2} \right\}$$

$$Q_{\phi a} = v^2 \rho(h) L s\phi s\theta \left\{ \frac{\mu_m}{2} \left(B_2^* - B_1^*\right) - d_t \left(1 - \mathrm{c}^2\,\phi\,\mathrm{s}^2\,\theta\right)^{1/2} \frac{h^*}{c\theta c\phi} \right\}$$

The generalized forces due to the Lorenz force acting perpendicular to the tether are given by Eq. (64) and Eq. (65) and repeated here.

$$Q_{\theta e} = \frac{IL^2\left(m_2 - m_1\right)}{2M}\left(c\phi c\theta s\phi B_r + s\phi c\phi s\theta B_t - c^2\phi B_n\right)$$

$$Q_{\phi e} = \frac{IL^2\left(m_2 - m_1\right)}{2M}\left(-s\theta B_r + c\theta B_t\right)$$

Suppose we wish to minimize the error 2-norm of the tether attitude with the equilibrium attitude, i.e. we desire to drive the states $\mathbf{y} = \mathbf{h}(\mathbf{x}) = [\theta, \phi]^T$ to some position close to the point $[\theta_e, \phi_e]^T$. Looking at the dynamics of the system, the control, $I = u(t)$, appears only in the second derivative of $\mathbf{y}$. Therefore, following the discussion in Ref 49 pp. 267-232, we may obtain the dynamic inversion by taking the second Lie derivative of $\mathbf{h}(\mathbf{x})$.

$$\mathbf{L_h f} = \frac{\partial \mathbf{h(x)}}{\partial \mathbf{x}} \mathbf{f} = \begin{bmatrix} 1000 \\ 0100 \end{bmatrix} \begin{bmatrix} \dot{\theta} \\ \dot{\phi} \\ f_3 \\ f_4 \end{bmatrix} = \begin{bmatrix} \dot{\theta} \\ \dot{\phi} \end{bmatrix}$$

$$\mathbf{L_h^2 f} = \frac{\partial \mathbf{h}\left(\mathbf{L_h f}\right)}{\partial \mathbf{x}} \mathbf{f} = \begin{bmatrix} 0010 \\ 0001 \end{bmatrix} \begin{bmatrix} f_1 \\ f_2 \\ f_3 \\ f_4 \end{bmatrix} = \begin{bmatrix} f_3 \\ f_4 \end{bmatrix}$$

Now to derive the controller, we write

$$\ddot{\mathbf{y}} = \begin{bmatrix} \ddot{\theta} \\ \ddot{\phi} \end{bmatrix} = \begin{bmatrix} \dot{x}_3 \\ \dot{x}_4 \end{bmatrix} = \frac{\partial^2 \mathbf{h}}{\partial \mathbf{x}^2} \mathbf{f} + \mathbf{G(x)} u$$

$$\ddot{\mathbf{y}} = \begin{bmatrix} 2\dot{\phi} t\phi \left(\dot{\theta} + \omega_o\right) - 3\omega_o^2 c\theta s\theta + \dfrac{Q_{\theta a}}{\mu_e L^2 c^2 \phi} \\ -c\phi s\phi \left(\left(\dot{\theta} + \omega_o\right)^2 + 3\omega_o^2 c^2 \theta\right) + \dfrac{Q_{\phi a}}{\mu_e L^2} \end{bmatrix} + \begin{bmatrix} \dfrac{Q_{\theta e}}{I \mu_e L^2 c^2 \phi} \\ \dfrac{Q_{\phi e}}{I \mu_e L^2} \end{bmatrix} u$$

Let the desired values of $\ddot{\theta}$ and $\ddot{\phi}$ be given by the vector $\mathbf{v}$. The controller will drive the states toward the desired values using a gain matrix $\mathbf{K}$.

$$\ddot{\mathbf{y}}_\mathbf{d} = \mathbf{v} = \begin{bmatrix} v_1 \\ v_2 \end{bmatrix} = \begin{bmatrix} -k_1 e_1 - k_2 \dot{e}_1 \\ -k_3 \dot{e}_2 - k_4 \dot{e}_2 \end{bmatrix} = \begin{bmatrix} -k_1 \left(y_1 - y_{d1}\right) - k_2 \left(\dot{y}_1 - \dot{y}_{d1}\right) \\ -k_3 \left(y_2 - y_{d2}\right) - k_4 \left(\dot{y}_2 - \dot{y}_{d2}\right) \end{bmatrix}$$

Where the error vector and gain matrix are respectively,

$$e = \begin{bmatrix} y_1 - y_{d1} \\ y_2 - y_{d2} \\ \dot{y}_1 - \dot{y}_{d1} \\ \dot{y}_2 - \dot{y}_{d2} \end{bmatrix} \text{ and } \mathbf{K} = \begin{bmatrix} k_1 & 0 & k_2 & 0 \\ 0 & k_3 & 0 & k_4 \end{bmatrix}$$

Setting the desired output equations containing the gain equal to the system dynamic equations, we can solve for $u(t)$.

$$\ddot{\mathbf{y}}_\mathbf{d} = \mathbf{v} = \frac{\partial^2 \mathbf{h}}{\partial \mathbf{x}^2} \mathbf{f} + u$$

$$u = \mathbf{G_s^{-1}(x)} \left[\mathbf{v} - \frac{\partial^2 \mathbf{h}}{\partial \mathbf{x}^2} \mathbf{f} \right] \tag{41}$$

The term $\mathbf{G}_s^{-1}(\mathbf{x})$ is the pseudo inverse of input vector/matrix $\mathbf{G}$ and is required for dynamic inversion since there are two controlled states, but only one input control.

Although the pseudo inverse cannot drive the tether attitude to the exact desired equilibrium point in general, it does minimize the error 2-norm. The proof is shown as follows.

Let $\mathbf{q} = \left[\mathbf{v} - \frac{\partial^2 \mathbf{h}}{\partial \mathbf{x}^2} \mathbf{f} \right]$. We can write the error norm as $e = \|\mathbf{G}u - \mathbf{q}\|^2$ and minimize this with respect to the control.

$$\begin{aligned} \frac{\partial e}{\partial u} &= \frac{\partial}{\partial u}\left(\left[\mathbf{G}u - \mathbf{q}\right]^T \left[\mathbf{G}u - \mathbf{q}\right] \right) = 0 \\ &= \left[\mathbf{G}u - \mathbf{q}\right]^T \mathbf{G} + \mathbf{G}^T \left[\mathbf{G}u - \mathbf{q}\right] = 0 \\ &= 2\mathbf{G}^T\mathbf{G}u - \mathbf{q}^T\mathbf{G} - \mathbf{G}^T\mathbf{q} = 0 \end{aligned}$$

Since $\mathbf{q}$ and $\mathbf{G}$ are both vectors,

$$\begin{aligned} & 2\mathbf{G}^T\mathbf{G}u - 2\mathbf{G}^T\mathbf{q} = 0 \\ \Rightarrow \quad & u = \left(\mathbf{G}^T\mathbf{G}\right)^{-1}\mathbf{G}^T\mathbf{q} = \frac{\mathbf{G}^T}{\|\mathbf{G}\|^2}\mathbf{q} = \mathbf{G}_s^{-1}\mathbf{q} \end{aligned}$$

The control law given by Eq. (41) was implemented using Simulink and the system was given a small perturbation from equilibrium. The output plots in Figure 25 show that the controller drives the in- and out-of-plane libration angles back toward the equilibrium point. Although the controller does not minimize energy or time, it does demonstrate that there is potential for controlling attitude, if required, using only the current in an electrodynamic tether. In reality, consideration must be given to the orbital change impacts of attitude controlling in this way. Other researchers have investigated tether length or tension control to dampen librations.[50] The next section will demonstrate how one may use optimal control methods over large time scales to maneuver the tether system to a new orbit while constraining the libration angles and rates to desired values.

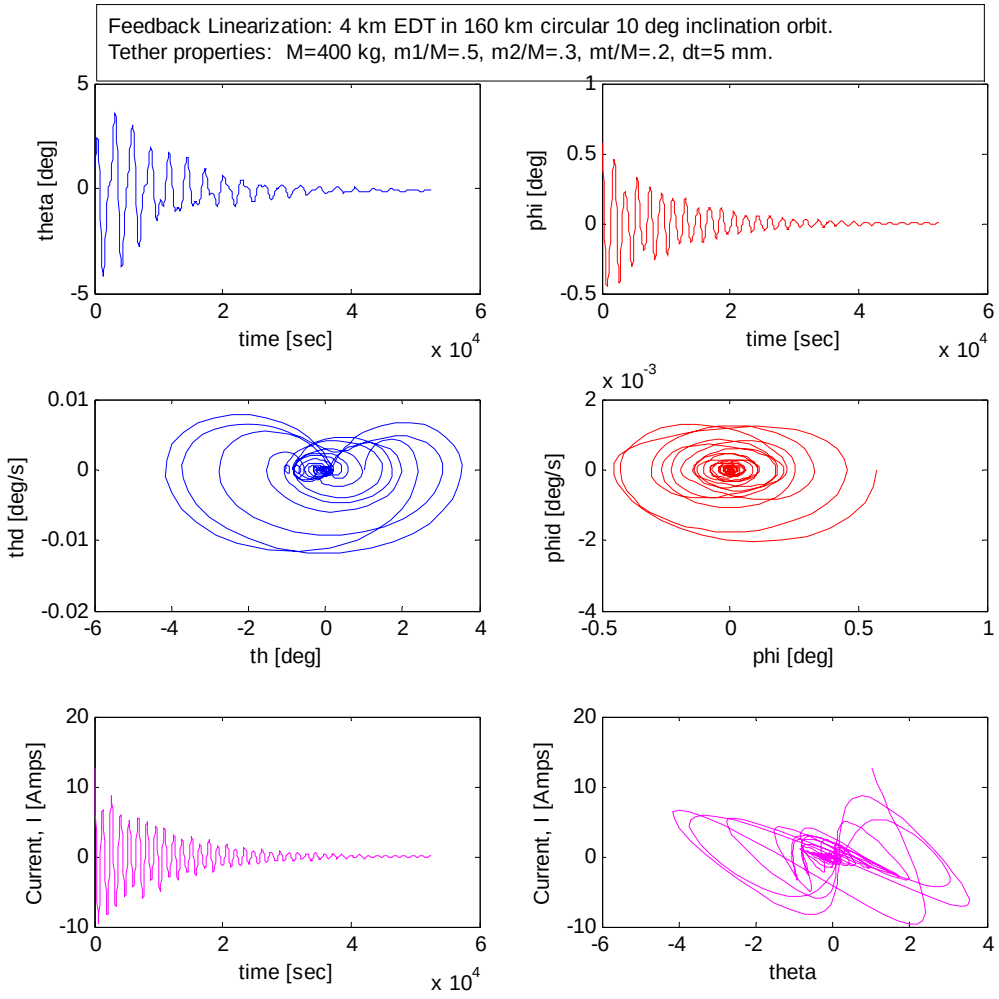

Figure 25. EDT Attitude Control Using Feedback Linearization

Libration Control over a Long Time Scale

When controlling an electrodynamic tether to reach a new orbit as discussed in the Chapter III, it was assumed that the tether was nadir-pointing and non-librating. This was done to introduce the method of averaging for solving the optimal control problem in Fourier space. In reality, however, we would need to account for the librations of the long tether. It has been shown that an unperturbed inert (unpowered) tether in a circular orbit librates in and out of plane about an equilibrium point without growth or decay. An uncontrolled EDT with a constant direct current running through it, however, will eventually go unstable as aptly pointed out by Pelaez, Lorenzini, Lopez-Rebollai, and Ruiz in Ref 10. The purpose of this section is to incorporate constraints on libration in the optimal control problem of Chapter III that will enable an optimal orbital change maneuver while simultaneously driving libration amplitude to a desired end state within specified bounds. Unfortunately, straightforward averaging of the derivative of the libration angle as we did with the orbital state derivative would yield zero. Control cannot be achieved for a state that is always zero, so a different approach is required to capture the librational motion in Fourier space to control the averaged state.

To simplify the problem, in-plane libration is ignored and attention is placed on controlling the out-of-plane libration. In-plane libration is not resonant with the periodic controller or the orbital motion (recall from the Equilibrium and Stability Section that $\omega_\theta = \sqrt{3}n$ where n is the mean motion of the satellite), thus it does not grow very quickly. For the design proposed here, months of constant thrusting are required to gain a few degrees of in-plane libration amplitude. Furthermore, the small in-plane librations may be managed by other mechanisms, such as controlling the drag on the upper and lower bodies thus imparting an aerodynamic torque out of phase with the pendular motion thus dampening this motion. With this justification in mind, we derive a new state that captures only the out-of-plane libration (hereafter simply called “libration” unless otherwise stated).

A constraint in Fourier space must not contain any functions of a fast time variable, i.e. trigonometric functions of ν. Averaging serves to eliminate dependence on this fast time variable leaving

only variables changing slowly with time. To accomplish this, a new state is devised; the mean square value of a tether's out-of-plane libration. Whether power is applied to the tether or not, the libration mean square is proportional to the maximum angle reached throughout the pendular cycle. For an unpowered (inert) librating EDT, the mean square value is exactly half of the square of the libration magnitude, i.e. $\phi_{rms}^2 = \frac{\phi_{\mathrm{m}}^2}{2}$. This relationship is approximate for a powered EDT as long as the perturbation due to the electromagnetic torque is relatively small. Deriving an expression that describes the librational mean square behavior provides a way to understand the behavior of the magnitude of the librational motion over a long time. Thus constraining the mean square trajectory for a given orbital maneuver is tantamount to bounding the envelope that contains the librational motion of the tether over long time durations.

Unfortunately, the librational equations of motion given in Eqs. (28) and (29) have no closed-form solution that will enable us to capture the libration amplitude changes over long time scales. The good news, however, is that assuming small libration angles we may linearize the equations of motion, thus decoupling the in- and out-of-plane libration equations of motion and, as previously mentioned, ignore the in-plane libration. Introducing the mean anomaly ν as the independent time variable we write

$$\begin{aligned} \ddot{\phi} + 4\phi &= \frac{Q_{\phi e}}{\mu_e L^2} = \frac{\left(m_2 - m_1\right)\gamma_m}{2M\mu_e\mu_g} I_m \sin i \left(\tilde{k}(T)\cos\nu - \tilde{h}(T)\sin\nu\right) \boldsymbol{\Psi}^T(\nu)\,\mathbf{u}(T) \\ &= \varepsilon \sin i \left(\tilde{k}\cos\nu - \tilde{h}\sin\nu\right)\left(u_1 + u_2\cos\nu + u_3\sin\nu + u_4\cos 2\nu + u_5\sin 2\nu\right) \end{aligned} \tag{42}$$

where dots indicate differentiation with respect to ν, i.e. $(\dot{}) = \frac{d(\,)}{d\nu}$. This equation is expressed using a partial equinoctial element set described in Chapter III where $\tilde{k} = \frac{k}{e}$ and $\tilde{h} = \frac{h}{e}$. Both $\tilde{k}$ and $\tilde{h}$ are order one quantities that are themselves averages that vary slowly with time. Adopting the convention used in Refs 9 and 10, the non-dimensional small parameter ε is defined as the ratio of the maximum electrodynamic torque to the gravity gradient torque and corresponds to the powered part of the expansion.

$$\varepsilon = \frac{\text{Max Electrodynamic Torque}}{\text{Gravity Gradient Torque}} = \frac{\left(m_2 - m_1\right)\gamma_m}{2M\mu_e\mu_g} I_m \tag{43}$$

For a 1.5 Amp, 500 kg tether system in low Earth orbit with an upper end mass of 230 kg and a lower end mass of 220 kg, this parameter is about 0.0026. The current control introduced in Chapter III as $I(\mathbf{u}(T),\nu)$, has a slowly varying part, $\mathbf{u}(T)=[u_1,u_2,u_3,u_4,u_5]^T$ and a periodic part that forms the basis in Fourier space $\boldsymbol{\Psi}(\nu)=[1,\cos\nu,\sin\nu,\cos 2\nu,\sin 2\nu]^T$. The normalized control current is therefore given by $I=I_m\boldsymbol{\Psi}^T(\nu)\mathbf{u}(T)$ where $\boldsymbol{\Psi}^T(\nu)\mathbf{u}(T)$ is an order one quantity. Recall that the slow time scale variable T is a scaled version the clock time t and the true anomaly. It is now necessary to formalize the relationship between the two time scales using a scaling parameter ε such that

$$T=\varepsilon t=\varepsilon\frac{\nu}{n} \tag{44}$$

The non-dimensional scale factor used here is the torque ratio defined in Eq. (43) (see Appendix F for details on scaling). Only small changes to the known periodic libration motion of the inert tether over short time spans will occur as long as the electrodynamic torque is small compared to the gravity gradient, i.e. $\varepsilon\ll 1$. In transforming the controls from the short time scale domain to Fourier space, we exchange a single control variable (current as a function of a fast time variable) for five control variables (the five Fourier coefficients in this case that are functions of slow time variables). Expanding the right-hand side term in the differential equation in Eq. (42) and through liberal use of trigonometric identities, we determine an exact solution to the linearized equation applying the method of undetermined coefficients.

$$\phi(\nu,T)=\phi_o(\nu,T)+\varepsilon\phi_1(\nu,\mathbf{u}(T))=\phi_m\cos 2(\nu-\nu_o)+\varepsilon\sin i\left(\tilde{k}K-\tilde{h}H\right) \tag{45}$$

where

$$K(\nu,\mathbf{u}(T))=\frac{u_2}{8}+\frac{1}{3}\left(u_1+\frac{u_4}{2}\right)\cos\nu+\frac{u_5}{6}\sin\nu-\frac{u_3}{8}\nu\cos 2\nu+\frac{u_2}{8}\nu\sin 2\nu-\frac{u_4}{10}\cos 3\nu-\frac{u_5}{10}\sin 3\nu$$

$$H(\nu,\mathbf{u}(T))=\frac{u_3}{8}+\frac{u_5}{6}\cos\nu-\frac{1}{3}\left(\frac{u_4}{2}-u_1\right)\sin\nu-\frac{u_2}{8}\nu\cos 2\nu+\frac{u_3}{8}\nu\sin 2\nu+\frac{u_5}{10}\cos 3\nu-\frac{u_4}{10}\sin 3\nu$$

One restriction due to the linearization is that the second term on the right hand side of Eq. (45) must be less than order one, i.e. $\varepsilon\nu\ll 1$. Therefore, to ensure accuracy of the solution, the duration is limited to $\nu\ll\frac{1}{\varepsilon}$ (note the explicit ν terms present in K and H). For a scaled maximum electrodynamic

torque of $\varepsilon = 0.0026$, this maximum allowable duration corresponds to about 60 orbital revolutions. Eventually a long duration optimal control problem will be discretized into smaller intervals that are much shorter than this limit so that the approximate solution is valid for each subinterval. Linking the subintervals together, the long term maneuver consists of the slowly varying "constant" states and Fourier coefficient controls within each subinterval. The first term on the right side of Eq. (45) represents the homogeneous solution indicating that a tether without any electrodynamic torque would continually librate at twice the orbital frequency. Perturbations come through the small electrodynamic torque of order ε imparted on the tether over a long time. Whether these perturbations destabilize or stabilize the libration depends on the slowly changing control terms contained in K and H. A thorough derivation of periodic libration angle solutions is provided in Ref 10 for an EDT with a steady dc current.

For an unpowered tether, or one where the center of mass is collocated with the center of force on the tether (thus no Lorenz torque), $\varepsilon \mathbf{u}(T) = \mathbf{0}$, or an equatorial orbit where $i = 0$, the solution to Eq. (45) is the homogeneous solution.

$$\phi_o(\nu, T) = \phi_m(T)\cos\left(2(\nu - \nu_0)\right)$$

where $\phi_m(T)$ is the initial amplitude of the librational motion which is approximately constant over a period, but changes slowly over time. Presuming that the periodic control may be started at any time during the libration cycle, for purposes here we assume the peak of a libration cycle corresponds with $\nu_0 = 0$ and write

$$\phi_o(\nu, T) = \phi_m(T)\cos 2\nu \tag{46}$$

Using this model, the only way to control the libration is through the $O(\varepsilon)$ term in Eq. (45).

We can now define the libration mean squared state as

$$z(\nu, T) = \frac{1}{2\pi}\int_{\nu}^{\nu+2\pi} \phi^2(\xi, T)\, d\xi = \phi_{rms}^2 \tag{47}$$

This state is always positive and is itself an average over a period by definition. Furthermore, for short time intervals such as a few periods when the libration amplitude change is negligible, the relationship between the state z and the amplitude may be expressed as

$$2z = 2\phi_{rms}^2 \approx \phi_m^2$$

Substituting Eq. (45) into Eq. (47) we write

$$\begin{aligned} z(\nu,T) &= \frac{1}{2\pi}\int_{\nu}^{\nu+2\pi} \phi^2(\xi,T)\,d\xi = \frac{1}{2\pi}\int_{\nu}^{\nu+2\pi} \left[\phi_o(\xi,T) + \varepsilon\phi_1(\xi,\mathbf{u}(T))\right]^2 d\xi \\ &= \frac{1}{2\pi}\int_{\nu}^{\nu+2\pi} \phi_o^2 + 2\varepsilon\phi_o\phi_1 + \varepsilon^2\phi_1^2 \; d\xi \end{aligned} \tag{48}$$

Because $\phi_o(\nu,T)$ and $\phi_1(\nu,\mathbf{u}(T))$ are both considered 2π periodic in ν over the small interval, the whole integrand in Eq. (48) is assumed 2π periodic. This assumption is valid since $\mathbf{u}(T)$ and $\phi_m(T)$ do not change significantly over the short 2π interval, therefore the limits of the definite integral may be considered from 0 to 2π without loss of generality. Thus, the secular change in z due to the Lorenz torque over one period is

$$\begin{aligned} z(T) &= \frac{1}{2\pi}\int_0^{2\pi} \phi_o^2 + 2\varepsilon\phi_o\phi_1 + \varepsilon^2\phi_1^2 d\nu \\ &= \frac{1}{2\pi}\int_0^{2\pi} \phi_o^2 + 2\varepsilon\phi_m\cos 2\nu \sin i\left(\tilde{k}K - \tilde{h}H\right) + \varepsilon^2 \sin^2 i\left(\tilde{k}K - \tilde{h}H\right)^2 d\nu \end{aligned} \tag{49}$$

Since the next step in the derivation will be to integrate, terms that will average to zero after integration may be omitted which yields

$$\begin{aligned} z(T) = \frac{1}{2\pi}\int_0^{2\pi} \phi_o^2 d\nu + \frac{\phi_m \sin i}{4}\frac{1}{2\pi}\int_0^{2\pi} \varepsilon\nu\cos 2\nu\left(\left(\tilde{h}u_2 - \tilde{k}u_3\right)\cos 2\nu + \left(\tilde{k}u_2 - \tilde{h}u_3\right)\sin 2\nu\right)d\nu \\ + \frac{\sin^2 i}{64}\frac{1}{2\pi}\int_0^{2\pi} \varepsilon^2\nu^2\left[\tilde{k}\left(u_3\cos 2\nu + u_2\sin 2\nu\right) + \tilde{h}\left(u_2\cos 2\nu - u_3\sin 2\nu\right)\right]^2 d\nu + O\left(\varepsilon^2\nu\right) \end{aligned} \tag{50}$$

The first integral term in Eq. (50) is the inert tether libration mean square value. Secular changes enter the system through the remaining terms with explicit dependence on ν. Over a single period the change in z is very small due to the scaling factor ε. Recalling Eq. (44), we substitute the slow time variable for $\varepsilon\nu$, consider it constant over the limits of the definite integral, and remove it from the integrand. This slow time variable affects the secular growth (or decay) of the z state only over large spans of time, so only the sinusoidal functions of ν are averaged through integration. Physically, the mean squared value of libration changes approximately linearly with T to first order over short time intervals. The plot in Figure

26 depicts the small, nearly linear change in the z state over one period. Substituting the slow time variable into Eq. (50) and expanding yields

$$z(T) = \frac{1}{2\pi}\int_0^{2\pi} \phi_o^2 d\nu + \frac{nT}{4}\phi_m \sin i \frac{1}{2\pi}\int_0^{2\pi}\left(\left(\tilde{h}u_2 - \tilde{k}u_3\right)\cos^2 2\nu + \left(\tilde{k}u_2 - \tilde{h}u_3\right)\frac{1}{2}\sin 4\nu\right)d\nu$$
$$+ \frac{n^2T^2\sin^2 i}{64}\frac{1}{2\pi}\int_0^{2\pi}\left[\tilde{k}^2\left(u_3^2\cos^2 2\nu + u_2^2\sin^2 2\nu\right) + \tilde{h}^2\left(u_2^2\cos^2 2\nu + u_3^2\sin^2 2\nu\right) - 2\tilde{h}\tilde{k}u_2u_3\right]d\nu + O(\varepsilon T)$$

Finally, we perform the integration with respect to true anomaly and take the derivative with respect to clock time for the desired secular change in z over a long time scale. Assuming that the averaged states x and control coefficients u in the previous equation vary slowly, the derivatives with respect to clock time will be small, i.e. $dx/dt = O(x\varepsilon)$ and $du/dt = O(u\varepsilon)$. The z state derivative is therefore

$$\frac{dz}{dt} = \varepsilon\frac{dz}{dT} = \varepsilon\frac{\sqrt{2z}n\sin i}{8}\left(\tilde{h}u_2 - \tilde{k}u_3\right) + \varepsilon^2\frac{n^2\sin^2 i}{64}\left(\left(u_2^2 + u_3^2\right) - 4\tilde{h}\tilde{k}u_2u_3\right)t + O\left(\phi_m\varepsilon^2 t\right) \qquad (51)$$

where $T = \varepsilon t$. Although the second term on the right hand side of the derivative in Eq. (51) causes quadratic growth (or decay) of the z state, it is of order ε^2 and may only be significant when considering larger time spans. This derivative will serve as a dynamic constraint in subsequent optimal control problems to manage the magnitude of libration while performing orbital maneuvers. Notice that using this model, the change in the libration mean square state is achieved primarily through the u_2 and u_3 coefficients corresponding to periodic control resonant with the orbital frequency. This is because in the satellite frame the local magnetic field vector varies with the orbital frequency, therefore resonating control current with this frequency can dampen (or excite) libration.

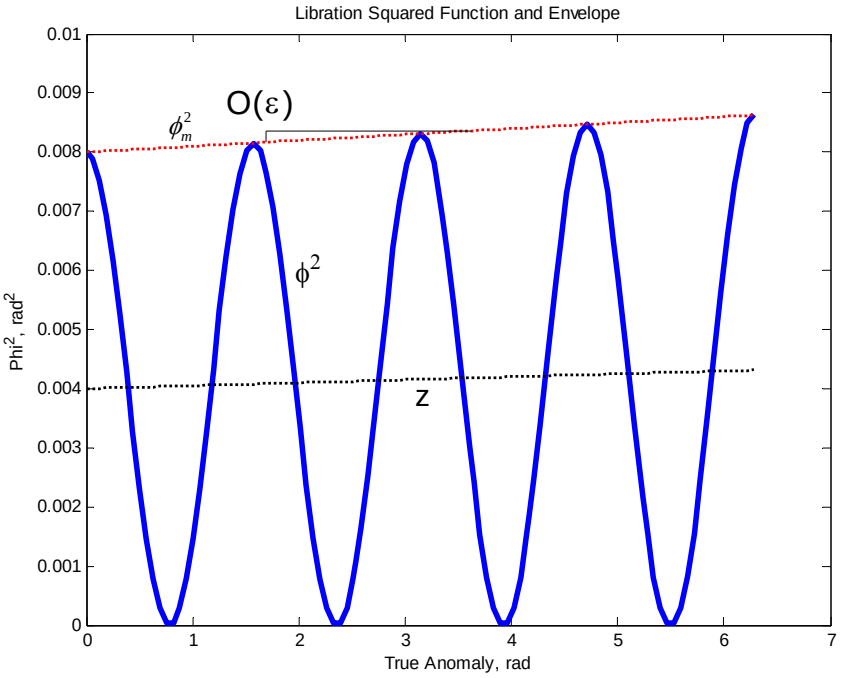

Figure 26. Libration Squared Function and Envelope

Optimal Maneuvering with Libration Control

With the dynamics of the mean square libration in hand, it is possible to optimally maneuver an EDT satellite to a new desired orbit while controlling the out-of-plane libration (within the limits of the dynamic model). The assumptions made for this section are that the in-plane libration is controlled using a separate mechanism (e.g. drag torque control) and that the out-of-plane librations are much larger than the in-plane librations, i.e. $\theta \ll \phi$. Furthermore, the eccentricity and the maximum possible electrodynamic torque for a given tether design are both small, i.e. $e \ll 1,\ \varepsilon \ll 1$. This method would work with eccentric orbits as well, but in deriving the asymptotic expansion for the libration angle, one would need to expand about the difference from the reference eccentricity. Because an EDT must orbit low enough to take advantage of the Earth's magnetic field, the orbit is nearly circular by necessity, so the problem posed here is for a nearly circular orbit. The optimal control problem is constructed in a manner similar to the ones

posed in Chapter III, but with the additional constraints on the mean square libration state, z, and may be written as the following.

Minimize Cost: $J = t_f$

Subject to:

$$\begin{aligned} &d\mathbf{x}/dt = \mathbf{f}(\mathbf{x},\mathbf{u}) \\ &\mathbf{e_0}\left(\mathbf{x}(T_0)\right) = \left[a_0, e_0, i_0, z_0\right]^T = [6648 \text{ km}, 0.005, 30^\circ, 0.0038]^T \\ &\mathbf{e_f}\left(\mathbf{x}(T_f)\right) = \left[a_f, i_f, z_f\right]^T = [6658 \text{ km}, 30.5^\circ, 0.0014]^T \\ &g_1\left(\mathbf{u}(T)\right) = I_{rms}^2 - 2.25 \le 0 \text{ Amps}^2 \end{aligned} \tag{52}$$

where $\mathbf{x}(T) = \left[a, h, k, i, z\right]^T$ represents the average states with averaged dynamics $\mathbf{f}\left(\mathbf{x}(T), \mathbf{u}(T)\right) \approx \Delta\mathbf{x}/\Delta T$ that are described by Eq. (51) and Eq. (11). Box constraints in Eq. (17) are still enforced as well and the rms current is defined by Eq. (14). The 500 kg, 4 km tether in this case is modeled using a 230 kg upper end body, and a 220 kg lower end body with the same current properties as the tether modeled in the Chapter III examples. Solving this problem using DIDO for the no drag case yields an optimal control solution (Figure 27) that drives the libration magnitude to the final desired value while executing the desired orbital maneuver (Figure 28). Similar to the minimum time solution obtained in Chapter III, much of the thrust is used to achieve the inclination change through the u_4 and u_5 control coefficients corresponding with the frequency components twice that of the orbital frequency. In this case, however, there is a small component of the periodic current allotted to u_2 and u_3 to drive the libration amplitude to the desired final state. The libration angle, ϕ, depicted in Figure 28 was propagated using the exact equations of motion given by Eq. (29) with a stiff ode solver (Matlab's ode23t) to verify the accuracy of the dynamic model and the assumptions. Control current is constantly phased with the librational motion to account for a small frequency shift due to numerical errors in the ode propagation, i.e.

$$\nu_c = \nu(1+\zeta)$$

where ν_c is the true anomaly argument used in the clock time domain controller given in Eq. (1) and ζ is a small parameter determined by observing the errors incurred during propagation of the homogenous solution to Eq. (46) (see Appendix H). The DIDO solution shows the z state history transformed into a

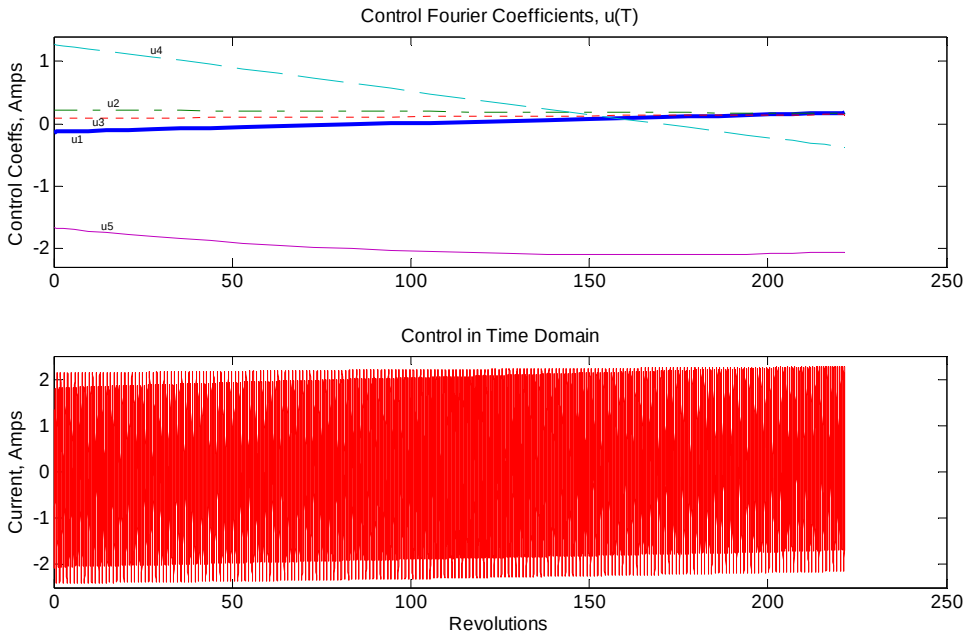

Figure 27. Control for Minimum Time Orbit Change with Libration Control, No Drag

libration angle history which forms an envelope for the rapidly varying libration angle. The propagated orbital trajectory and maximum libration angle envelope matches well with the propagated values indicating that the proposed model is sufficient for this problem.

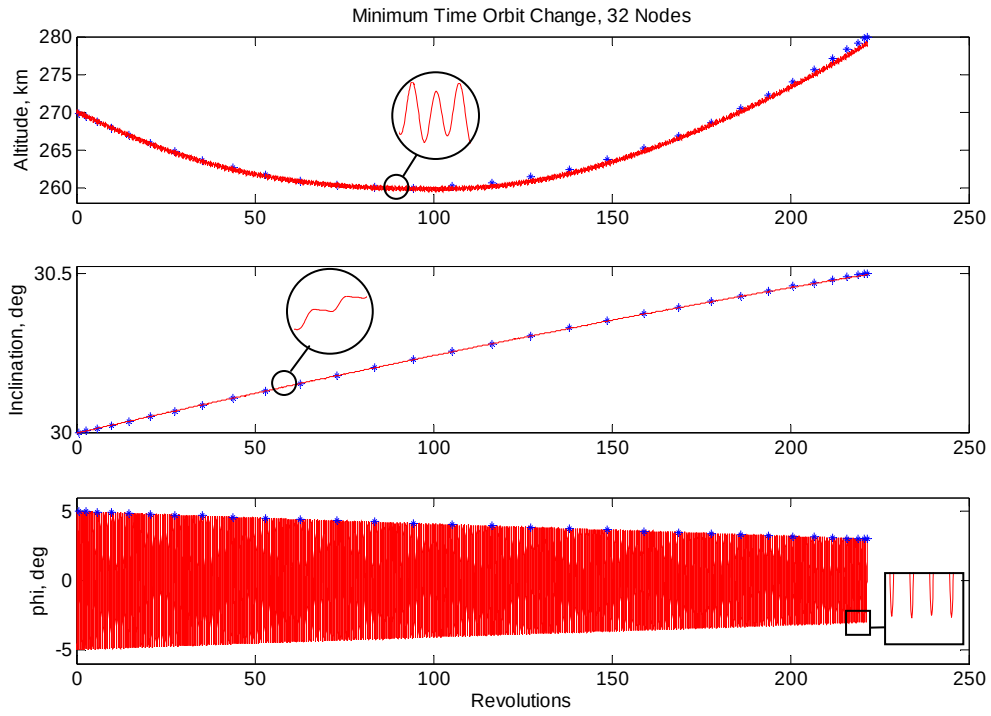

Figure 28. Minimum Time Orbit Change State Trajectory, No Drag. Stars indicate DIDO derived libration envelope; lines indicate propagated instantaneous state.

For comparison, a similar constant eccentricity optimal maneuver was executed without any restriction on the libration mean square state. The constraints in Eq. (52) were enforced with the following exception and addition.

$$\mathbf{e_f}\left(\mathbf{x}\left(T_f\right)\right) = \left[a_f, i_f\right]^T = [6658\text{ km}, 30.5^\circ]^T$$
$$g_2\left(\mathbf{u}\left(T\right)\right) = h^2 + k^2 - e_0^2 = 0$$

The additional path constraint is written to enforce a constant eccentricity maneuver. The resulting control profile (Figure 29) and trajectory (Figure 30) demonstrate that the maneuver is only marginally quicker (by a single revolution) but the libration amplitude, left uncontrolled, remains practically unchanged for this time span. Given enough time, however, this amplitude can grow in a thrusting tether, so it is important to manage the libration while maneuvering an EDT. This is especially true for a tether that is long, carries a

large control current, or has a large mass differential between the upper and lower masses resulting in a large electrodynamic torque when the EDT is active.

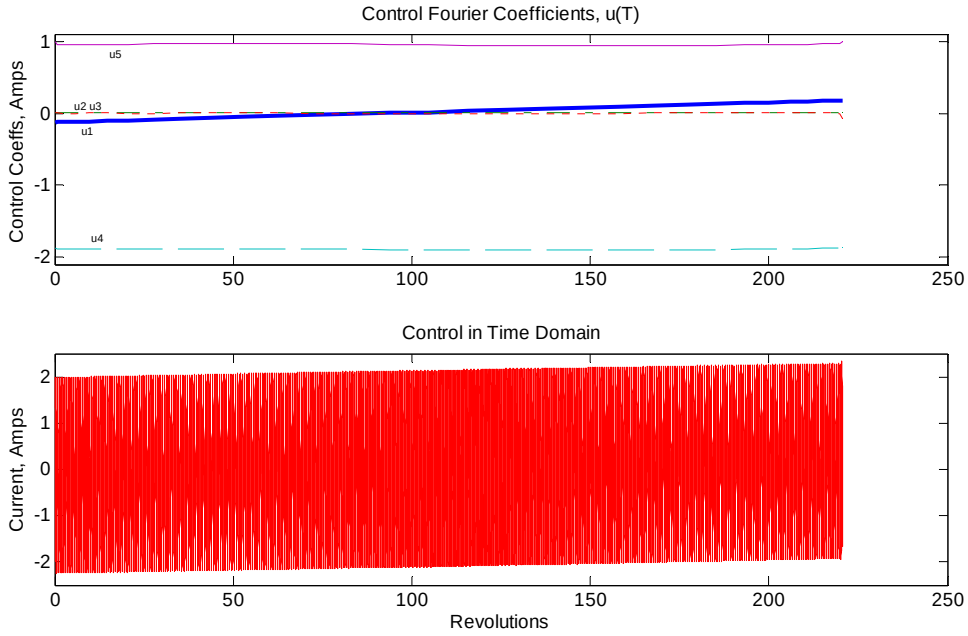

Figure 29. Control Profile for a Minimum Time Orbit Change with No Libration Control, No Drag

Including a state in the dynamics that captures the magnitude of the out-of-plane tether libration provides a higher fidelity constraint model that enables more accurate optimal control of an EDT. Since the long time scale equations of motion for orbit transfers assume a near nadir-pointing tether, bounding the libration is even more critical. The results of this section demonstrate that it is possible to control tether libration while simultaneously maneuvering to a new orbit using periodic control of the EDT current over a long time scale.

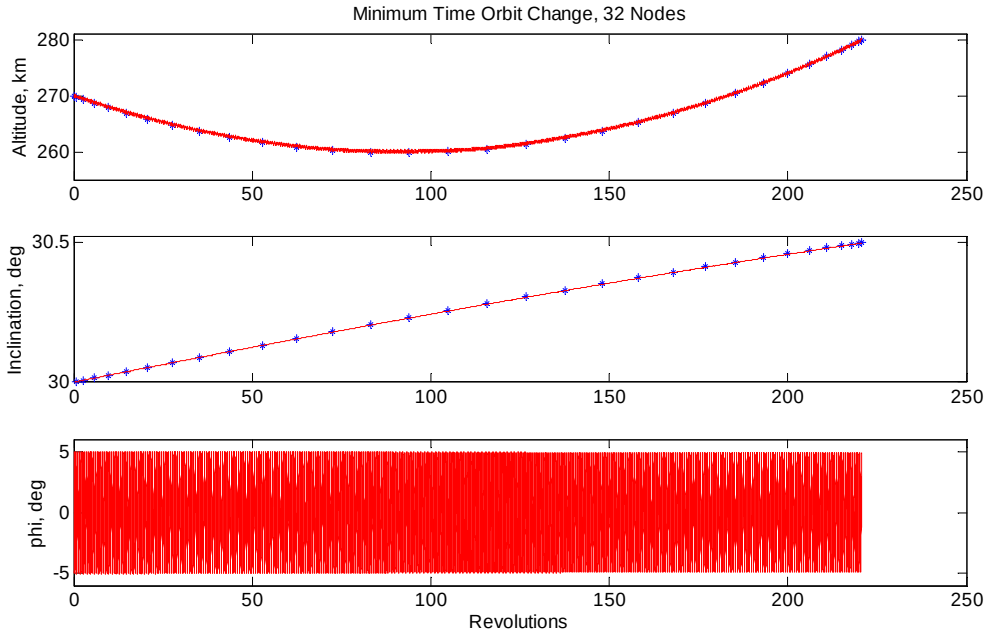

Figure 30. Minimum Time Orbit Change State Trajectory without Libration Control

When drag is included in the dynamic model (i.e. $D \neq 0$ in Eq.(11)), the controls initially boost the satellite to take advantage of the lower atmospheric density at higher altitudes allowing more power to be dedicated to cranking the inclination in the same manner as the example in Chapter III. The controls are shown in Figure 31 with the resulting trajectory in Figure 32. With drag, this maneuver takes three more days to complete than its no-drag counterpart, requiring a total of 270 revolutions.

Although we do not demonstrate definitive optimality of the control solution, compliance with one transversality condition necessary for optimality is shown. Because there is no explicit time dependence in the Lagrangian of the Hamiltonian of this optimal control problem we have $\dot{\bar{H}} = 0$. The Lagrangian of the Hamiltonian was defined in Chapter III as

$$\bar{H} = H + \mu_g g_1 + \boldsymbol{\mu}_x^T \mathbf{x} + \boldsymbol{\mu}_u^T \mathbf{u}$$

where the Hamiltonian is defined by $H = \boldsymbol{\lambda}^T \mathbf{f}$ given the Mayer cost chosen in this example and $\boldsymbol{\lambda}$ represents the costates. Recall that the covector functions associated with the path constraint, state-variable

box constraints and control-variable constraints are represented by μ_g , $\boldsymbol{\mu}_x$ and $\boldsymbol{\mu}_u$ respectively.

Furthermore, since the problem posed here is a minimum final time problem we have $\bar{H}\left(t_f\right) = -1$, so we have a condition that holds throughout the trajectory, namely

$$\bar{H}\left(t\right) = -1 \tag{53}$$

DIDO uses the Covector Mapping Principle to produce adjoints and the Hamiltonian as part of the solution. To check this optimality condition we plotted the output Hamiltonian and discovered that it indeed satisfied Eq. (53) throughout the maneuver within a tolerance of 0.002.

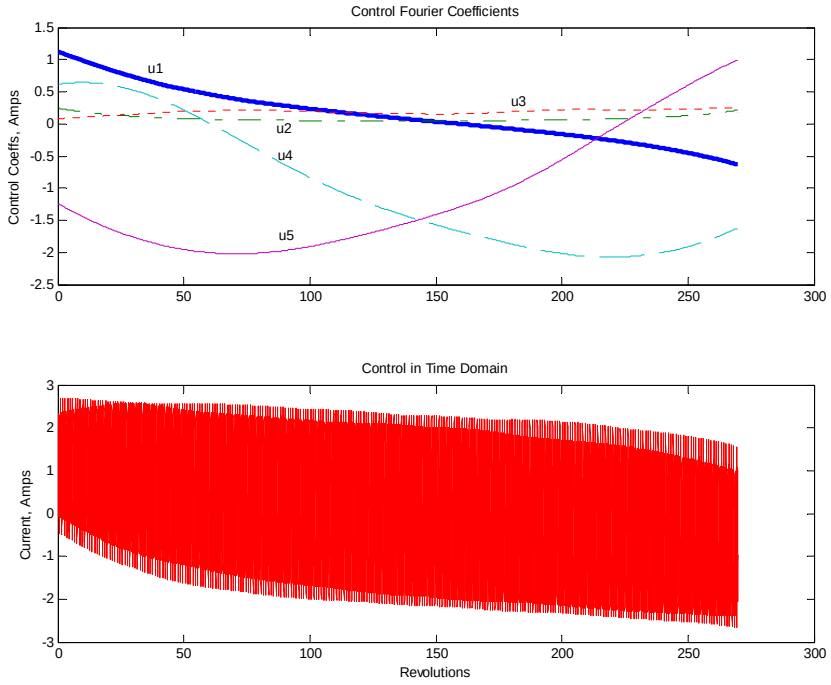

Figure 31. Control Profile for a Minimum Time Orbit Change with Libration Control and Drag

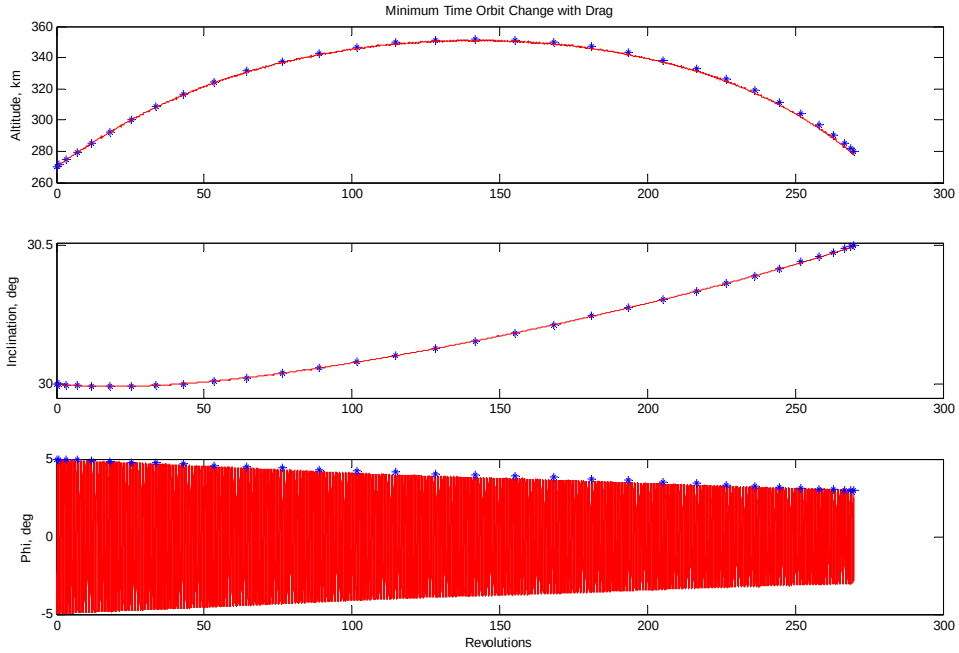

Figure 32. Minimum Time Orbit Change State Trajectory with Drag

VI. Summary, Conclusions and Future Work

This research demonstrates how using the method of averaging and multiple time scales can be used to achieve optimal controls for systems exhibiting periodic behavior, such as maneuvering low thrust satellites. Optimal control problems for maneuvering electrodynamic tethers were posed using averaged state dynamics and constraints and then solved using a pseudospectral optimization method. It was shown that some classes of complex optimal control problems that use instantaneous state dynamics requiring hundreds or thousands of collocation node points for accurate solutions in the clock time domain can be reduced to relatively simple problems in Fourier space using only tens of node points. Using this method of large time scale optimal control, it is possible to determine optimal solutions of nearly periodic systems more accurately and more quickly than optimization using the instantaneous states. For long term maneuvers spanning days, weeks or months, it may be difficult or impossible to achieve accurate solutions that use instantaneous state dynamics due to numerical round off errors. Using averaged state dynamics, however, small periodic behavior over each orbit is ignored enabling the optimizer to determine a trajectory for the averaged state, thus optimizing only the secular behavior. This greatly reduces the scale of the problem for the optimizer. This method of optimal control in Fourier space could assist engineers with initial trade studies to determine design and performance parameters for a tether or any other low thrust maneuvering satellite.

It was further shown that this method of large time scale optimal control may be adapted to accommodate dynamics operating over multiple time scales. For the electrodynamic tether controller model, it was necessary to include the effects of a tilted Earth magnetic dipole which rotates once per day, slower than the orbital rate of the satellite system. None of the controllers described in the literature addressed a tilted Earth magnetic dipole or an atmospheric drag model for electrodynamic tethers in orbit transfer, so a model was derived that included both. The periodic controller was modified to include terms resonant with the Earth's rotation and more accurate results were achieved and verified against a "truth" model.

To provide an even higher fidelity controller model, optimal libration control was also examined. It was shown that a rapidly changing state such as libration may be controlled in Fourier Space by defining a mean square state and using the averaged dynamic equations of motion as constraints in the optimal control problem. In this manner, it was possible to achieve minimum time orbit transfers that simultaneously drove down libration amplitude. Using this method of large time scale optimal control in concert with instantaneous state controllers operating in real time could enable maneuvering electrodynamic tether satellites to achieve long term transfers unachievable using instantaneous state controllers alone.

Optimal controls for low thrust satellites performing orbital maneuvers using multiple time scales is a wide open field with plenty of areas to be explored. The following is a list of recommended follow on research.

Apply the method of multiple time scale optimal control to systems subject to a different class of dynamic equations of motion. In this research, optimal control problems were reduced in Fourier space because we exploited what we knew about the problem, namely that the dynamic system had a fast time periodic piece and a slowly varying secular piece. There are many other systems that fall into this category that could use this method. Additionally, we are not constrained to periodic systems. A basis in Fourier space was chosen here because of the periodic nature of the orbital mechanics, however a different problem might be better served in a polynomial space with an orthogonal polynomial basis.

Demonstrate a powered sun-synchronous orbit. Non-thrusting satellites may be placed in sun-synchronous orbits that take advantage of the Earth's oblateness in such a way that the orbital plane precesses once per year. However, these orbits are typically constrained by altitude, inclination and eccentricity. A continuously thrusting system however could potentially achieve otherwise unachievable sun-synchronous orbits. One advantage would be that a satellite could reside in a desired orbit while maintaining optimal solar panel orientation with respect to the sun at all times.

Demonstrate optimal control using a higher fidelity model. Other periodic effects may be included into the dynamic model. A diurnally varying atmosphere, by definition, differs on the day and night sides. The controller, as described by Eq. (1), already contains control coefficients to affect

perturbations resonant with the orbital motion such as diurnally varying phenomena. When we introduced the Earth's rotating tilted magnetic dipole into the model, we had an effect that is not resonant with the first two harmonics of the Eq. (1) controller. New terms were be added to the controller to accommodate new perturbation effects (Eq. (25)). There may be other multiple time scale effects to consider in the model that operate at different frequencies.

Appendix A: Derivation of Libration Equations of Motion

In developing an orbital maneuvering controller, it is important to understand the attitude behavior of the tether motion when subjected to electrodynamic and aerodynamic forces. Because of the length of the tether, gravity gradient restoring torques can be significant. In order to make the equations as general as possible for 2-ball tether designs, few assumptions were made with regard to the mass distribution. The tether is modeled as two end-masses connected by a straight tether in constant tension with a uniform mass distribution.

The conservative gravitational force plays a large role in the tether attitude dynamics and lends itself well to the development of equations of motion using the Lagrangian method. Constructing the Lagrangian, we need adequate expressions for both the kinetic and potential energies. Using the coordinates defined in Figure 33, we can write the endmass and tether velocities and thus the kinetic energy.

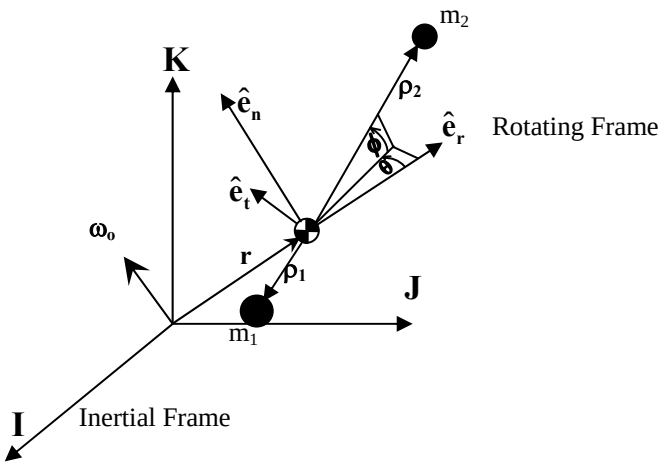

Figure 33. Rotating Frame Coordinates

The inertial frame is centered at the center of the Earth. The rotating frame is located at a position $\mathbf{r}$ with respect to the inertial frame and is centered at the system COM. It consists of three mutually orthogonal unit vectors; $\hat{\mathbf{e}}_\mathbf{r}$ in the zenith direction, $\hat{\mathbf{e}}_\mathbf{t}$ in the transverse direction and $\hat{\mathbf{e}}_\mathbf{n}$ completing the triad in the direction of the angular momentum perpendicular to the orbital plane. The vectors along the straight tether extending from the COM to mass 1 and mass 2 are $\boldsymbol{\rho}_1$ and $\boldsymbol{\rho}_2$ respectively.

Kinetic Energy

The kinetic energy for the system is derived by summing the separate kinetic energies for the end-masses and the integrated kinetic energy across the length of the tether. The velocity for mass 1 and its square are

$$\mathbf{v}_1 = \dot{\mathbf{r}} + \dot{\boldsymbol{\rho}}_1 = \dot{\mathbf{r}} + \boldsymbol{\rho}_1' + (\boldsymbol{\omega}_o + \boldsymbol{\omega}_e) \times \boldsymbol{\rho}_1 = \dot{\mathbf{r}} + \boldsymbol{\rho}_1' + \boldsymbol{\Omega} \times \boldsymbol{\rho}_1$$
$$\mathbf{v}_1 \cdot \mathbf{v}_1 = (\dot{\mathbf{r}} + \boldsymbol{\rho}_1' + \boldsymbol{\Omega} \times \boldsymbol{\rho}_1) \cdot (\dot{\mathbf{r}} + \boldsymbol{\rho}_1' + \boldsymbol{\Omega} \times \boldsymbol{\rho}_1)$$
$$= \dot{\mathbf{r}} \cdot \dot{\mathbf{r}} + 2\dot{\mathbf{r}} \cdot \boldsymbol{\rho}_1' + 2\dot{\mathbf{r}} \cdot (\boldsymbol{\Omega} \times \boldsymbol{\rho}_1) + \boldsymbol{\rho}_1' \cdot \boldsymbol{\rho}_1' + 2\boldsymbol{\rho}_1' \cdot (\boldsymbol{\Omega} \times \boldsymbol{\rho}_1) + (\boldsymbol{\Omega} \times \boldsymbol{\rho}_1) \cdot (\boldsymbol{\Omega} \times \boldsymbol{\rho}_1)$$

where $\boldsymbol{\omega}_e$ is the angular velocity of the straight tether in the rotating frame, $\boldsymbol{\omega}_o$ is the angular velocity of the rotating frame with respect to the inertial frame and $\boldsymbol{\Omega} = \boldsymbol{\omega}_o + \boldsymbol{\omega}_e$. Primed vectors indicate radial derivatives with respect to the rotating frame (e-frame). Given the length of the straight tether, L, we may write the relative position vectors $\boldsymbol{\rho}_1$ and $\boldsymbol{\rho}_2$ in terms of a reduced mass and L.

$$\boldsymbol{\rho}_1 = -\frac{\mu_m}{M_1} L \hat{\boldsymbol{\rho}}$$
$$\boldsymbol{\rho}_2 = \frac{\mu_m}{M_2} L \hat{\boldsymbol{\rho}}$$

where $\hat{\boldsymbol{\rho}}$ is the unit vector in the direction along the straight tether from m_1 to m_2. The reduced mass μ_m is given by

$$\mu_m = \frac{\left(m_1 + \frac{m_t}{2}\right)\left(m_2 + \frac{m_t}{2}\right)}{m_1 + m_2 + m_t} = \frac{M_1 M_2}{(M_1 + M_2)} = \frac{M_1 M_2}{M}$$

where $M_1 = m_1 + \frac{m_t}{2}$, $M_2 = m_2 + \frac{m_t}{2}$ and $M = m_1 + m_2 + m_t$, the total mass. Derivation for this 3-body reduced mass is found in Appendix B. Considering the appropriate substitutions for $\boldsymbol{\rho}_1$ and $\boldsymbol{\rho}_2$, the kinetic energy of mass 1 is

$$T_1 = \frac{1}{2} m_1 \mathbf{v}_1 \cdot \mathbf{v}_1$$
$$= \frac{m_1}{2} \dot{\mathbf{r}} \cdot \dot{\mathbf{r}} + \frac{m_1 \mu_m}{2M_1} \left\{ -2\dot{\mathbf{r}} \cdot \mathbf{L}' - 2\dot{\mathbf{r}} \cdot \boldsymbol{\Omega} \times \mathbf{L} + \frac{\mu_m}{M_1} \left(\mathbf{L}' \cdot \mathbf{L}' + 2\mathbf{L}' \cdot \boldsymbol{\Omega} \times \mathbf{L} + (\boldsymbol{\Omega} \times \mathbf{L}) \cdot (\boldsymbol{\Omega} \times \mathbf{L}) \right) \right\}$$

where $\mathbf{L}'$ is the time derivative of L w.r.t. the e-frame. Likewise the kinetic energy for mass 2 is

$$T_2 = \frac{1}{2} m_2 \mathbf{v}_2 \cdot \mathbf{v}_2 =$$
$$\frac{m_2}{2} \dot{\mathbf{r}} \cdot \dot{\mathbf{r}} + \frac{m_2 \mu_m}{2M_2} \left\{ +2\dot{\mathbf{r}} \cdot \mathbf{L}' + 2\dot{\mathbf{r}} \cdot \boldsymbol{\Omega} \times \mathbf{L} + \frac{\mu_m}{M_2} \left(\mathbf{L}' \cdot \mathbf{L}' + 2\mathbf{L}' \cdot \boldsymbol{\Omega} \times \mathbf{L} + (\boldsymbol{\Omega} \times \mathbf{L}) \cdot (\boldsymbol{\Omega} \times \mathbf{L}) \right) \right\}$$

Note that the fourth term in braces vanishes since $\mathbf{L}' \cdot \boldsymbol{\Omega} \times \mathbf{L} = 0$.

The kinetic energy of the tether, however, must be integrated from tip to tip (i.e. $-\rho_1$ to ρ_2 as shown in Figure 34)

$$T_t = \frac{1}{2} \int_{-\rho_1}^{\rho_2} \mathbf{v}_t \cdot \mathbf{v}_t \, dm$$

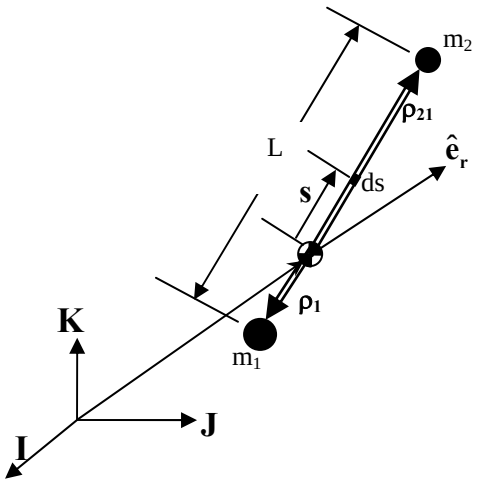

Figure 34. Straight Tether Integration

where the velocity of any given element ds along the tether is

$$\mathbf{v}_t = \dot{\mathbf{r}} + \dot{\mathbf{s}} = \dot{\mathbf{r}} + \mathbf{s}' + \boldsymbol{\Omega} \times \mathbf{s}$$

and a mass element for a tether of uniform density is

$$dm = \frac{m_t}{L} ds$$

Substituting in appropriate terms, the tether kinetic energy may be written

$$T_t = \frac{1}{2} \frac{m_t}{L} \int_{-\rho_1}^{\rho_2} \dot{\mathbf{r}} \cdot \dot{\mathbf{r}} + 2\dot{\mathbf{r}} \cdot \mathbf{s}' + 2\dot{\mathbf{r}} \cdot \boldsymbol{\Omega} \times \mathbf{s} + \mathbf{s}' \cdot \mathbf{s}' + 2\mathbf{s}' \cdot \boldsymbol{\Omega} \times \mathbf{s} + (\boldsymbol{\Omega} \times \mathbf{s}) \cdot (\boldsymbol{\Omega} \times \mathbf{s}) ds$$

Recognizing that a tether section that spans length s stretches in linear proportion to the overall tether stretch, i.e. $\mathbf{s}' = {}^{s}\!/_{L}\, \mathbf{L}' = \frac{s\dot{L}}{L} \hat{\boldsymbol{\rho}}$ and we can write the kinetic energy integrand in terms of the scalar s.

$$\begin{aligned} T_t = \frac{m_t}{2L} \{ & \dot{\mathbf{r}} \cdot \dot{\mathbf{r}} L + 2\dot{\mathbf{r}} \cdot \hat{\boldsymbol{\rho}} \int_{-\rho_1}^{\rho_2} \frac{s\dot{L}}{L} ds + 2\dot{\mathbf{r}} \cdot \boldsymbol{\Omega} \times \hat{\boldsymbol{\rho}} \int_{-\rho_1}^{\rho_2} s ds + \left(\frac{\dot{L}}{L} \right)^2 \int_{-\rho_1}^{\rho_2} s^2 ds + 2\hat{\boldsymbol{\rho}} \cdot \boldsymbol{\Omega} \times \hat{\boldsymbol{\rho}} \left(\frac{\dot{L}}{L} \right) \int_{-\rho_1}^{\rho_2} s^2 ds + \\ & + (\boldsymbol{\Omega} \times \hat{\boldsymbol{\rho}}) \cdot (\boldsymbol{\Omega} \times \hat{\boldsymbol{\rho}}) \int_{-\rho_1}^{\rho_2} s^2 ds \} \end{aligned} \tag{54}$$

Since $-\rho_1 = -\frac{\mu_m}{M_1} L$ and $\rho_2 = \frac{\mu_m}{M_2} L$, we can rewrite the integration limits and the tether kinetic energy becomes

$$\begin{aligned} T_t = \frac{m_t}{2L} \{ & \dot{\mathbf{r}} \cdot \dot{\mathbf{r}} L + 2\dot{\mathbf{r}} \cdot \hat{\boldsymbol{\rho}} \frac{\dot{L}}{L} \frac{L^2}{2} \left(\frac{{\mu_m}^2}{{M_2}^2} - \frac{{\mu_m}^2}{{M_1}^2} \right) + 2\dot{\mathbf{r}} \cdot \boldsymbol{\Omega} \times \hat{\boldsymbol{\rho}} \frac{L^2}{2} \left(\frac{{\mu_m}^2}{{M_2}^2} - \frac{{\mu_m}^2}{{M_1}^2} \right) + \\ & \left(\frac{\dot{L}}{L} \right)^2 \frac{L^3}{3} \left(\frac{{\mu_m}^3}{{M_2}^3} + \frac{{\mu_m}^3}{{M_1}^3} \right) + (\boldsymbol{\Omega} \times \hat{\boldsymbol{\rho}}) \cdot (\boldsymbol{\Omega} \times \hat{\boldsymbol{\rho}}) \frac{L^3}{3} \left(\frac{{\mu_m}^3}{{M_2}^3} + \frac{{\mu_m}^3}{{M_1}^3} \right) \} \end{aligned}$$

Where the fifth term in the braces of Eq. (54) drops out since $\hat{\boldsymbol{\rho}} \cdot \boldsymbol{\Omega} \times \hat{\boldsymbol{\rho}} = 0$.

Thus we are left with

$$\begin{aligned} T_t = & \frac{m_t}{2} \dot{\mathbf{r}} \cdot \dot{\mathbf{r}} + m_t \dot{L} \dot{\mathbf{r}} \cdot \hat{\boldsymbol{\rho}} \left(\frac{m_1 - m_2}{2M} \right) + m_t L \dot{\mathbf{r}} \cdot \boldsymbol{\Omega} \times \hat{\boldsymbol{\rho}} \left(\frac{m_1 - m_2}{2M} \right) + \\ & m_t \frac{\dot{L}^2}{6} \left(\frac{{M_1}^3 + {M_2}^3}{M^3} \right) + (\boldsymbol{\Omega} \times \hat{\boldsymbol{\rho}}) \cdot (\boldsymbol{\Omega} \times \hat{\boldsymbol{\rho}}) \frac{m_t L^2}{6} \left(\frac{{M_1}^3 + {M_2}^3}{M^3} \right) \end{aligned}$$

Note that

$$\frac{\mu_m{}^2}{M_2{}^2}-\frac{\mu_m{}^2}{M_1{}^2}=\frac{M_1{}^2-M_2{}^2}{M^2}=\frac{m_1{}^2+m_1m_t-m_2{}^2-m_2m_t}{M^2}=\frac{(m_1-m_2)(m_1+m_2+m_t)}{M^2}=\frac{m_1-m_2}{M}$$

The total kinetic energy of the system is then

$$\begin{aligned}T&=T_1+T_2+T_t\\&=\frac{1}{2}M\dot{\mathbf{r}}\cdot\dot{\mathbf{r}}+\left\{\mu_m\left(\frac{-m_1}{M_1}+\frac{m_2}{M_2}\right)+\frac{m_t}{2}\left(\frac{m_1-m_2}{M}\right)\right\}\left(\dot{L}\dot{\mathbf{r}}\cdot\hat{\boldsymbol{\rho}}+L\dot{\mathbf{r}}\cdot\boldsymbol{\Omega}\times\hat{\boldsymbol{\rho}}\right)+\\&\left\{\frac{m_1\mu_m{}^2}{2M_1{}^2}+\frac{m_2\mu_m{}^2}{2M_2{}^2}+\frac{m_t}{6}\left(\frac{M_1{}^3+M_2{}^3}{M^3}\right)\right\}\left(\dot{L}^2+L^2\left(\boldsymbol{\Omega}\times\hat{\boldsymbol{\rho}}\right)\cdot\left(\boldsymbol{\Omega}\times\hat{\boldsymbol{\rho}}\right)\right)\end{aligned}$$

The term in the first set of braces vanishes as shown below.

$$\begin{aligned}\mu_m\left(\frac{-m_1}{M_1}+\frac{m_2}{M_2}\right)+\frac{m_t}{2}\left(\frac{m_1-m_2}{M}\right)&=\frac{-M_2m_1+M_1m_2+\frac{m_t}{2}(m_1-m_2)}{M}\\&=\frac{-m_1\left(m_2+\frac{m_t}{2}\right)+m_2\left(m_1+\frac{m_t}{2}\right)+\frac{m_t}{2}(m_1-m_2)}{M}=0\end{aligned}$$

Furthermore, the quantity $\left(\boldsymbol{\Omega}\times\hat{\boldsymbol{\rho}}\right)\cdot\left(\boldsymbol{\Omega}\times\hat{\boldsymbol{\rho}}\right)$ is actually $\boldsymbol{\Omega}^T\mathbf{J}\boldsymbol{\Omega}$ or $\boldsymbol{\Omega}\cdot\overline{\overline{\mathbf{J}}}\cdot\boldsymbol{\Omega}$ in matrix and tensor form respectively where $\overline{\overline{\mathbf{J}}}$ is the specific inertia tensor (see Appendix C). Thus the total kinetic energy for the system is

$$T=\frac{1}{2}M\dot{\mathbf{r}}\cdot\dot{\mathbf{r}}+\frac{1}{2}\left\{\mu_m{}^2\left(\frac{m_1}{M_1{}^2}+\frac{m_2}{M_2{}^2}\right)+\frac{m_t}{3}\left(\frac{M_1{}^3+M_2{}^3}{M^3}\right)\right\}\left(\dot{L}^2+L^2\boldsymbol{\Omega}\cdot\overline{\overline{\mathbf{J}}}\cdot\boldsymbol{\Omega}\right)$$

The mass term in braces may be shown to reduce to an equivalent reduced mass μ_e as shown in Appendix B.

$$\mu_e=\mu_m{}^2\left(\frac{m_1}{M_1{}^2}+\frac{m_2}{M_2{}^2}\right)+\frac{m_t}{3}\left(\frac{M_1{}^3+M_2{}^3}{M^3}\right)=\mu_m-\frac{m_t}{6}$$

The final form of the total kinetic energy is

$$\boxed{T=\frac{1}{2}M\dot{\mathbf{r}}\cdot\dot{\mathbf{r}}+\frac{1}{2}\mu_e\left(\dot{L}^2+L^2\boldsymbol{\Omega}\cdot\overline{\overline{\mathbf{J}}}\cdot\boldsymbol{\Omega}\right)}\qquad(55)$$

The first term on the right hand side of Eq. (55) is the translational energy of the whole system acting through the system COM. The second term accounts for the rotational energy acting through the COM and the relative motion energy between the two end-masses.

Potential Energy

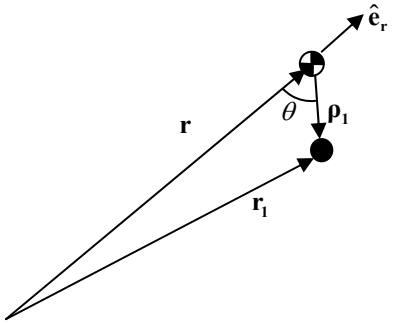

Figure 35. Position of Endmass 1

The potential energy is derived for each end-mass at its distance from the center of the Earth. The potential energy of the tether wire is integrated for each elemental mass along the length of the wire. To obtain the potential relative to the COM, a binomial expansion of the potential energy expression is used. For mass 1, the potential energy may be expressed in terms of the radius vector to the COM of the system, $\mathbf{r}$, and the m_1 position vector relative to the COM

$$V_1 = \frac{-\mu_g m_1}{r_1} = \frac{-\mu_g m_1}{r\left(1 + 2\dfrac{\boldsymbol{\rho}_1 \cdot \hat{\mathbf{e}}_\mathbf{r}}{r} + \dfrac{\rho_1^{\,2}}{r^2}\right)^{1/2}}$$

where we have used the geometry in Figure 35 and the law of cosines to infer that

$$r_1^{\,2} = r^2 + \rho_1^{\,2} - 2r\rho_1\cos\theta = r^2\left(1 + \frac{\rho_1^{\,2}}{r^2} + \frac{2\boldsymbol{\rho}_1 \cdot \hat{\mathbf{e}}_\mathbf{r}}{r}\right)$$

$$r_1 = r\left(1 + \frac{\rho_1^{\,2}}{r^2} + \frac{2\boldsymbol{\rho}_1 \cdot \hat{\mathbf{e}}_\mathbf{r}}{r}\right)^{\frac{1}{2}}$$

An expression for r_1^{-1} is derived using a binomial expansion and ignoring terms greater than or equal to $\mathcal{O}\left\{\dfrac{\rho^3}{r^3}\right\}$.

$$r_1^{-1} \approx r^{-1}\left\{1-\frac{\boldsymbol{\rho}_1\cdot\hat{\mathbf{e}}_\mathbf{r}}{r}-\frac{1}{2}\frac{\rho_1^{\,2}}{r^2}+\frac{3}{2}\left(\frac{\boldsymbol{\rho}_1\cdot\hat{\mathbf{e}}_\mathbf{r}}{r}\right)^2\right\}$$

Thus the potential energy of mass 1 is

$$V_1 = -\mu_g m_1 r_1^{-1} \approx \frac{-\mu_g m_1}{r}\left\{1-\frac{\boldsymbol{\rho}_1\cdot\hat{\mathbf{e}}_\mathbf{r}}{r}+\frac{3}{2}\left(\frac{\boldsymbol{\rho}_1\cdot\hat{\mathbf{e}}_\mathbf{r}}{r}\right)^2-\frac{1}{2}\frac{\rho_1^{\,2}}{r^2}\right\}$$

Substituting in the expressions for $\boldsymbol{\rho}_1$ and $\boldsymbol{\rho}_2$ we obtain

$$V_1 \approx \frac{-\mu_g m_1}{r}\left\{1+\frac{\mu_m L}{M_1}\left(\frac{\hat{\boldsymbol{\rho}}\cdot\hat{\mathbf{e}}_\mathbf{r}}{r}\right)+\frac{3}{2}\frac{\mu_m^{\,2}L^2}{M_1^{\,2}}\left(\frac{\hat{\boldsymbol{\rho}}\cdot\hat{\mathbf{e}}_\mathbf{r}}{r}\right)^2-\frac{1}{2}\frac{\mu_m^{\,2}L^2}{M_1^{\,2}r^2}\right\}$$
$$=\frac{-\mu_g m_1}{r}\left\{1+\frac{\mu_m L}{M_1 r}\left(\hat{\boldsymbol{\rho}}\cdot\hat{\mathbf{e}}_\mathbf{r}\right)+\frac{1}{2}\frac{\mu_m^{\,2}L^2}{M_1^{\,2}r^2}\left(3\left(\hat{\boldsymbol{\rho}}\cdot\hat{\mathbf{e}}_\mathbf{r}\right)^2-1\right)\right\}$$

Similarly, the potential energy of mass 2 is

$$V_2 \approx \frac{-\mu_g m_2}{r}\left\{1-\frac{\mu_m L}{M_2 r}\left(\hat{\boldsymbol{\rho}}\cdot\hat{\mathbf{e}}_\mathbf{r}\right)+\frac{1}{2}\frac{\mu_m^{\,2}L^2}{M_2^{\,2}r^2}\left(3\left(\hat{\boldsymbol{\rho}}\cdot\hat{\mathbf{e}}_\mathbf{r}\right)^2-1\right)\right\}$$

The potential energy of the tether is the integration of all the elemental potential energies along the tether length.

$$V_t = -\mu_g \int_{-\rho_1}^{\rho_2}\frac{1}{\mathbf{r}+\mathbf{s}\cdot\hat{\mathbf{e}}_\mathbf{r}}dm \text{ where } dm=\frac{m_t}{L}ds$$

Using a binomial expansion,

$$V_t \approx \frac{-\mu_g m_t}{Lr}\int_{-\rho_1}^{\rho_2} 1-s\frac{\hat{\boldsymbol{\rho}}\cdot\hat{\mathbf{e}}_\mathbf{r}}{r}+\frac{3}{2}s^2\left(\frac{\hat{\boldsymbol{\rho}}\cdot\hat{\mathbf{e}}_\mathbf{r}}{r}\right)^2-\frac{1}{2}\frac{s^2}{r^2}ds$$
$$=\frac{-\mu_g m_t}{Lr}\left(s-\frac{s^2}{2r}\left(\hat{\boldsymbol{\rho}}\cdot\hat{\mathbf{e}}_\mathbf{r}\right)+\frac{s^3}{2r^2}\left(\hat{\boldsymbol{\rho}}\cdot\hat{\mathbf{e}}_\mathbf{r}\right)^2-\frac{s^3}{6r^2}\right)\Bigg|_{-\rho_1=\frac{-\mu_m L}{M_1}}^{\rho_2=\frac{\mu_m L}{M_2}}$$
$$=\frac{-\mu_g m_t}{Lr}\left\{L+\frac{L^2}{2r}\left(\frac{M_2^{\,2}-M_1^{\,2}}{M^2}\right)\left(\hat{\boldsymbol{\rho}}\cdot\hat{\mathbf{e}}_\mathbf{r}\right)+\frac{L^3}{2r^2}\left(\frac{M_1^{\,3}+M_2^{\,3}}{M^3}\right)\left(\left(\hat{\boldsymbol{\rho}}\cdot\hat{\mathbf{e}}_\mathbf{r}\right)^2-\frac{1}{3}\right)\right\}$$
$$=\frac{-\mu_g m_t}{r}\left\{1+\frac{L}{2r}\left(\frac{m_2-m_1}{M}\right)\left(\hat{\boldsymbol{\rho}}\cdot\hat{\mathbf{e}}_\mathbf{r}\right)+\frac{L^2}{2r^2}\left(\frac{M_1^{\,3}+M_2^{\,3}}{M^3}\right)\left(\left(\hat{\boldsymbol{\rho}}\cdot\hat{\mathbf{e}}_\mathbf{r}\right)^2-\frac{1}{3}\right)\right\}$$

The total potential energy is then

$$
\begin{aligned}
V &= V_1 + V_2 + V_t \\
&\approx -\frac{\mu_g M}{r} - \frac{\mu_g L}{r^2}\left\{\frac{\mu_m m_1}{M_1} - \frac{\mu_m m_2}{M_2} + \frac{m_t}{2}\left(\frac{m_2 - m_1}{M}\right)\right\}\left(\hat{\boldsymbol{\rho}}\cdot\hat{\mathbf{e}}_{\mathbf{r}}\right) + \\
&-\frac{\mu_g L^2}{2r^3}\left\{\frac{{M_2}^2 m_1 + {M_1}^2 m_2}{M^2} + \frac{m_t}{3}\left(\frac{{M_1}^3 + {M_2}^3}{M^3}\right)\right\}\left(3\left(\hat{\boldsymbol{\rho}}\cdot\hat{\mathbf{e}}_{\mathbf{r}}\right)^2 - 1\right)
\end{aligned}
$$

The first term in braces vanishes to zero as shown.

$$
\begin{aligned}
&\frac{\mu_m m_1}{M_1} - \frac{\mu_m m_2}{M_2} + \frac{m_t}{2}\left(\frac{m_2 - m_1}{M}\right) = \frac{M_2 m_1 - M_1 m_2 + \frac{m_t}{2}\left(m_2 - m_1\right)}{M} \\
&= \frac{\left(m_2 + \frac{m_t}{2}\right)m_1 - \left(m_1 + \frac{m_t}{2}\right)m_2 + \frac{m_t}{2}\left(m_2 - m_1\right)}{M} = 0
\end{aligned}
$$

The second term in braces is the equivalent reduced mass, μ_e. The total potential energy is then

$$
\boxed{V \approx -\frac{\mu_g M}{r} - \frac{\mu_g L^2}{2r^3}\mu_e\left(3\left(\hat{\boldsymbol{\rho}}\cdot\hat{\mathbf{e}}_{\mathbf{r}}\right)^2 - 1\right)} \tag{56}
$$

The first term in (56) is the potential energy of the entire system mass acting as a point mass at the COM. The second term is the gravity gradient potential due to the center of gravity offset from the COM.

The Lagrangian Equations of Motion

With the kinetic and potential energies in hand (equations (55) and (56)), we may now construct the Lagrangian function, $\mathcal{L} = T - V$, and form the Lagrangian equations of motion.

$$
\mathcal{L} = \frac{1}{2}Mv^2 + \frac{1}{2}\mu_e\left(\dot{L}^2 + L^2\boldsymbol{\Omega}\cdot\bar{\bar{\mathbf{J}}}\cdot\boldsymbol{\Omega}\right) + \frac{\mu_g M}{r} + \frac{\mu_g\mu_e L^2}{2r^3}\left(3\left(\hat{\boldsymbol{\rho}}\cdot\hat{\mathbf{e}}_{\mathbf{r}}\right)^2 - 1\right)
$$

To get the equations of motion in terms of the in-plane and out-of-plane libration angles of the straight tether, we need reference frames and coordinates with which to evaluate the vector operations to obtain scalars. The body frame and the rotating frame (e-frame) will serve well for this purpose. The rotational energy term, $L^2\boldsymbol{\Omega}\cdot\bar{\bar{\mathbf{J}}}\cdot\boldsymbol{\Omega}$, is evaluated using the body frame depicted in Figure 36. The orbital rotation may

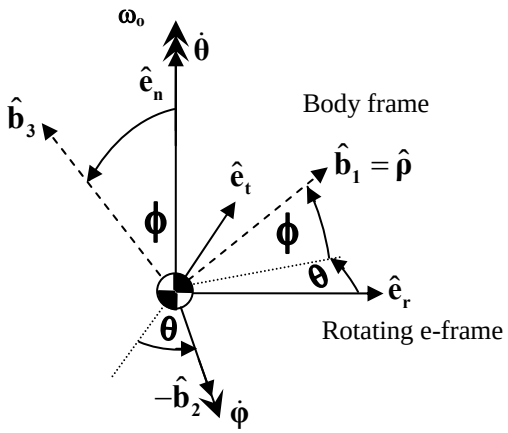

Figure 36. Body Frame and Rotating Frame

be expressed in body coordinates as $\omega_o = \begin{bmatrix} \omega \sin\phi \\ 0 \\ \omega \cos\phi \end{bmatrix}_b$ and similarly the tether rotation in the rotating frame may be expressed in body coordinates as $\omega_e = \begin{bmatrix} \dot{\theta} \sin\phi \\ -\dot{\phi} \\ \dot{\theta} \cos\phi \end{bmatrix}_b$.

Letting $s\theta = \sin\theta$ and $c\theta = \cos\theta$ we may write the total inertial angular rate of the tether system in body coordinates as

$$\mathbf{\Omega} = \boldsymbol{\omega}_\mathbf{o} + \boldsymbol{\omega}_\mathbf{e} = \begin{bmatrix} \left(\dot{\theta} + \omega\right) s\phi \\ -\dot{\phi} \\ \left(\dot{\theta} + \omega\right) c\phi \end{bmatrix}_b$$

The specific inertia tensor may be expressed in body coordinates as well in matrix form. Approximating the tether as a thin rod with zero inertia about the $\hat{\mathbf{b}}_1$ axis, we write

$$\mathbf{J}L^2 = \begin{bmatrix} 0 & 0 & 0 \\ 0 & L^2 & 0 \\ 0 & 0 & L^2 \end{bmatrix}_b$$

thus

$$L^2 \mathbf{\Omega} \cdot \bar{\bar{\mathbf{J}}} \cdot \mathbf{\Omega} = L^2 \mathbf{\Omega}^T \mathbf{J} \mathbf{\Omega} = L^2 \left(\dot{\phi}^2 + c^2\phi \left(\dot{\theta} + \omega\right)^2 \right)$$

where ω is not constant in general and is equal to the rate of change of the true anomaly, $\dot{\nu}$. To evaluate $\left(\hat{\boldsymbol{\rho}}\cdot\hat{\mathbf{e}}_{\mathbf{r}}\right)^2$, the e-frame is convenient. In the rotating e-frame, the length vector and its derivative may be written

$$\mathbf{L} = L\begin{bmatrix}\cos\phi\cos\theta\\ \cos\phi\sin\theta\\ \sin\phi\end{bmatrix}_e = L\hat{\boldsymbol{\rho}}$$

$$\dot{\mathbf{L}} = \mathbf{L}' + \boldsymbol{\omega}_{\mathbf{e}}\times\mathbf{L} = \dot{L}\hat{\boldsymbol{\rho}} + L\dot{\hat{\boldsymbol{\rho}}} = \dot{L}\begin{bmatrix}\cos\phi\cos\theta\\ \cos\phi\sin\theta\\ \sin\phi\end{bmatrix}_e + L\begin{bmatrix}-\dot{\theta}\cos\phi\sin\theta-\dot{\phi}\sin\phi\cos\theta\\ \dot{\theta}\cos\phi\cos\theta-\dot{\phi}\sin\phi\sin\theta\\ \dot{\phi}\cos\phi\end{bmatrix}_e$$

$$\hat{\boldsymbol{\rho}} = \begin{bmatrix}c\phi c\theta\\ c\phi s\theta\\ s\phi\end{bmatrix}_e,\ \hat{\boldsymbol{\rho}}\cdot\hat{\mathbf{e}}_{\mathbf{r}} = c\phi c\theta,\ \left(\hat{\boldsymbol{\rho}}\cdot\hat{\mathbf{e}}_{\mathbf{r}}\right)^2 = c^2\phi c^2\theta$$

The Lagrangian is then

$$\mathcal{L} = \frac{1}{2}Mv^2 + \frac{1}{2}\mu_e\left(\dot{L}^2 + L^2\left(\dot{\phi}^2 + c^2\phi\left(\dot{\theta}+\dot{\nu}\right)^2\right)\right) + \frac{\mu_g M}{r} + \frac{\mu_g\mu_e L^2}{2r^3}\left(3c^2\phi c^2\theta - 1\right)$$

The in-plane libration equation of motion may be obtained as follows.

$$\frac{\partial\mathcal{L}}{\partial\dot{\theta}} = \mu_e L^2 c^2\phi\left(\dot{\theta}+\dot{\nu}\right),\ \frac{d}{dt}\left(\frac{\partial\mathcal{L}}{\partial\dot{\theta}}\right) = \mu_e L^2 c^2\phi\left(\ddot{\theta}+\ddot{\nu}\right) + \mu_e\left(\left(-2L^2 c\phi s\phi\dot{\phi}\right) + 2L\dot{L}c^2\phi\right)\left(\dot{\theta}+\dot{\nu}\right)$$

$$\frac{\partial\mathcal{L}}{\partial\theta} = \frac{-3\mu_g\mu_e L^2}{r^3}c^2\phi c\theta s\theta$$

$$\frac{d}{dt}\left(\frac{\partial\mathcal{L}}{\partial\dot{\theta}}\right) - \frac{\partial\mathcal{L}}{\partial\theta} = Q_\theta$$

$$\boxed{\mu_e L^2\left(c^2\phi\left(\ddot{\theta}+\ddot{\nu}\right) + 2\left(\frac{\dot{L}}{L}c^2\phi - \dot{\phi}c\phi s\phi\right)\left(\dot{\theta}+\dot{\nu}\right) + \frac{3\mu_g}{r^3}c^2\phi c\theta s\theta\right) = Q_\theta} \qquad (57)$$

The out-of-plane libration equation of motion is similarly obtained.

$$\frac{\partial\mathcal{L}}{\partial\dot{\phi}} = \mu_e L^2\dot{\phi},\ \frac{d}{dt}\left(\frac{\partial\mathcal{L}}{\partial\dot{\phi}}\right) = \mu_e\left(L^2\ddot{\phi} + 2L\dot{L}\dot{\phi}\right)$$

$$\frac{\partial\mathcal{L}}{\partial\phi} = -\mu_e L^2\left(c\phi s\phi\left(\dot{\theta}+\dot{\nu}\right)^2 + \frac{3\mu_g}{r^3}c\phi s\phi c^2\theta\right)$$

$$\frac{d\mathcal{L}}{dt}\left(\frac{\partial\mathcal{L}}{\partial\dot{\phi}}\right) - \frac{\partial\mathcal{L}}{\partial\phi} = Q_\phi$$

$$\boxed{\mu_e L^2\left(\ddot{\phi}+2\frac{\dot{L}}{L}\dot{\phi}+c\phi s\phi\left(\left(\dot{\theta}+\dot{\nu}\right)^2+\frac{3\mu_g}{r^3}c^2\theta\right)\right)=Q_\phi} \tag{58}$$

The motion along the length of the tether is free when the tether is slack, but constrained when the tether is in tension. This equation of motion is given by

$$\frac{d}{dt}\left(\frac{\partial\mathcal{L}}{\partial\dot{L}}\right)=\mu_e\ddot{L}$$
$$\frac{\partial\mathcal{L}}{\partial L}=\mu_e L\left(\dot{\phi}^2+c^2\phi\left(\dot{\theta}+\dot{\nu}\right)^2+\frac{\mu_g}{r^3}\left(3c^2\phi c^2\theta-1\right)\right)$$
$$\frac{d}{dt}\left(\frac{\partial\mathcal{L}}{\partial L'}\right)-\frac{\partial\mathcal{L}}{\partial L}=Q_L$$

$$\boxed{\mu_e L\left(\frac{\ddot{L}}{L}-\dot{\phi}^2-c^2\phi\left(\dot{\theta}+\dot{\nu}\right)^2-\frac{\mu_g}{r^3}\left(3c^2\phi c^2\theta-1\right)\right)=Q_L} \tag{59}$$

To complete the right sides of these equations of motion, we need to write the non-conservative generalized forces acting on the system.

Non-Conservative Generalized Forces

There are two external non-conservative forces considered in these equations of motion, aerodynamic drag and Lorenz force due to the current in the wire interacting with the Earth's magnetic field. At the operational altitudes of interest, the magnitudes of both of these forces cannot be neglected. In this section we will derive the generalized forces on the tether due to these effects.

Aerodynamic Drag

Although the air density is very low in the stratosphere, drag is not negligible. Over many orbits, the atmospheric drag will eventually cause the tether orbit to decay if there is no restoring force. The air is too thin to model as a fluid, i.e. the molecular mean free path is large compared to the dimensions of the satellite. Therefore we use a free-molecular flow model and only consider a drag force opposite the direction of the velocity. This force acts on both end-masses and the tether itself. Each end-mass has a different ballistic coefficient and the system COM is not, in general, in the center of the tether.

Furthermore the atmospheric density varies exponentially along the length of the tether, thus the impact force of incoming atmospheric particles varies with height along the wire as shown in Figure 37. Due to the uneven distribution of aerodynamic forces about the COM, there will be aerodynamic torque acting on the tether system.

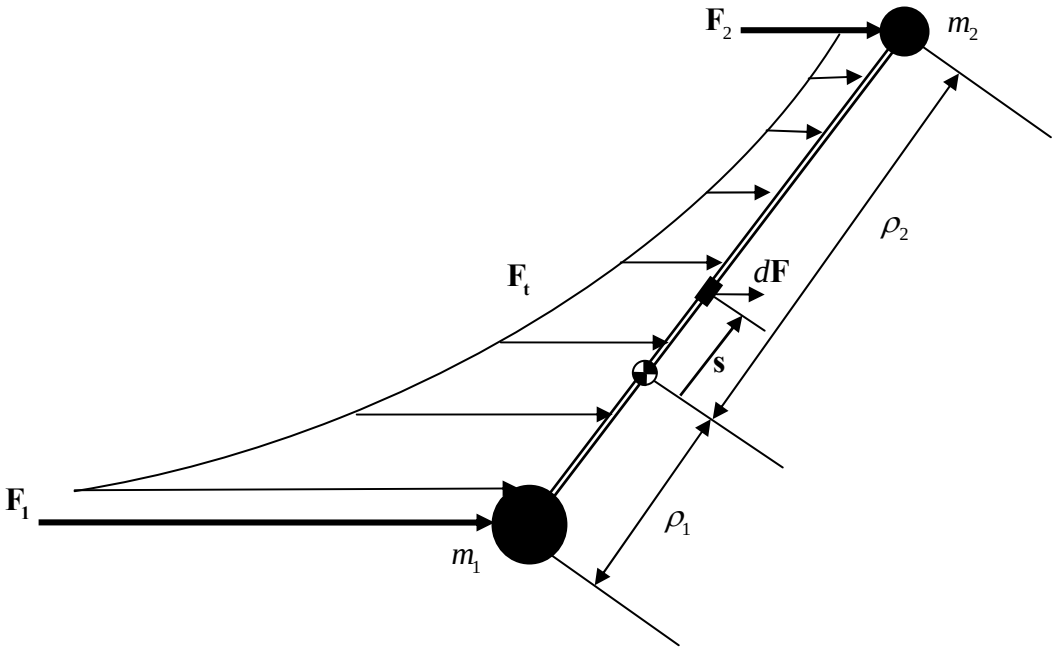

Figure 37. Tether Subject to Atmospheric Drag

The generalized in-plane aerodynamic torque is given by

$$Q_{\theta a} = \mathbf{F}_1 \cdot \frac{\partial \mathbf{v}_1}{\partial \dot{\theta}} + \mathbf{F}_2 \cdot \frac{\partial \mathbf{v}_2}{\partial \dot{\theta}} + \mathbf{M}_t \cdot \frac{\partial \boldsymbol{\Omega}}{\partial \dot{\theta}}$$

but

$$\frac{\partial \mathbf{v}_1}{\partial \dot{\theta}} = \frac{\partial \left(\dot{\mathbf{r}} + \dot{\boldsymbol{\rho}}_1 \right)}{\partial \dot{\theta}} = \frac{\partial \dot{\boldsymbol{\rho}}_1}{\partial \dot{\theta}} = \frac{\partial \left(\boldsymbol{\rho}_1' + \boldsymbol{\Omega} \times \boldsymbol{\rho}_1 \right)}{\partial \dot{\theta}} = \frac{\partial \boldsymbol{\rho}_1'}{\partial \dot{\theta}} + \boldsymbol{\Omega} \times \frac{\partial \boldsymbol{\rho}_1}{\partial \dot{\theta}} + \frac{\partial \boldsymbol{\Omega}}{\partial \dot{\theta}} \times \boldsymbol{\rho}_1 = \frac{\partial \boldsymbol{\Omega}}{\partial \dot{\theta}} \times \boldsymbol{\rho}_1$$

since $\frac{\partial \dot{\mathbf{r}}}{\partial \dot{\theta}} = \frac{\partial \boldsymbol{\rho}_1'}{\partial \dot{\theta}} = \frac{\partial \boldsymbol{\rho}_1}{\partial \dot{\theta}} = 0$. Recalling that $\boldsymbol{\Omega} = \boldsymbol{\omega}_o + \boldsymbol{\omega}_e$, we have

$$\frac{\partial \mathbf{v}_1}{\partial \dot{\theta}} = \frac{\partial \left(\boldsymbol{\omega}_o + \boldsymbol{\omega}_e \right)}{\partial \dot{\theta}} \times \boldsymbol{\rho}_1 = \frac{\partial \boldsymbol{\omega}_e}{\partial \dot{\theta}} \times \boldsymbol{\rho}_1 \text{ since } \frac{\partial \boldsymbol{\omega}_o}{\partial \dot{\theta}} = 0.$$

Similarly $\frac{\partial \mathbf{v}_2}{\partial \dot{\theta}} = \frac{\partial \boldsymbol{\omega}_\mathbf{e}}{\partial \dot{\theta}} \times \boldsymbol{\rho}_2$, thus the aerodynamic torque reduces to

$$Q_{\theta a} = \mathbf{F}_1 \cdot \frac{\partial \boldsymbol{\omega}_\mathbf{e}}{\partial \dot{\theta}} \times \boldsymbol{\rho}_1 + \mathbf{F}_2 \cdot \frac{\partial \boldsymbol{\omega}_\mathbf{e}}{\partial \dot{\theta}} \times \boldsymbol{\rho}_2 + \mathbf{M}_\mathbf{t} \cdot \frac{\partial \boldsymbol{\Omega}}{\partial \dot{\theta}}$$

The forces on the end-masses depend on the respective ballistic coefficients and air densities and vehicle velocity. For the purpose of computing the aerodynamic forces on both end-masses, the velocity due to orbital motion is considered far greater than the velocity of each end-mass relative to the COM due to rotation. Also, the tether is considerably shorter than the distance to the center of the Earth, so the directions of $\mathbf{F}_1$ and $\mathbf{F}_2$ are approximately parallel with the velocity vector of the COM. In the force computations, we use $\mathbf{v}_\mathbf{a}$ as the velocity of air molecules impinging on the vehicle. Ignoring the rotation of the atmosphere since this velocity contribution is miniscule compared to the orbital velocity in low Earth orbit, we can write the air velocity in the rotating e-frame (designated with a subscript "e") in terms of the flight path angle γ (Figure 38) as

$$\mathbf{v}_\mathbf{a} = v\hat{\mathbf{v}}_\mathbf{a} = v\begin{bmatrix} -\sin\gamma \\ -\cos\gamma \\ 0 \end{bmatrix}_e \quad \text{where } \hat{\mathbf{v}}_\mathbf{a} = \begin{bmatrix} -\sin\gamma \\ -\cos\gamma \\ 0 \end{bmatrix}_e = \left(\dot{r}^2 + r^2\left(\dot{\nu} + \dot{\omega}_p\right)^2\right)^{-1/2} \begin{bmatrix} -\dot{r} \\ -r\left(\dot{\nu} + \dot{\omega}_p\right) \\ 0 \end{bmatrix}_e$$

$$v_a{}^2 = v^2$$

Thus, the aerodynamic force on mass 1 is described as

$$\mathbf{F}_1 = \frac{1}{2} C_{d1} A_1 \rho_0 e^{\frac{-\left(h + \hat{\boldsymbol{\rho}}_1 \cdot \hat{\mathbf{e}}_\mathbf{r}\right)}{h^*}} v_a{}^2 \hat{\mathbf{v}}_\mathbf{a} = \frac{1}{2} C_{d1} A_1 \rho_0 e^{\frac{-\left(h - \frac{\mu_m L}{M_1} c\phi c\theta\right)}{h^*}} v^2 \begin{bmatrix} -s\gamma \\ -c\gamma \\ 0 \end{bmatrix}_e$$

where h is the altitude of the COM, h^* is the characteristic height of the atmosphere, ω_p is the argument of perigee, C_{d1} is the effective coefficient of drag on M_1, A_1 is the presented area of mass 1, and ρ_0 is the atmospheric density at the COM altitude. Also

$$\frac{\partial \boldsymbol{\omega}_\mathbf{e}}{\partial \dot{\theta}} \times \boldsymbol{\rho}_1 = \frac{-\mu_m L}{M_1} \begin{bmatrix} -c\phi s\theta \\ c\phi c\theta \\ 0 \end{bmatrix}_e \quad \text{and} \quad \frac{\partial \boldsymbol{\omega}_\mathbf{e}}{\partial \dot{\theta}} \times \boldsymbol{\rho}_2 = \frac{\mu_m L}{M_2} \begin{bmatrix} -c\phi s\theta \\ c\phi c\theta \\ 0 \end{bmatrix}_e$$

The torque about the perpendicular to the orbital plane about the COM due to the drag on mass 1 is

$$\mathbf{F_1}\cdot\frac{\partial\boldsymbol{\omega}_\mathbf{e}}{\partial\dot{\theta}}\times\boldsymbol{\rho}_\mathbf{1}=\frac{1}{2}C_{d1}A_1\rho_0 e^{\frac{-\left(h-\frac{\mu_m L}{M_1}c\phi c\theta\right)}{h^*}}v^2\frac{\mu_m Lc\phi}{M_1}\left(-s\gamma s\theta+c\gamma c\theta\right)$$
$$=\frac{1}{2}B_1^*\rho_0 e^{\frac{-\left(h-\frac{\mu_m L}{M_1}c\phi c\theta\right)}{h^*}}v^2\mu_m Lc\phi\left(c\gamma c\theta-s\gamma s\theta\right)$$

where $B_1^*=\dfrac{C_{d1}A_1}{M_1}$ is the effective ballistic coefficient with M_1 in the denominator, not m_1. Likewise, the aerodynamic force on mass 2 is

$$\mathbf{F}_2=\frac{1}{2}C_{d2}A_2\rho_0 e^{\frac{-(h+\hat{\boldsymbol{\rho}}_2\cdot\hat{\mathbf{e}}_\mathbf{r})}{h^*}}v^2\hat{\mathbf{v}}_\mathbf{a}=\frac{1}{2}C_{d2}A_2\rho_0 e^{\frac{-\left(h+\frac{\mu_m L}{M_2}c\phi c\theta\right)}{h^*}}v^2\begin{bmatrix}-s\gamma\\-c\gamma\\0\end{bmatrix}_e$$

with a corresponding aerodynamic torque of

$$\mathbf{F_2}\cdot\frac{\partial\boldsymbol{\omega}_\mathbf{e}}{\partial\dot{\theta}}\times\boldsymbol{\rho}_\mathbf{2}=-\frac{1}{2}C_{d2}A_2\rho_0 e^{\frac{-\left(h+\frac{\mu_m L}{M_2}c\phi c\theta\right)}{h^*}}v_a{}^2\frac{\mu_m Lc\phi}{M_2}\left(-s\gamma s\theta+c\gamma c\theta\right)$$
$$=-\frac{1}{2}B_2^*\rho_0 e^{\frac{-\left(h+\frac{\mu_m L}{M_2}c\phi c\theta\right)}{h^*}}v^2\mu_m Lc\phi\left(-s\gamma s\theta+c\gamma c\theta\right)$$

The moment due to the varying air drag on the tether must be integrated along the tether length. An infinitesimal force acting on an element of surface area on the tether is proportional to the presented area to

the air flow, the velocity squared, the coefficient of drag, and the air density at that position on the tether. Its direction is in the direction of the air flow.

$$d\mathbf{F} = \frac{C_{dt}}{2}\rho(h)v_a{}^2 dA\hat{\mathbf{v}}_\mathbf{a}$$

The elemental area presented to the air stream is $dA = \cos\alpha d_t ds$ where α is the angle of attack as shown in Figure 38 and d_t is the tether diameter (tether wire modeled as a long cylinder). Using a coefficient of drag for an infinitely long cylinder of approximately two (i.e. $C_{dt} \approx 2$), we may express the moment on tether alone due to drag as (see Ref 51 pp 250-251)

$$\mathbf{M}_\mathbf{t} = \oiint \mathbf{s}\times d\mathbf{F} = \int_{-\rho_1}^{\rho_2} (\hat{\boldsymbol{\rho}}\times\hat{\mathbf{v}}_\mathbf{a}) s dF = (\hat{\boldsymbol{\rho}}\times\hat{\mathbf{v}}_\mathbf{a}) \int_{-\rho_1}^{\rho_2} s\rho(h_s)v_a{}^2 dA = (\hat{\boldsymbol{\rho}}\times\hat{\mathbf{v}}_\mathbf{a}) v_a{}^2 \cos\alpha d_t \int_{-\rho_1}^{\rho_2} s\rho(h_s) ds$$

where h_s is the altitude of the element which may be written $h_s = (h\hat{\mathbf{e}}_\mathbf{r} + s\hat{\boldsymbol{\rho}})\cdot\hat{\mathbf{e}}_\mathbf{r} = h + s\cos\phi\cos\theta$. For a more thorough discussion of the tether coefficient of drag, see Ref 52. Integrating in this manner presumes that $\cos\alpha > 0$ since a negative value would imply force acting on the backside of the elemental area, thus only the area presented to the air stream is considered.

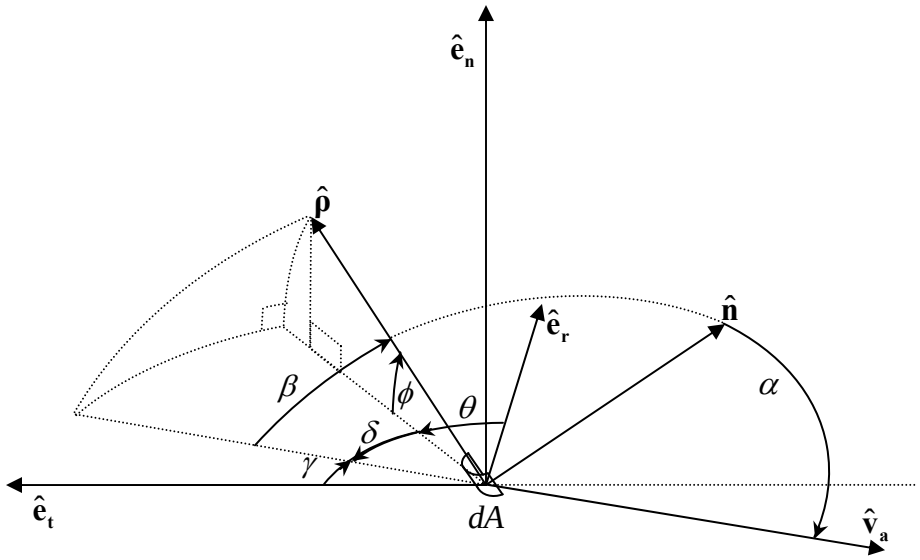

Figure 38. Tether Element and Drag Geometry

The angle of attack is defined as the angle between the unit inward normal to the elemental area, $\hat{\mathbf{n}}$, and the air stream velocity unit vector, $\hat{\mathbf{v}}_{\mathbf{a}}$ as shown in Figure 38. Using the angles defined in this figure we can determine the angle of attack in terms of the libration angles, θ and ϕ, and the flight path angle, γ, using the following spherical trigonometry relation.

$$\cos\beta = \cos\phi\cos\delta + \sin\phi\sin\delta\cos\left(\frac{\pi}{2}\right) = \cos\phi\cos\delta$$

$$\delta = \frac{\pi}{2} - \theta - \gamma \quad \therefore \quad \cos\delta = \cos\left(\frac{\pi}{2} - (\theta+\gamma)\right) = \sin(\theta+\gamma)$$

$$\cos\beta = \cos\phi\sin(\theta+\gamma)$$

$$\beta = \frac{\pi}{2} - \alpha \quad \text{since } \hat{\mathbf{n}}, \hat{\mathbf{v}}_{\mathbf{a}} \text{ and } \hat{\boldsymbol{\rho}} \text{ all lie in the same plane and } \hat{\boldsymbol{\rho}} \perp \hat{\mathbf{n}}$$

$$\therefore \quad \sin\alpha = \cos\beta = \cos\phi\sin(\theta+\gamma)$$

$$\cos\alpha = \left(1-\sin^2\alpha\right)^{1/2} = \left(1-\cos^2\phi\sin^2(\theta+\gamma)\right)^{1/2}$$

Notice that for a circular orbit, $\gamma = 0$ for all time. Additionally, if there is no out of plane motion then $\cos\alpha = \cos\theta$.

Air density is modeled as an exponentially decaying atmosphere with characteristic height (or scale height) h^*. Letting ρ_0 be the reference density at the altitude of the center of mass, then the density at the tether element location is

$$\rho(h_s) = \rho_0 e^{\frac{-(h+s\cos\phi\cos\theta)}{h^*}} = \rho_0 e^{-h/h^*} e^{\frac{-s\cos\phi\cos\theta}{h^*}} = \rho(h) e^{\frac{-s\cos\phi\cos\theta}{h^*}}$$

$$\text{where } \rho(h) = \rho_0 e^{-h/h^*}$$

Substituting these values into the tether moment equation yields

$$\mathbf{M}_{\mathbf{t}} = v^2\rho_0 e^{-h/h^*} d_t \left(1-\cos^2\phi\sin^2(\theta+\gamma)\right)^{1/2} (\hat{\boldsymbol{\rho}}\times\hat{\mathbf{v}}_{\mathbf{a}}) \int_{-\mu_m L/M_1}^{\mu_m L/M_2} s e^{\frac{-s\cos\theta\cos\phi}{h^*}} ds$$

$$\mathbf{M}_{\mathbf{t}} = v^2\rho(h) d_t \left(1-\cos^2\phi\sin^2(\theta+\gamma)\right)^{1/2} (\hat{\boldsymbol{\rho}}\times\hat{\mathbf{v}}_{\mathbf{a}}) \left(\frac{h^*}{c\phi c\theta}\right)^2 e^{\frac{-c\theta c\phi s}{h^*}} \left(-\frac{c\phi c\theta}{h^*} s - 1\right)\Bigg|_{-\mu_m L/M_1}^{\mu_m L/M_2}$$

$$= v^2\rho(h) C \left\{ e^{\frac{-c\theta c\phi\mu_m L}{h^* M_2}} \left(\frac{-c\theta c\phi\mu_m L}{h^* M_2} - 1\right) - e^{\frac{+c\theta c\phi\mu_m L}{h^* M_1}} \left(\frac{c\theta c\phi\mu_m L}{h^* M_1} - 1\right) \right\} (\hat{\boldsymbol{\rho}}\times\hat{\mathbf{v}}_{\mathbf{a}})$$

where $C = d_t \left(1-\cos^2\phi\sin^2(\theta+\gamma)\right)^{1/2} \left(\frac{h^*}{c\phi c\theta}\right)^2$.

Now the torque effect on θ due to the aerodynamic drag on the tether alone is

$$\frac{d\boldsymbol{\Omega}}{d\dot{\theta}}\cdot\mathbf{M}_{\mathbf{t}} =$$
$$v^2\rho(h)C\left\{e^{\frac{-c\theta c\phi\mu_m L}{h^* M_2}}\left(\frac{-c\theta c\phi\mu_m L}{h^* M_2}-1\right)-e^{\frac{+c\theta c\phi\mu_m L}{h^* M_1}}\left(\frac{c\theta c\phi\mu_m L}{h^* M_1}-1\right)\right\}\left(c\phi\left(s\gamma s\theta-c\gamma c\theta\right)\right)$$

where $\boldsymbol{\Omega}=\begin{bmatrix}\dot{\phi}s\theta\\-\dot{\phi}c\theta\\\dot{\nu}+\dot{\theta}\end{bmatrix}_e$ $\therefore$ $\dfrac{d\boldsymbol{\Omega}}{d\dot{\theta}}=\begin{bmatrix}0\\0\\1\end{bmatrix}_e$ and

$$\mathbf{M}_{\mathbf{t}}=v^2\rho(h)C\left\{e^{\frac{-c\theta c\phi\mu_m L}{h^* M_2}}\left(\frac{-c\theta c\phi\mu_m L}{h^* M_2}-1\right)-e^{\frac{+c\theta c\phi\mu_m L}{h^* M_1}}\left(\frac{c\theta c\phi\mu_m L}{h^* M_1}-1\right)\right\}\begin{bmatrix}c\gamma s\phi\\-s\gamma s\phi\\c\phi\left(s\gamma s\theta-c\gamma c\theta\right)\end{bmatrix}_e$$

since $\hat{\boldsymbol{\rho}}\times\hat{\mathbf{v}}_{\mathbf{a}}=\begin{vmatrix}\hat{\mathbf{e}}_{\mathbf{r}} & \hat{\mathbf{e}}_{\mathbf{t}} & \hat{\mathbf{e}}_{\mathbf{n}}\\ c\phi c\theta & c\phi s\theta & s\phi\\ -s\gamma & -c\gamma & 0\end{vmatrix}=\begin{bmatrix}c\gamma s\phi\\-s\gamma s\phi\\c\phi\left(s\gamma s\theta-c\gamma c\theta\right)\end{bmatrix}_e$

The total aerodynamic drag torque affecting θ is therefore

$$Q_{\theta a}=\mathbf{F}_{\mathbf{1}}\cdot\frac{\partial\dot{\boldsymbol{\rho}}_{\mathbf{1}}}{\partial\dot{\theta}}+\mathbf{F}_2\cdot\frac{\partial\dot{\boldsymbol{\rho}}_{\mathbf{2}}}{\partial\dot{\theta}}+\mathbf{M}_{\mathbf{t}}\cdot\frac{\partial\boldsymbol{\Omega}}{\partial\dot{\theta}}$$

$$Q_{\theta a}=v^2\rho(h)c\phi\left(c\gamma c\theta-s\gamma s\theta\right)\left\{\frac{\mu_m L}{2}\left(B_1^* e^{\frac{\mu_m Lc\phi c\theta}{M_1 h^*}}-B_2^* e^{\frac{-\mu_m Lc\phi c\theta}{M_2 h^*}}\right)-\right.$$
$$\left.C\left(e^{\frac{-c\theta c\phi\mu_m L}{h^* M_2}}\left(\frac{-c\theta c\phi\mu_m L}{h^* M_2}-1\right)-e^{\frac{+c\theta c\phi\mu_m L}{h^* M_1}}\left(\frac{c\theta c\phi\mu_m L}{h^* M_1}-1\right)\right)\right\} \qquad (60)$$

Notice that this expression reduces significantly if the assumption that the atmospheric density does not vary significantly across the length of the tether. Looking at the expansion of the exponential terms in Eq. (60) and letting $p_1=\dfrac{\mu_m Lc\phi c\theta}{M_1 h^*}$ and $p_2=\dfrac{\mu_m Lc\phi c\theta}{M_2 h^*}$ we write for a circular orbit ($\gamma=0$)

$$Q_{\theta a}=v^2\rho(h)c\phi c\theta\left\{\frac{\mu_m L}{2}\left(B_1^*\left(1+p_1+\frac{p_1^2}{2}\right)-B_2^*\left(1-p_2+\frac{p_2^2}{2}\right)\right)-\right.$$
$$\left.d_t\left(1-\mathrm{c}^2\phi\,\mathrm{s}^2\theta\right)^{1/2}\left(\frac{h^*}{c\phi c\theta}\right)^2\left(\left(1-p_2+\frac{p_2^2}{2}\right)(-p_2-1)-\left(1+p_1+\frac{p_1^2}{2}\right)(p_1-1)\right)\right\} \qquad (61)$$

$$= v^2 \rho(h) c\phi c\theta \left\{ \frac{\mu_m L}{2} \left(B_1^* (1+p_1) - B_2^* (1-p_2) \right) - d_t \left(1 - \mathrm{c}^2 \phi \mathrm{s}^2 \theta\right)^{1/2} \left(\frac{h^*}{c\phi c\theta} \right)^2 \left(p_2^2 - p_1^2 \right) \right\}$$

$$Q_{\theta a} = v^2 \rho(h) c\phi c\theta \left\{ \frac{\mu_m L}{2} \left(B_1^* (1+p_1) - B_2^* (1-p_2) \right) - \right.$$
$$\left. d_t \left(1 - \mathrm{c}^2 \phi \mathrm{s}^2 \theta\right)^{1/2} \left(\frac{h^*}{c\phi c\theta} \right)^2 \left(\left(\frac{c\phi c\theta}{h^*} \right)^2 \mu_m^2 L^2 \left(\frac{1}{M_2^2} - \frac{1}{M_1^2} \right) \right) \right\}$$

The last term in the braces is rewritten as

$$\mu_m^2 L^2 \left(\frac{1}{M_2^2} - \frac{1}{M_1^2} \right) = \left(\frac{(m_1 - m_2) L^2}{M} \right) = -2\rho_t L$$

where we have used the mass term equalities given in the kinetic energy discussion in Appendix A and the definition of the COM offset distance ρ_t given in (66). Therefore the in-plane torque is

$$Q_{\theta a} = \rho(h) v^2 L c\phi c\theta \left\{ \frac{\mu_m}{2} \left(B_1^* (1+p_1) - B_2^* (1-p_2) \right) + 2 d_t \rho_t \left(1 - \mathrm{c}^2 \phi \mathrm{s}^2 \theta\right)^{1/2} \right\}$$

which is accurate for $\left(\frac{L}{h^*} \right)^2 \ll 1$. This assumption would mean that the length of the tether is much smaller than the characteristic height of the atmosphere. For altitudes up to about 160 km, $h^* \approx 7km$. Between 160 and 400 km, h^* ranges from 30 to 60 km. If we desire a first order approximation, namely that $\frac{L}{h^*} \ll 1$, then the torque due to the tether drag would be derived as follows.

$$Q_{\theta a} = v^2 \rho(h) c\phi c\theta \left\{ \frac{\mu_m L}{2} \left(B_1^* - B_2^* \right) - d_t \left(1 - \mathrm{c}^2 \phi \mathrm{s}^2 \theta\right)^{1/2} \left(\frac{h^*}{c\phi c\theta} \right)^2 \left(- \frac{c\theta c\phi \mu_m L}{h^* M_2} - \frac{c\theta c\phi \mu_m L}{h^* M_1} \right) \right\}$$
$$= v^2 \rho(h) L c\phi c\theta \left\{ \frac{\mu_m}{2} \left(B_1^* - B_2^* \right) - d_t \left(1 - \mathrm{c}^2 \phi \mathrm{s}^2 \theta\right)^{1/2} \left(\frac{h^*}{c\phi c\theta} \right) \left(\frac{\mu_m}{M_2} + \frac{\mu_m}{M_1} \right) \right\}$$

recognizing that $\mu_m \left(\frac{1}{M_2} + \frac{1}{M_1} \right) = 1$.

And the total aerodynamic drag torque with this simplifying assumption is

$$Q_{\theta a} = v^2 \rho(h) L c\phi c\theta \left\{ \frac{\mu_m}{2} \left(B_1^* - B_2^* \right) - \frac{d_t h^*}{c\phi c\theta} \left(1 - \mathrm{c}^2 \phi \mathrm{s}^2 \theta\right)^{1/2} \right\} \tag{62}$$

To derive the torque affecting the out-of-plane libration angle ϕ we follow the same process.

$$Q_{\phi a} = \mathbf{F_1} \cdot \frac{\partial \mathbf{v_1}}{\partial \dot{\phi}} + \mathbf{F}_2 \cdot \frac{\partial \mathbf{v_2}}{\partial \dot{\phi}} + \mathbf{M_t} \cdot \frac{\partial \mathbf{\Omega}}{\partial \dot{\phi}}$$

where $\frac{\partial \mathbf{v_1}}{\partial \dot{\phi}} = \frac{\partial \dot{\boldsymbol{\rho}}_1}{\partial \dot{\phi}} = \frac{\mu_m L}{M_1}\begin{bmatrix} s\phi c\theta \\ s\phi s\theta \\ -c\phi \end{bmatrix}_e$, $\frac{\partial \mathbf{v_2}}{\partial \dot{\phi}} = \frac{\partial \dot{\boldsymbol{\rho}}_2}{\partial \dot{\phi}} = \frac{\mu_m L}{M_2}\begin{bmatrix} -s\phi c\theta \\ -s\phi s\theta \\ c\phi \end{bmatrix}_e$ and $\frac{\partial \mathbf{\Omega}}{\partial \dot{\phi}} = \begin{bmatrix} s\theta \\ -c\theta \\ 0 \end{bmatrix}_e$

The moments are

$$\mathbf{F_1} \cdot \frac{\partial \mathbf{v_1}}{\partial \dot{\phi}} = \frac{1}{2} C_{d1} A_1 \rho_0 e^{\frac{-\left(h - \frac{\mu_m L}{M_1} c\theta c\phi\right)}{h^*}} v^2 \frac{\mu_m L}{M_1} s\phi\left(-s\gamma c\theta - c\gamma s\theta\right)$$

$$= \frac{-\mu_m L}{2} \rho_0 e^{-h/h^*} v^2 s\phi\left(s\gamma c\theta + c\gamma s\theta\right) B_1^* e^{\frac{\mu_m L c\theta c\phi}{M_1 h^*}}$$

$$\mathbf{F}_2 \cdot \frac{\partial \mathbf{v_2}}{\partial \dot{\phi}} = \frac{1}{2} C_{d2} A_2 \rho_0 e^{\frac{-\left(h + \frac{\mu_m L}{M_2} c\theta c\phi\right)}{h^*}} v^2 \frac{\mu_m L}{M_2} s\phi\left(s\gamma c\theta + c\gamma s\theta\right)$$

$$= \frac{\mu_m L}{2} \rho_0 e^{-h/h^*} v^2 s\phi\left(s\gamma c\theta + c\gamma s\theta\right) B_2^* e^{\frac{-\mu_m L c\theta c\phi}{M_2 h^*}}$$

$$\mathbf{M_t} \cdot \frac{\partial \mathbf{\Omega}}{\partial \dot{\phi}} = v^2 \rho_0 e^{-h/h^*} C \left\{ e^{\frac{-c\theta c\phi \mu_m L}{h^* M_2}} \left(\frac{-c\theta c\phi \mu_m L}{h^* M_2} - 1 \right) - e^{\frac{+c\theta c\phi \mu_m L}{h^* M_1}} \left(\frac{c\theta c\phi \mu_m L}{h^* M_1} - 1 \right) \right\} s\phi\left(s\gamma c\theta + c\gamma s\theta\right)$$

The total moment about the COM affecting ϕ due to aerodynamic drag is

$$Q_{\phi a} = v^2 \rho(h) s\phi\left(s\gamma c\theta + c\gamma s\theta\right) \left\{ \frac{\mu_m L}{2} \left(B_2^* e^{\frac{-\mu_m L c\theta c\phi}{M_2 h^*}} - B_1^* e^{\frac{\mu_m L c\theta c\phi}{M_1 h^*}} \right) + \right.$$

$$\left. C \left(e^{\frac{-c\theta c\phi \mu_m L}{h^* M_2}} \left(\frac{-c\theta c\phi \mu_m L}{h^* M_2} - 1 \right) - e^{\frac{+c\theta c\phi \mu_m L}{h^* M_1}} \left(\frac{c\theta c\phi \mu_m L}{h^* M_1} - 1 \right) \right) \right\}$$

When the tether is significantly shorter than the characteristic height of the atmosphere $\left(\frac{L}{h^*} \ll 1\right)$, the air density is considered constant along the tether and the following simplifications can be made using the same procedure that produced Eq. (62).

$$Q_{\phi a} = v^2 \rho(h) s\phi\left(s\gamma c\theta + c\gamma s\theta\right) \left\{ \frac{\mu_m L}{2} \left(B_2^* - B_1^* \right) - C \frac{\mu_m L c\theta c\phi}{h^*} \left(\frac{1}{M_2} + \frac{1}{M_1} \right) \right\}$$

$$Q_{\phi a} = v^2 \rho(h) s\phi \left(s\gamma c\theta + c\gamma s\theta\right)\left\{\frac{\mu_m L}{2}\left(B_2^* - B_1^*\right) - d_t\left(1 - \mathrm{c}^2\,\phi\,\mathrm{s}^2\left(\theta+\gamma\right)\right)^{1/2}\frac{Lh^*}{c\theta c\phi}\right\}$$

Furthermore, for circular orbits $\gamma = 0$ for all time and we have

$$Q_{\phi a} = v^2 \rho(h) s\phi s\theta L\left\{\frac{\mu_m}{2}\left(B_2^* - B_1^*\right) - d_t\left(1 - \mathrm{c}^2\,\phi\,\mathrm{s}^2\,\theta\right)^{1/2}\frac{h^*}{c\theta c\phi}\right\} \tag{63}$$

As we shall see later, this torque affecting out-of-plane libration vanishes near the equilibrium point where $\theta \to 0,\ \phi \to 0$.

The generalized force due to air drag along the tether length is a force given by

$$Q_{La} = \mathbf{F_1}\cdot\frac{\partial \mathbf{v_1}}{\partial \dot{L}} + \mathbf{F}_2\cdot\frac{\partial \mathbf{v_2}}{\partial \dot{L}} + \mathbf{M_t}\cdot\frac{\partial \mathbf{\Omega}}{\partial \dot{L}}$$

Since $\frac{\partial \mathbf{\Omega}}{\partial \dot{L}} = 0$ the last term drops out. The remaining two are determined by

$$\frac{\partial \mathbf{v_1}}{\partial \dot{L}} = \frac{\partial \dot{\boldsymbol{\rho}}_1}{\partial \dot{L}} = \frac{-\mu_m}{M_1}\begin{bmatrix} c\phi c\theta \\ c\phi s\theta \\ s\phi \end{bmatrix}_e \text{ and } \frac{\partial \mathbf{v_2}}{\partial \dot{L}} = \frac{\partial \dot{\boldsymbol{\rho}}_2}{\partial \dot{L}} = \frac{\mu_m}{M_2}\begin{bmatrix} c\phi c\theta \\ c\phi s\theta \\ s\phi \end{bmatrix}_e$$

$$\mathbf{F_1}\cdot\frac{\partial \mathbf{v_1}}{\partial \dot{L}} = \frac{1}{2}C_{d1}A_1\rho_0 v^2 e^{\frac{-\left(h - \frac{\mu_m L}{M_1}c\phi c\theta\right)}{h^*}}\frac{\mu_m}{M_1}c\phi\left(s\gamma c\theta + c\gamma s\theta\right)$$

$$\mathbf{F}_2\cdot\frac{\partial \mathbf{v_2}}{\partial \dot{L}} = -\frac{1}{2}C_{d2}A_2\rho_0 v^2 e^{\frac{-\left(h + \frac{\mu_m L}{M_2}c\phi c\theta\right)}{h^*}}\frac{\mu_m}{M_2}c\phi\left(s\gamma c\theta + c\gamma s\theta\right)$$

$$Q_{La} = \frac{\mu_m}{2}v^2\rho(h)c\phi\left(s\gamma c\theta + c\gamma s\theta\right)\left(B_1^* e^{\frac{\mu_m L c\phi c\theta}{M_1 h^*}} - B_2^* e^{\frac{-\mu_m L c\phi c\theta}{M_2 h^*}}\right)$$

When $L/h^* \ll 1$, then the equation reduces.

$$Q_{La} = \frac{\mu_m}{2}v^2\rho(h)c\phi\left(s\gamma c\theta + c\gamma s\theta\right)\left(B_1^* - B_2^*\right)$$

If the tether is in a circular orbit such that $\gamma = 0$ then the equation further reduces to

$$Q_{La} = \frac{\mu_m}{2}v^2\rho(h)c\phi s\theta\left(B_1^* - B_2^*\right)$$

Lorenz Force

When there is a current driven through the conducting tether wire in a magnetic field a force is created in the direction mutually perpendicular to the local magnetic field lines and the current direction according to the relation $d\mathbf{F}_e = Id\mathbf{L}\times\mathbf{B}$ where I is the current, $\mathbf{B}$ is the Earths magnetic flux density and $\mathbf{L}$ is the length vector along the direction of the straight tether. For a uniform current in a straight line electromagnetic tether we simply have $\mathbf{F}_e = I\mathbf{L}\times\mathbf{B}$. Using a non-tilted dipole model of the Earth's magnetic field, we can write the magnetic flux density direction as a function of true anomaly, ν, magnetic inclination, i, and the argument of perigee, ω_p. The magnitude depends on the magnetic dipole of the Earth, γ_m $\left(\approx 8e6\ \frac{N}{A\cdot m}km^3\right)$, and the radial distance from the Earth's center, r. The magnetic flux density is modeled here as

$$\mathbf{B} = \frac{\gamma_m}{r^3}\begin{bmatrix} -2\sin\left(\omega_p+\nu\right)\sin i \\ \cos\left(\omega_p+\nu\right)\sin i \\ \cos i \end{bmatrix}_e = \begin{bmatrix} B_r \\ B_t \\ B_n \end{bmatrix}_e$$

On the surface of Earth, $B = \frac{\gamma_m}{r^3} = \frac{8e6}{6378^3} = 3e^{-}5\frac{N}{A\cdot m}$. Another 250 km up from the surface, the value is about $2.7e^{-}5\frac{N}{A\cdot m}$.

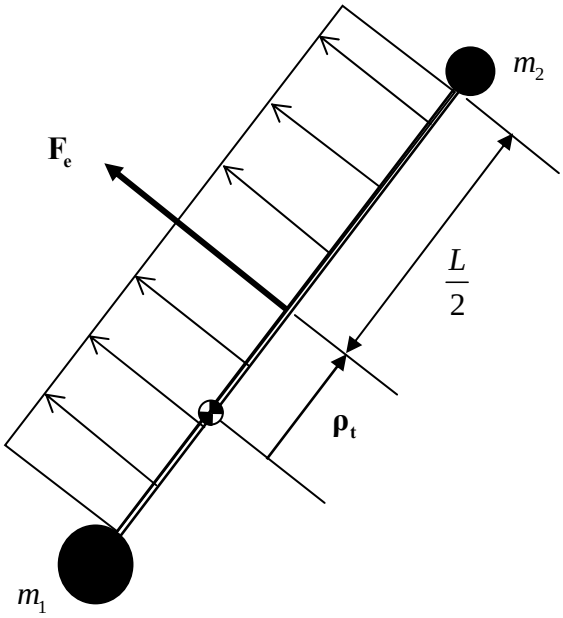

Figure 39. Electrodynamic Tether with Lorenz Force Loading

A rotating Earth with a tilted dipole would yield a time varying magnetic field, however we will assume that the motion of the satellite is much faster than the rotational motion of the Earth. This assumption was relaxed in Chapter III where multiple time scale optimization was addressed, however for derivation purposes the rotating tilted dipole of the Earth's magnetic field may be ignored without loss of generality. The electromagnetic force along the tether length varies as the cube of the distance to the center of the earth. This resultant force may be written as

$$\mathbf{F_e} = \int_L d\mathbf{F} = \int_{-\rho_1}^{\rho_2} I\hat{\boldsymbol{\rho}} \times \mathbf{B} ds = \int_{-\rho_1}^{\rho_2} I\hat{\boldsymbol{\rho}} \times \hat{\mathbf{b}} \frac{\gamma_m}{(r-s)^3} ds = I\gamma_m \left(\hat{\boldsymbol{\rho}} \times \hat{\mathbf{b}}\right) \int_{-\rho_1}^{\rho_2} \frac{1}{(r-s)^3} ds$$

Using a binomial expansion of the integrand, we have

$$\mathbf{F_e} = I\gamma_m \left(\hat{\boldsymbol{\rho}} \times \hat{\mathbf{b}}\right) \int_{-\rho_1}^{\rho_2} r^{-3} \left(1 - \frac{s}{r} + \left(\frac{s}{r}\right)^2\right) ds = \frac{I\gamma_m}{r^3} \left(\hat{\boldsymbol{\rho}} \times \hat{\mathbf{b}}\right) \left(s - \frac{s^2}{2r} + \frac{s^3}{3r^2} + h.o.t.\right) \Bigg|_{-\rho_1 = -\frac{\mu_m L}{M_1}}^{\rho_2 = \frac{\mu_m L}{M_2}}$$

Ignoring the higher order terms, following through with mass term substitutions and rearranging we write

$$\mathbf{F_e} = \frac{IL\gamma_m}{r^3} \left(\hat{\boldsymbol{\rho}} \times \hat{\mathbf{b}}\right) \left(1 - \left(\frac{m_1 - m_2}{2M}\right) \frac{L}{r} + \left(\frac{1}{12} + \left(\frac{m_1 - m_2}{2M}\right)^2\right) \frac{L^2}{r^2}\right)$$

A simplifying approximation is that the length of the tether is significantly shorter than the distance between the center of mass and the center of the Earth $\left(L/r \ll 1\right)$. This means that the magnetic field strength and direction is approximately the same across the length of the tether. The model is then simply a uniform force distribution along the tether as shown in Figure 39. For analyses in which we have already assumed the length to be short compared to the atmospheric scale height (40-50 km) when modeling the atmospheric drag, this approximation is justified. The resultant force, $\mathbf{F_e}$, may be used to determine the moment about the COM with moment arm $\boldsymbol{\rho}_\mathbf{t} = \dfrac{\left(m_2 - m_1\right)L}{2M}\hat{\boldsymbol{\rho}}$. The force is

$$\mathbf{F_e} = I\mathbf{L}\times\mathbf{B} = IL\hat{\boldsymbol{\rho}}\times\mathbf{B}$$

$$\text{where } \hat{\boldsymbol{\rho}}\times\mathbf{B} = \begin{vmatrix} \hat{\mathbf{e}}_\mathbf{r} & \hat{\mathbf{e}}_t & \hat{\mathbf{e}}_n \\ c\phi c\theta & c\phi s\theta & s\phi \\ B_r & B_t & B_n \end{vmatrix} \text{ and } \mathbf{F_e} = IL\begin{bmatrix} B_n c\phi s\theta - B_t s\phi \\ B_r s\phi - B_n c\phi c\theta \\ B_t c\phi c\theta - B_r c\phi s\theta \end{bmatrix}_e$$

The torque affecting the θ state is

$$Q_{\theta e} = \mathbf{F_e}\cdot\frac{\partial\mathbf{v}}{\partial\dot{\theta}} = \mathbf{F_e}\cdot\frac{\partial\left(\dot{\mathbf{r}}+\dot{\boldsymbol{\rho}}_\mathbf{t}\right)}{\partial\dot{\theta}} = \mathbf{F_e}\cdot\left(\frac{\partial\dot{\mathbf{r}}}{\partial\dot{\theta}} + \frac{\partial\boldsymbol{\rho}_\mathbf{t}'}{\partial\dot{\theta}} + \frac{\partial\left(\boldsymbol{\Omega}+\boldsymbol{\rho}_\mathbf{t}\right)}{\partial\dot{\theta}}\right) = \mathbf{F_e}\cdot\left(\frac{\partial\boldsymbol{\Omega}}{\partial\dot{\theta}}\times\boldsymbol{\rho}_\mathbf{t} + \boldsymbol{\Omega}\times\frac{\partial\boldsymbol{\rho}_\mathbf{t}}{\partial\dot{\theta}}\right)$$

$$\text{where } \frac{\partial\dot{\mathbf{r}}}{\partial\dot{\theta}} = \frac{\partial\boldsymbol{\rho}_\mathbf{t}'}{\partial\dot{\theta}} = \frac{\partial\boldsymbol{\rho}_\mathbf{t}}{\partial\dot{\theta}} = 0$$

$$Q_{\theta e} = \mathbf{F_e}\cdot\left(\frac{\partial\boldsymbol{\Omega}}{\partial\dot{\theta}}\times\boldsymbol{\rho}_\mathbf{t}\right) = \frac{\partial\boldsymbol{\Omega}}{\partial\dot{\theta}}\cdot\boldsymbol{\rho}_\mathbf{t}\times\mathbf{F_e} = \frac{\partial\boldsymbol{\Omega}}{\partial\dot{\theta}}\cdot\mathbf{M_e}$$

$$Q_{\theta e} = \frac{IL^2\left(m_2 - m_1\right)}{2M}\left(c\phi c\theta s\phi B_r + s\phi c\phi s\theta B_t - c^2\phi B_n\right) \tag{64}$$

The torque affecting ϕ is

$$Q_{\phi e} = \mathbf{F_e}\cdot\frac{\partial\mathbf{v}}{\partial\dot{\phi}} = \frac{\partial\boldsymbol{\Omega}}{\partial\dot{\phi}}\cdot\boldsymbol{\rho}_\mathbf{t}\times\mathbf{F_e} \text{ where } \frac{\partial\boldsymbol{\Omega}}{\partial\dot{\phi}} = \begin{bmatrix} s\theta \\ -c\theta \\ 0 \end{bmatrix}_e$$

$$Q_{\phi e} = \frac{IL^2\left(m_2 - m_1\right)}{2M}\left(-s\theta B_r + c\theta B_t\right) \tag{65}$$

There is no tension in the wire created by the Lorenz force since the force is perpendicular to the wire so no work is being done to move the end-bodies toward or away from each other.

$$Q_{Le} = \frac{\partial \mathbf{v}}{\partial \dot{L}} \cdot \mathbf{F_e} \text{ where } \frac{\partial \mathbf{v}}{\partial \dot{L}} = \frac{\partial\left(\boldsymbol{\rho}' + \boldsymbol{\Omega} \times \boldsymbol{\rho}\right)}{\partial \dot{L}} = \frac{\partial \boldsymbol{\rho}'}{\partial \dot{L}} = \frac{\partial\left(\dot{L}\hat{\boldsymbol{\rho}}\right)}{\partial \dot{L}} = \hat{\boldsymbol{\rho}} = \begin{bmatrix} c\phi c\theta \\ c\phi s\theta \\ s\phi \end{bmatrix}_e$$

$$Q_{Le} = \hat{\boldsymbol{\rho}} \cdot \mathbf{F_e} = 0 \text{ since } \hat{\boldsymbol{\rho}} \perp \mathbf{F_e}$$

The total generalized forces (torques) are the sum of those due to the electrodynamic and aerodynamic forces.

$$Q_\theta = Q_{\theta a} + Q_{\theta e}$$
$$Q_\phi = Q_{\phi a} + Q_{\phi e}$$
$$Q_L = Q_{La} + Q_{Le}$$

Now these values may be substituted into the right hand sides of the equations of motion (Eqs. (57), (58) and (59)). For purposes of this research, the electrodynamic tether will be controlled using the current in the wire.

Appendix B: Reduced Mass Derivation

In order to capture the mass of the tether and end-masses of the "dumbbell" tether model, a reduced mass is used to simplify the equations of motion. Starting with the geometry depicted in Figure 40, we can write the positions of ρ_1, ρ_2 and ρ_t relative to the COM.

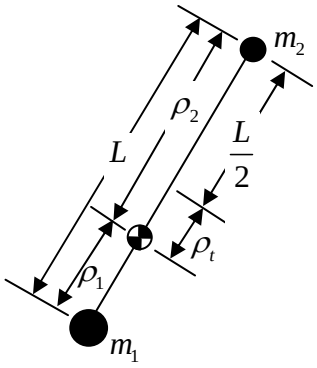

Figure 40. Tether Mass Distribution Geometry

Calculating the distances from each end-mass to the COM we have

$$\rho_1 = \frac{m_t \frac{L}{2} + m_2 L}{m_1 + m_2 + m_t} = \frac{M_2}{M} L = \frac{\mu_m}{M_1} L$$

$$\rho_2 = \frac{m_t \frac{L}{2} + m_1 L}{m_1 + m_2 + m_t} = \frac{M_1}{M} L = \frac{\mu_m}{M_2} L$$

where $M_1 = m_1 + \frac{m_t}{2}$, $M_2 = m_2 + \frac{m_t}{2}$, $M = m_1 + m_2 + m_t$ and $\mu_m = \frac{M_1 M_2}{M}$.

The distance from the system COM and the tether COM located at the midpoint of the tether is given by

$$\rho_t = \frac{m_1\left(-\frac{L}{2}\right) + m_2\left(\frac{L}{2}\right)}{m_1 + m_2 + m_t} = \frac{\left(m_2 - m_1\right)}{2M} L \tag{66}$$

The equivalent reduced mass, μ_e, given in equations (55) and (56) may be reduced as follows.

$$\mu_e = \mu_m{}^2\left(\frac{m_1}{M_1{}^2}+\frac{m_2}{M_2{}^2}\right)+\frac{m_t}{3}\left(\frac{M_1{}^3+M_2{}^3}{M^3}\right)$$
$$= \mu_m{}^2\left(\frac{m_1+\frac{m_t}{2}}{M_1{}^2}+\frac{m_2+\frac{m_t}{2}}{M_2{}^2}-\frac{1}{2}\left(\frac{m_t}{M_1{}^2}+\frac{m_t}{M_2{}^2}\right)\right)+\frac{m_t}{3}\left(\frac{M_1{}^3+M_2{}^3}{M^3}\right)$$

$$= \mu_m{}^2\left(\frac{M_1}{M_1{}^2}+\frac{M_2}{M_2{}^2}-\frac{m_t}{2}\left(\frac{1}{M_1{}^2}+\frac{1}{M_2{}^2}\right)\right)+\frac{m_t}{3}\left(\frac{M_1{}^3+M_2{}^3}{M^3}\right)$$
$$= \mu_m-\frac{m_t}{2}\frac{M\left(M_2{}^2+M_1{}^2\right)}{M^3}+\frac{m_t}{3}\left(\frac{M_1{}^3+M_2{}^3}{M^3}\right)$$
$$= \mu_m-\frac{m_t}{6M^3}\left\{3\left(M_1+M_2\right)\left(M_2{}^2+M_1{}^2\right)-2\left(M_1{}^3+M_2{}^3\right)\right\}$$
$$= \mu_m-\frac{m_t}{6M^3}\left\{M_1{}^3+3M_1{}^2M_2+3M_1M_2{}^2-M_2{}^3\right\}$$
$$= \mu_m-\frac{m_t}{6M^3}\left(M_1+M_2\right)^3=\mu_m-\frac{m_t}{6M^3}M^3$$
$$= \mu_m-\frac{m_t}{6}$$

Notice that if we approximate the tether mass as zero we are left with the more familiar two body reduced mass.

$$\mu_e=\left(\mu_m-\frac{m_t}{6}\right)\Bigg|_{m_t=0}=\frac{m_1m_2}{m_1+m_2}$$

Many analysts prefer to model the system as a dominant end-mass with all other masses negligible. An example is the space shuttle or space station with $m_t, m_2 \ll m_1$. In this case, mass terms become

$$M = M_1, \mu_m = \frac{M_1M_2}{M_1} = M_2 = m_2+\frac{m_t}{2}$$

and the equivalent reduced mass reduces to

$$\mu_e = m_2+\frac{m_t}{2}-\frac{m_t}{6}=m_2+\frac{m_t}{3}$$

Notice that $\left(m_2 + \frac{m_t}{3}\right)L^2$ is the moment of inertia of a mass on the end of a rigid rod about an axis through the other end of the rod.

It may be desirable to simulate the tether using finite elements. The elements may be modeled as straight bar links with no end-masses, only tether mass. In this case the reduced masses for each element may be approximated in the following manner.

$$m_1 = m_2 = 0$$
$$\Rightarrow \mu_m = \frac{m_t}{4}, \mu_e = \frac{m_t}{12}$$

This effective mass, when multiplied by L^2, is the moment of inertia about the center of a uniform density rod.

Appendix C: Tether Moment Of Inertia

The derivation of the specific inertia dyadic is derived in several dynamics texts (see [53] for example), but will be repeated here for convenience. From a vector product identity, we may write

$$\begin{aligned}(\boldsymbol{\Omega}\times\hat{\boldsymbol{\rho}})\cdot(\boldsymbol{\Omega}\times\hat{\boldsymbol{\rho}}) &= \sum(\boldsymbol{\Omega}\cdot\boldsymbol{\Omega})(\hat{\boldsymbol{\rho}}\cdot\hat{\boldsymbol{\rho}})-(\boldsymbol{\Omega}\cdot\hat{\boldsymbol{\rho}})^2\\ &= \sum\boldsymbol{\Omega}\cdot(\hat{\boldsymbol{\rho}}\cdot\hat{\boldsymbol{\rho}})\mathbf{I}\cdot\boldsymbol{\Omega}-(\boldsymbol{\Omega}\cdot\hat{\boldsymbol{\rho}})(\boldsymbol{\Omega}\cdot\hat{\boldsymbol{\rho}})\\ &= \sum\boldsymbol{\Omega}\cdot\left(\rho^2\mathbf{I}\right)\cdot\boldsymbol{\Omega}-(\boldsymbol{\Omega}\cdot\hat{\boldsymbol{\rho}})(\hat{\boldsymbol{\rho}}\cdot\boldsymbol{\Omega})\\ &= \sum\boldsymbol{\Omega}\cdot\left(\rho^2\mathbf{I}\right)\cdot\boldsymbol{\Omega}-\boldsymbol{\Omega}\cdot(\hat{\boldsymbol{\rho}}\hat{\boldsymbol{\rho}})\cdot\boldsymbol{\Omega}\\ &= \sum\boldsymbol{\Omega}\cdot\left(\rho^2\mathbf{I}-\hat{\boldsymbol{\rho}}\hat{\boldsymbol{\rho}}\right)\cdot\boldsymbol{\Omega}\\ &= \boldsymbol{\Omega}\cdot\overline{\overline{\mathbf{J}}}\cdot\boldsymbol{\Omega}\end{aligned}$$

The specific inertia tensor is given by $\overline{\overline{\mathbf{J}}}$. This tensor expression in matrix form is

$$(\boldsymbol{\Omega}\times\hat{\boldsymbol{\rho}})\cdot(\boldsymbol{\Omega}\times\hat{\boldsymbol{\rho}}) = \boldsymbol{\Omega}^T\left[\rho^2\mathbf{I}-\hat{\boldsymbol{\rho}}\hat{\boldsymbol{\rho}}^T\right]\boldsymbol{\Omega} = \boldsymbol{\Omega}^T\mathbf{J}\boldsymbol{\Omega}$$

Because $\hat{\boldsymbol{\rho}}$ is a unit vector, we recognize that $\hat{\boldsymbol{\rho}}\cdot\hat{\boldsymbol{\rho}} = \rho^2 = 1$. In our case, we can express the vectors in the rotating e-frame, thus the quantity $(\boldsymbol{\Omega}\times\boldsymbol{\rho})\cdot(\boldsymbol{\Omega}\times\boldsymbol{\rho})$ may be computed as follows.

$$(\boldsymbol{\Omega}\times\hat{\boldsymbol{\rho}}) = \begin{vmatrix}\hat{\mathbf{e}}_\mathbf{r} & \hat{\mathbf{e}}_\mathbf{t} & \hat{\mathbf{e}}_\mathbf{n}\\ \dot{\phi}s\theta & -\dot{\phi}c\theta & \dot{\nu}+\dot{\theta}\\ c\phi c\theta & c\phi s\theta & s\phi\end{vmatrix} = \begin{bmatrix}-\dot{\phi}c\theta s\phi-(\dot{\nu}+\dot{\theta})c\phi s\theta\\ c\phi c\theta(\dot{\nu}+\dot{\theta})-\dot{\phi}s\phi s\theta\\ \dot{\phi}c\phi\end{bmatrix}_e$$

$$\begin{aligned}(\boldsymbol{\Omega}\times\hat{\boldsymbol{\rho}})\cdot(\boldsymbol{\Omega}\times\hat{\boldsymbol{\rho}}) &= \dot{\phi}^2c^2\theta s^2\phi+2\dot{\phi}(\dot{\nu}+\dot{\theta})c\phi c\theta s\phi s\theta+c^2\phi s^2\theta(\dot{\nu}+\dot{\theta})^2+\\ &\quad c^2\phi c^2\theta(\dot{\nu}+\dot{\theta})^2-2\dot{\phi}(\dot{\nu}+\dot{\theta})c\phi c\theta s\phi s\theta+\dot{\phi}^2s^2\theta s^2\phi+\dot{\phi}^2c^2\phi\\ &= c^2\phi(\dot{\nu}+\dot{\theta})^2+\dot{\phi}^2\end{aligned}$$

This result is of course the same as that achieved using the specific inertia tensor in the kinetic energy formulation. Using the equivalent mass μ_e which accounts for end-masses and the tether mass, the radius of gyration can be taken as that of a very thin rod.

Appendix D: Operational Limitations

Choosing a proper maximum allowable rms control current is important to ensure feasible EDT designs. Permitting too much current can cause a flexible tether to curve too much, tus negating the "dumbbell" model used by the controller. If the EDT system is not capable of driving enough average current through the wire, then drag will overpower the electrodynamic thrust and the EDT will reenter the atmosphere. The subject of this appendix is to determine bounds on the maximum allowable current with which we may constrain the optimal control problems presented in Chapter III through Chapter V.

Preventing Reentry

There are many forces acting on the electrodynamic tether besides gravity. The predominant two are the drag force and, when the electrodynamic tether is actively thrusting, the Lorenz force (see Figure 1). If the cumulative drag force is greater than the Lorenz thrust, then the EDT will reenter the atmosphere. To determine the tether system design requirements to compensate for atmospheric drag to prevent reentry we look at approximate models for the atmosphere and Earth's magnetic field. The atmosphere is modeled as having exponentially decaying air density with a scale height $h^* = 44$ km and a reference altitude and density of $h_o = 250$ km and $\rho_o = 6e-11$ kg/m^3 respectively. In a circular orbit the drag force will always act opposite the direction of motion (i.e. the $-\hat{\mathbf{e}}_\mathbf{t}$ direction). The drag magnitude on the two endmasses is

$$F_{a1} + F_{a2} = \frac{1}{2} v^2 \rho_o e^{\frac{-(h-h_{ref})}{h^*}} \left(C_{d1}A_1 + C_{d1}A_1\right) = \frac{1}{2}\left(\frac{\mu_g}{r}\right)\rho(h)\left(C_{d1}A_1 + C_{d2}A_2\right) \tag{67}$$

where $\rho(h) = \rho_o e^{\frac{-(h-h_{ref})}{h^*}}$. The drag force on the tether alone is approximated using a constant force distribution along the tether. This approximation is adequate for this calculation when the COM of the system is close to the midpoint of the tether. Justification of this approximation is shown as follows. Letting $dA = d_t ds$, the force due to the drag on the tether alone is

$$F_{tether} = \int dF = \frac{1}{2} C_{dt} v^2 \int \rho dA = \frac{1}{2} C_{dt} v^2 \rho(h) d_t \int_{-L/2}^{L/2} e^{\frac{-s}{h^*}} ds = C_{dt} v^2 \rho(h) d_t h^* \sinh\left(\frac{L}{2h^*}\right)$$

Letting $z = \frac{L}{2h^*}$, an expansion of the hyperbolic sine function is

$$\sinh(z) = z + \frac{z^3}{6} + h.o.t$$

If we are willing to ignore $O(z^3)$ terms, then we may let $\sinh(z) = z$ and write

$$F_{tether} = \frac{1}{2} C_{dt} v^2 \rho(h) d_t L$$

where we recognize that $d_t L$ is the cross sectional area of the tether. Only in very long tethers ($L > 35$ km) at low altitudes ($h < 250$ km) could the $O(z^3)$ terms be too significant to ignore. The total aerodynamic drag force on the entire system is the sum of the drag forces on both end masses and on the tether itself.

$$D = \frac{1}{2} v^2 \rho(h)\left(F_{a1} + F_{a2} + F_{tether}\right) = \frac{1}{2}\left(\frac{\mu_g}{r}\right)\rho(h)\left(C_{d1}A_1 + C_{d2}A_2 + C_{dt}Ld_t\right) \tag{68}$$

The maximum Lorenz force on the other hand depends on the maximum average current that is permitted through the wire and, for the nadir-pointing tether in a circular orbit, will only have a component of thrust in the positive velocity direction $\hat{\mathbf{e}}_\mathbf{t}$ perpendicular to the normal component of the local magnetic field.

$$F = \left(I_m L \hat{\mathbf{e}}_\mathbf{r} \times \mathbf{B}\right) \cdot \hat{\mathbf{e}}_\mathbf{t}$$

For a circular orbit the force magnitude is

$$F = I_m L B_o \left(\frac{r_o}{r}\right)^3 \cos i \tag{69}$$

where the circular reference orbit is taken to be at a 250 km altitude where $B_o = 2.7e-5 \ \frac{\mathrm{N}}{\mathrm{A}\cdot\mathrm{m}}$. The magnetic flux density component normal to the orbital plane decays as the magnetic inclination i approaches 90 degrees, and thus so does the transverse force component of a nadir-pointing EDT. For a given orbit in a drag environment, the average Lorenz force must be greater than the average drag or the EDT will lose altitude quickly and burn up on reentry.

It is desirable to graph the force balance altitudes for various tether designs from which we can perform design trade studies. Knowing the lowest feasible altitude one can achieve for various electrodynamic tether designs, one can determine a control strategy that avoids inadvertent reentry. The ratio of average forces given in Eq. (68) and Eq. (69) is

$$\frac{F}{D} = \frac{I_m L B_o \left(\frac{r_o}{r}\right)^3 \cos i}{\frac{1}{2}\frac{\mu_g}{r_o}\left(\frac{r_o}{r}\right)\rho_o e^{\frac{-(h-h_0)}{h^*}}\left(C_{d1}A_1 + C_{d2}A_2 + C_{dt}Ld_t\right)}$$

Separating the reference altitude parameters (r_o, B_o and ρ_o) and assuming that the coefficients of drag are all approximately 2, we write the force ratio in terms of the radial distance or equivalently the altitude.

$$\frac{F}{D} = \frac{I_m L B_o \cos i}{v_o^2 \rho_o A}\left(\frac{r_o}{r}\right)^2 \exp\left[\frac{r_o}{h^*}\left(\frac{r}{r_o} - 1\right)\right] \tag{70}$$

where $A = A_1 + A_2 + d_t L$ is the total system cross sectional area. To avoid drag induced orbit decay, the average available Lorenz force must overcome the average drag force, i.e. $\frac{F}{D} \geq 1$. A graph depicting the force ratio as given by Eq. (70) is shown in Figure 41 for a 2 Amp EDT in a circular equatorial orbit with the force balance condition depicted as a vertical dashed line. The graph clearly shows that long skinny tethers permit orbits at lower altitudes than short wide tethers which are more susceptible to drag and do not generate as much thrust. Varying design parameters such as the maximum average current or orbit parameters such as the inclination will shift along the curves according to Eq. (70). For instance, increasing the orbit inclination reduces average normal component of the magnetic flux density. This component is the only one that contributes to forward thrust in a nadir-pointing EDT, so reducing it

diminishes the system's boosting capability and as a result the available thrusting force to overcome drag is reduced thus reducing the margin to the force balance altitude (or forces higher force balance altitude). Increasing the maximum allowable control current increases the available thrusting force and shifts the curves right, resulting in a lower force balance altitude (or increases margin to force balance altitude). This graph is useful for design trade studies to determine the minimum force required to maintain a given orbit. The upper bound on the generated force is limited by the tether quasi-equilibrium curvature described in Appendix D.

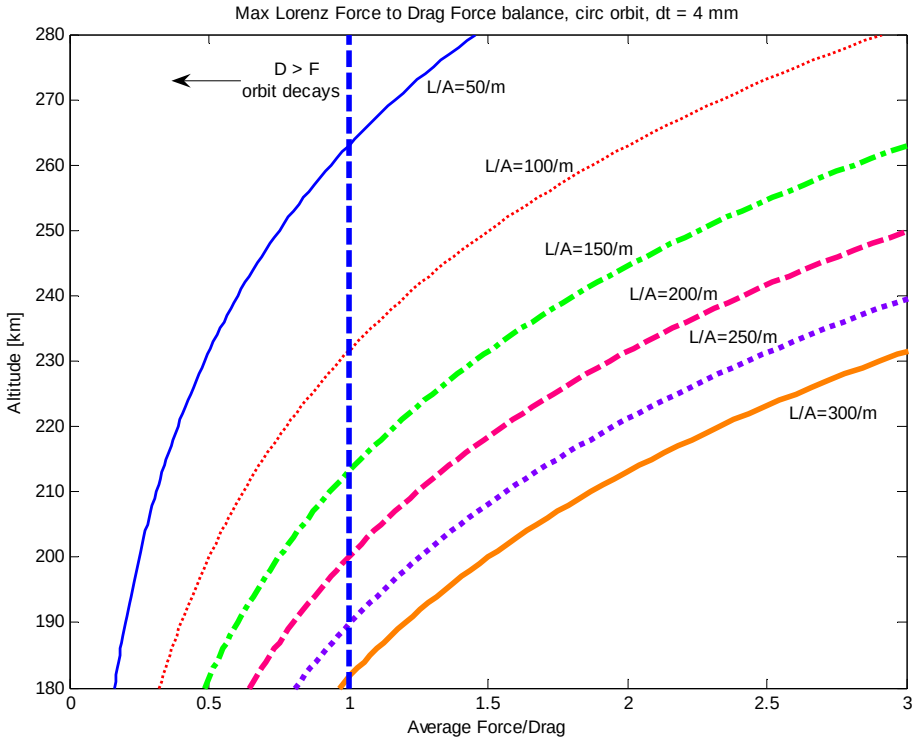

Figure 41. Maximum Lorenz Force to Drag Force Ratio at the Magnetic Equator

It is should be recognized that there are other considerations that factor into the design requirements such as ohmic losses in the conducting wire, cosine losses due to non-vertical wire orientation in a spinning or librating tether, and even non-operation during eclipse times. The design limits presented here represent an absolute lower bound on the average current, therefore the peak current available for a

real system would need to be higher than this average value. The upper bound on the allowable control current is driven by the tether length and diameter, and is described in the following section.

Validity of a Straight Tether Model

To control an electrodynamic tether, it is important to understand the tether shape. Simpler control laws using current through the conducting wire are available when we assume that the tether lies along a straight line between the two end-masses. To justify this approximation, we need an adequate shape model with which we can determine the tether constraints that maintain a relatively straight line. For a given orbit, the EDT's maximum current, length and diameter all factor into the tether shape and vibration dynamics. These parameters must be considered to ensure feasible control solutions. An approximate model using spectral separation developed by Von Flotow (Ref 54 pp 76-77) will serve this purpose. An outline of these approximations is given here.

Because the dynamics of the flexible tether experiences fast motion (longitudinal vibration along the tether) and slow motion (lateral vibration), we may view the slow dynamics as forming an equilibrium with respect to the fast dynamics. A quasi-equilibrium state may be reached in slow time when the lateral force distribution along a vertical wire is balanced by gravity gradient and tension forces. Viewing the quasi-equilibrium in this manner permits us to determine an instantaneous tether shape using the following equation.

$$\frac{\partial}{\partial s}\left(\tau \frac{\partial \mathbf{R}}{\partial s}\right) + \mathbf{f}_{\mathbf{ext}} = 0$$

where s is the distance along the strained arc-length of the tether subject to tension, τ , and external forces per unit length, $\mathbf{f}_{\mathbf{ext}}$, such as drag and Lorenz forces (Figure 42).

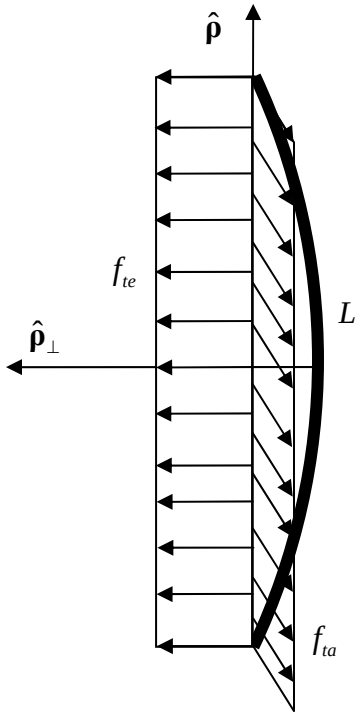

Figure 42. Tether Curvature Due To Lorenz and Aerodynamic Force Distribution

The vector position of the tether is $\mathbf{R}$, thus the equilibrium radius of curvature is its magnitude R. The tether does not curve very much and we can approximate it as that of a circular arc of radius R. If we assume that the tether mass is much less than the end-body masses, then we can assume the tension is independent of s. At equilibrium conditions with these assumptions, the tether radius of curvature is $R = \frac{\tau}{f_t}$ where f_t is the total external force density component in the $\hat{\mathbf{e}}_{\mathbf{t}}$ direction perpendicular to the line between m_1 and m_2. This lateral force density is measured in units of force per unit length. Tether curvature in the $\hat{\mathbf{e}}_{\mathbf{r}} - \hat{\mathbf{e}}_{\mathbf{t}}$ plane is depicted in Figure 43 with $\phi = 0$.

The curve angle ψ may be written

$$2\psi = \frac{L}{R} \Rightarrow \psi = \frac{Lf_t}{2\tau} \tag{71}$$

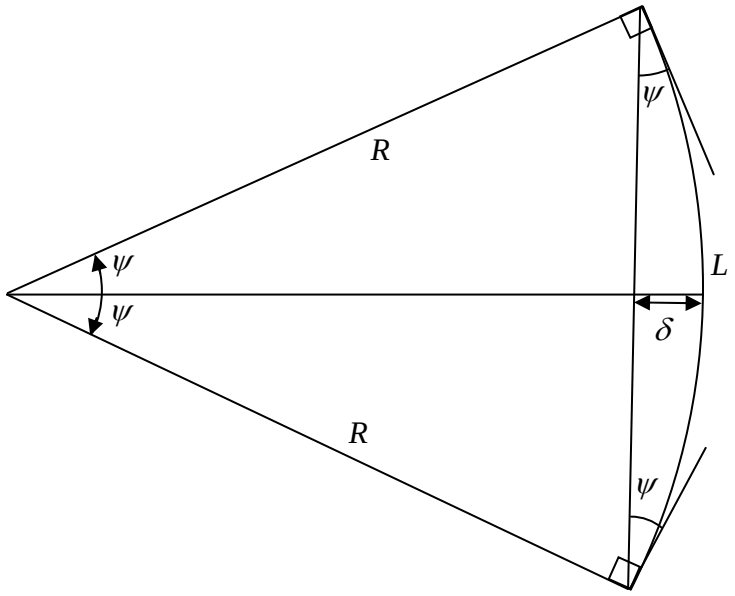

Figure 43. Curved Tether Geometry

The tether shape is determined by its tension, length and transverse component of external forces acting on it. To justify a straight-line tether assumption in the dynamic equations and subsequent control laws, we cannot allow the tether to curve appreciably under the distributed loads along the tether to the extent that the resultant force is significantly smaller than that of a straight tether. From Figure 43 we see that the arc portion $R\psi$ is slightly longer than the vertical component of the wire that effectively produces thrust in the $\hat{\boldsymbol{\rho}}_{\perp}$ direction, $R\sin\psi$. This difference results in the straight-line model error given by

$$e_{slm} = R(\sin\psi - \psi) = R\left(\psi - \frac{\psi^3}{6} - \psi + h.o.t.\right) = -\frac{R\psi^3}{6}$$

where we have made use of a Taylor expansion for ψ about zero and ignored terms higher than order three. If we desire the straight tether thrust approximation to remain within 95% that of the actual curved tether, we require that

$$R\sin\psi \geq 0.95 * R\psi \;\Rightarrow\; \sin\psi \geq 0.95\psi$$

therefore,

$$\sin\psi_{\lim} \approx \psi_{\lim} - \frac{\psi_{\lim}^3}{6} = 0.95\psi_{\lim}$$
$$\psi_{\lim}^2 = 6(1-.95) = 0.3$$
$$\psi_{\lim} = \pm 0.548$$

To obtain the force per unit length f_t we include electrodynamic and atmospheric effects, f_{te} and f_{ta}. The maximum electrodynamic force per unit length for a given $I_{\max}$ is

$$f_{te} = \left.\frac{\left\| I_{\max}\mathbf{L}\times\mathbf{B}\right\|}{L}\right|_{\text{mag equator}} = -I_{\max}B_n$$

where B_n is the $\hat{\mathbf{e}}_\mathbf{n}$ component in the rotating frame of the Earth's magnetic flux density. At 250 km, this magnetic flux density is about 2.7 e-5 N/(A-m) (rounded average from International Geomagnetic Reference Field).

The maximum aerodynamic force per unit length of the wire in nadir-pointing equilibrium and circular orbit is

$$f_{ta} = v^2\rho(h)\cos\alpha d_t\Big|_{\theta=\phi=\alpha=0} = \frac{\mu_g}{a}\rho(h)d_t$$

so the total lateral force density is

$$f_t = f_{te} + f_{ta} = -I_{\max}B_n + \frac{\mu_g}{a}\rho(h)d_t \tag{72}$$

At 250 km where the atmospheric density is about 6e-11 kg/m^3, this force density is about 1.8e-5 N/m. Using $\psi_{\lim}$ to determine f_t using Eq. (71) then substituting into Eq. (72) yields a maximum allowable current that permits the straight tether line assumption.

$$I_{\max} = \frac{1}{B_n}\left(\frac{2\tau\psi_{\lim}}{L} - \frac{\mu_g}{a}\rho(h)d_t\right)$$

For a 2 km tether in a 250 km orbit with a tension at nadir-pointing equilibrium of about .7 N, this maximum current equates to about 13 Amps. A tether carrying 13 Amps of current will have a radius of curvature and mid-point sag distance given respectively by

$$R = \frac{\tau}{f_t} = \frac{.7}{13 \cdot (2.7e-5)} = 1920 \text{ m}$$

$$\delta = \frac{L^2}{8R} = 260 \text{ m}$$

Von Flotow's paper provides a formula for the period of the first lateral mode of vibration as

$$P_{lat} = 2L\sqrt{\frac{\delta_t}{\tau}}$$

where δ_t is the mass density of the tether. For a uniform density tether, this is simply $\delta_t = m_t / L$ and the period of lateral vibration is

$$P_{lat} = 2\sqrt{\frac{Lm_t}{\tau}}$$

For a 400 kg tether system described above (10% of which is tether mass), this period would equate to 676 seconds. Having bounded the maximum allowable control current, we may now pose optimal control problems that can achieve feasible solutions.

Appendix E: Tether Tension Curves

There are two sets of graphs in this Appendix. The first set represents solutions to equation (40) for various altitudes, mass ratios, ballistic coefficient ratios and tether lengths. In all cases, the numerical solutions use a 400 kg system with a tether thickness of 5 mm. The second set of graphs show the in-plane equilibrium conditions at which the tether tension is zero. Equilibrium conditions above the curves are where the tether is in tension, while regions under the curves represent non-tension conditions where the tether would be slack. The slack conditions must be avoided when determining the EDT control strategy in which case we may bound the θ state to meet the constraints established by Eq. (39) for all libration angles and not just at equilibrium.

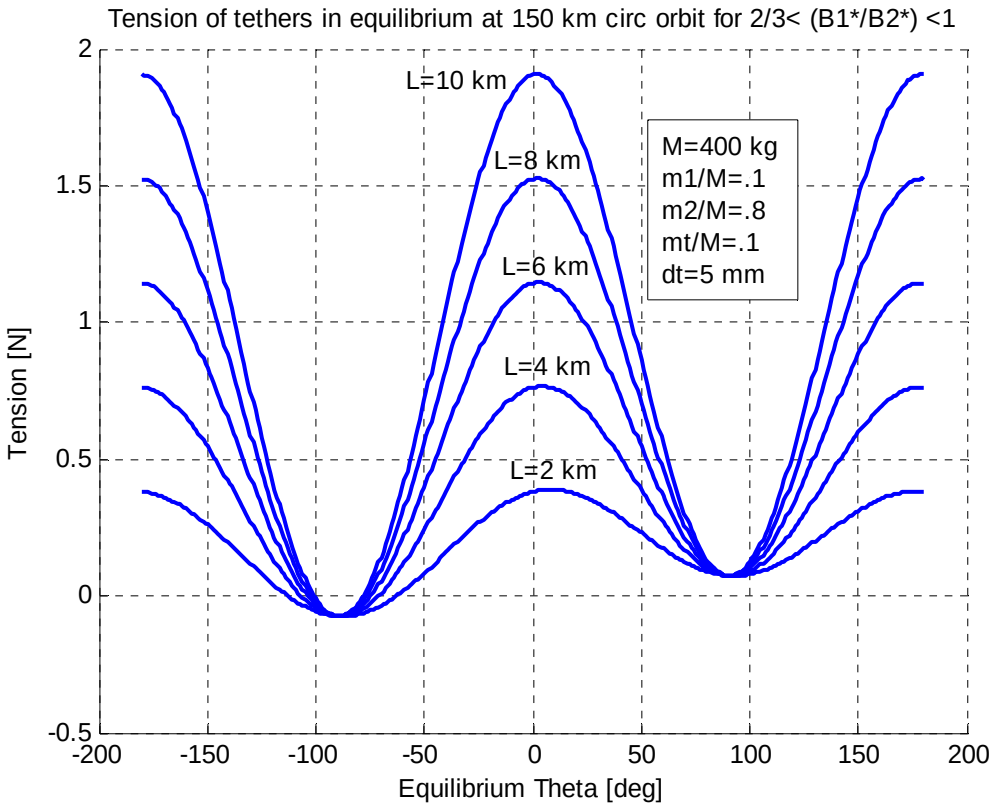
Tension of tethers in equilibrium at 150 km circ orbit for 2/3< (B1*/B2*) <1
L=10 km
L=8 km
L=6 km
L=4 km
L=2 km
M=400 kg
m1/M=.1
m2/M=.8
mt/M=.1
dt=5 mm
Tension [N]
Equilibrium Theta [deg]
2
1.5
1
0.5
0
-0.5
-200
-150
-100
-50
0
50
100
150
200

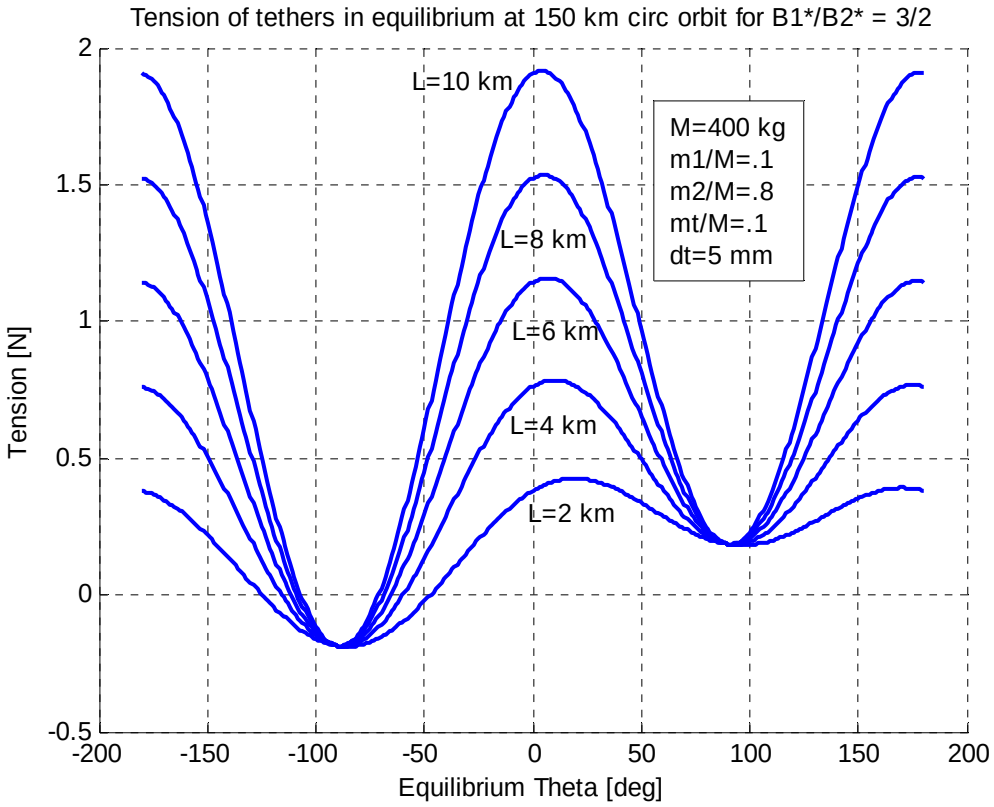
Tension of tethers in equilibrium at 150 km circ orbit for B1*/B2* = 3/2
L=10 km
L=8 km
L=6 km
L=4 km
L=2 km
M=400 kg
m1/M=.1
m2/M=.8
mt/M=.1
dt=5 mm
Tension [N]
Equilibrium Theta [deg]
2
1.5
1
0.5
0
-0.5
-200
-150
-100
-50
0
50
100
150
200

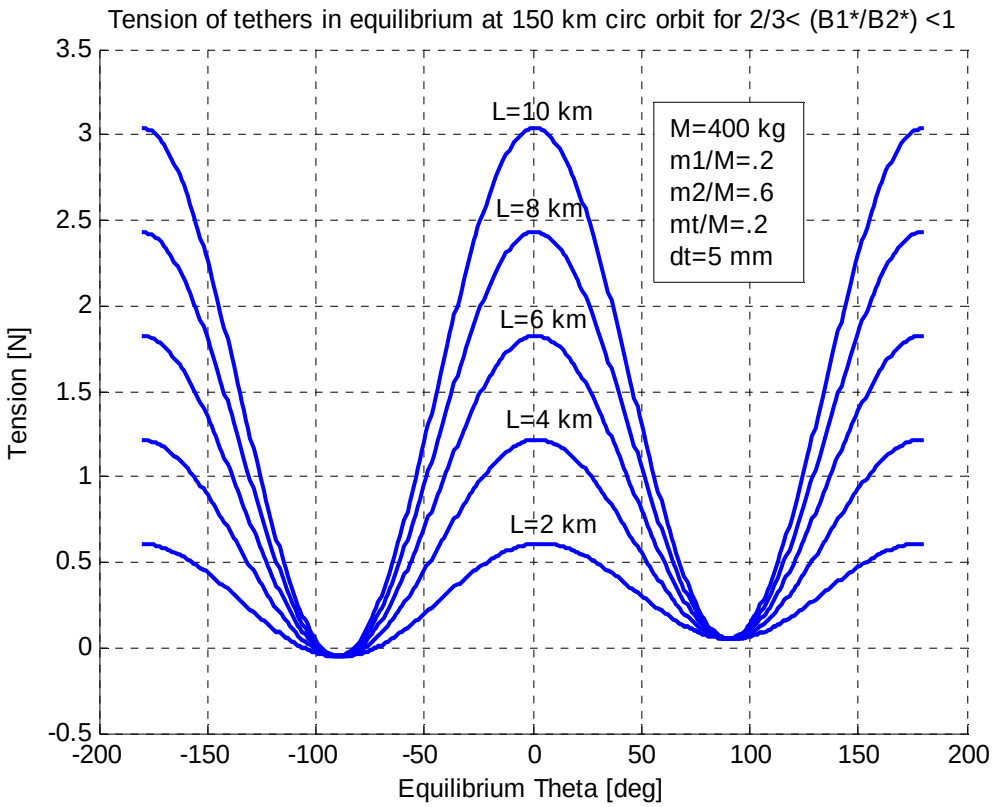
Tension of tethers in equilibrium at 150 km circ orbit for 2/3< (B1*/B2*) <1
L=10 km
L=8 km
L=6 km
L=4 km
L=2 km
M=400 kg
m1/M=.2
m2/M=.6
mt/M=.2
dt=5 mm
Tension [N]
Equilibrium Theta [deg]
3.5
3
2.5
2
1.5
1
0.5
0
-0.5
-200
-150
-100
-50
0
50
100
150
200

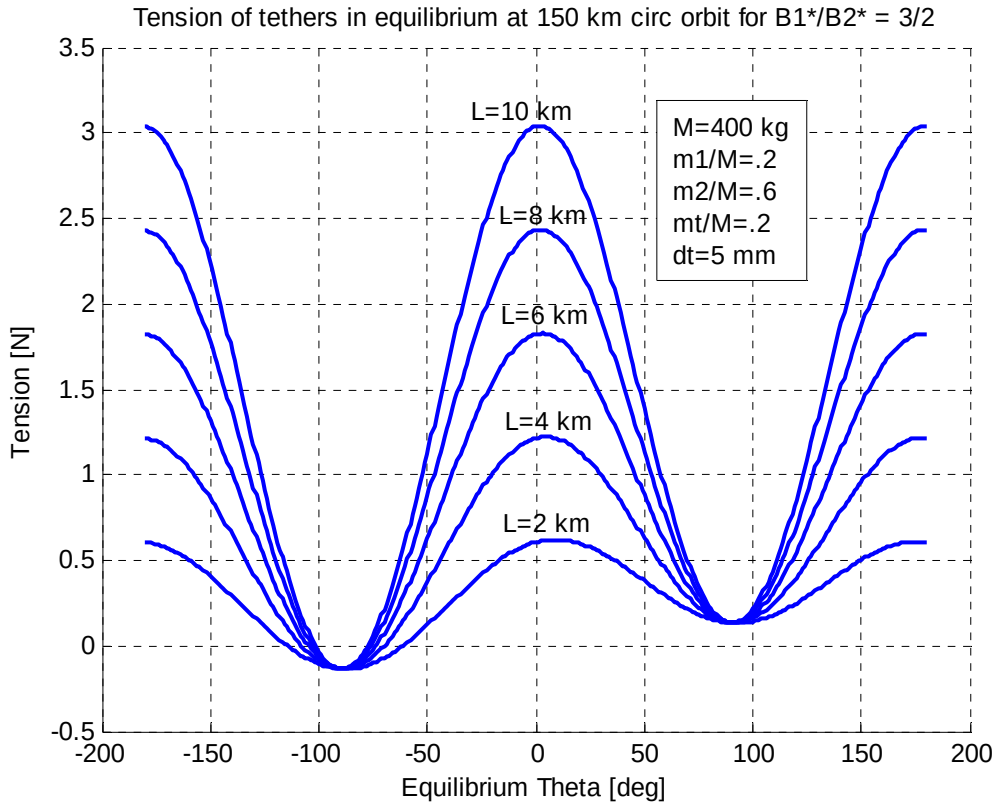
Tension of tethers in equilibrium at 150 km circ orbit for B1*/B2* = 3/2
L=10 km
L=8 km
L=6 km
L=4 km
L=2 km
M=400 kg
m1/M=.2
m2/M=.6
mt/M=.2
dt=5 mm
Tension [N]
Equilibrium Theta [deg]
3.5
3
2.5
2
1.5
1
0.5
0
-0.5
-200
-150
-100
-50
0
50
100
150
200

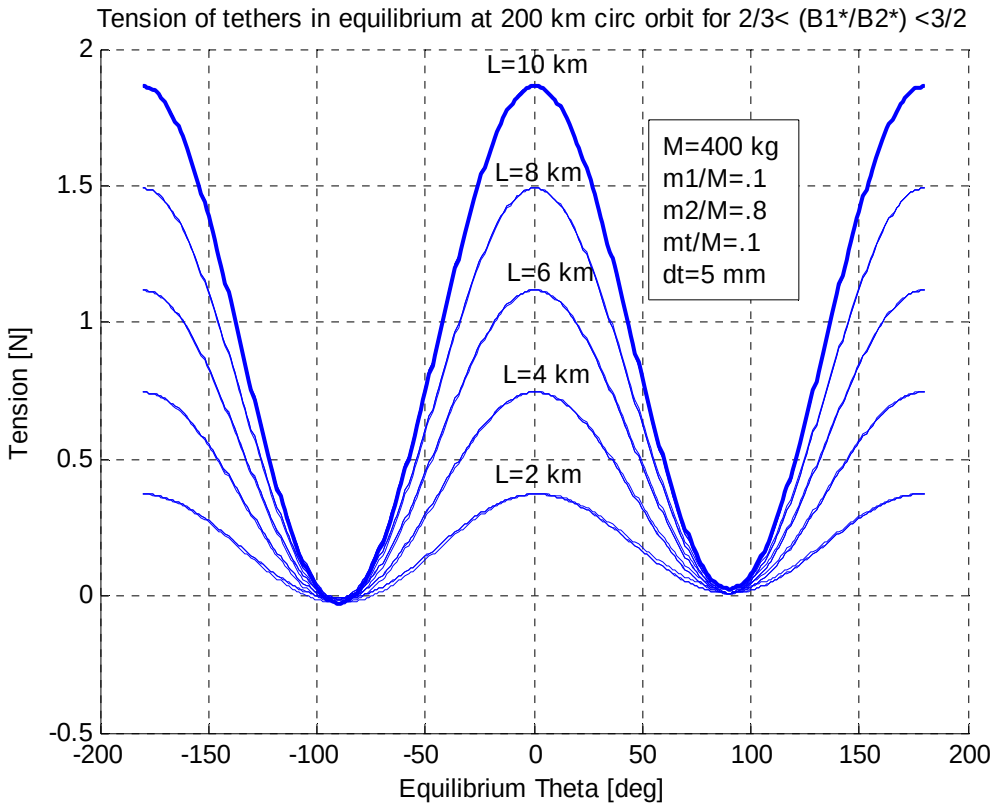
Tension of tethers in equilibrium at 200 km circ orbit for 2/3< (B1*/B2*) <3/2
L=10 km
L=8 km
L=6 km
L=4 km
L=2 km
M=400 kg
m1/M=.1
m2/M=.8
mt/M=.1
dt=5 mm
Tension [N]
Equilibrium Theta [deg]
2
1.5
1
0.5
0
-0.5
-200
-150
-100
-50
0
50
100
150
200

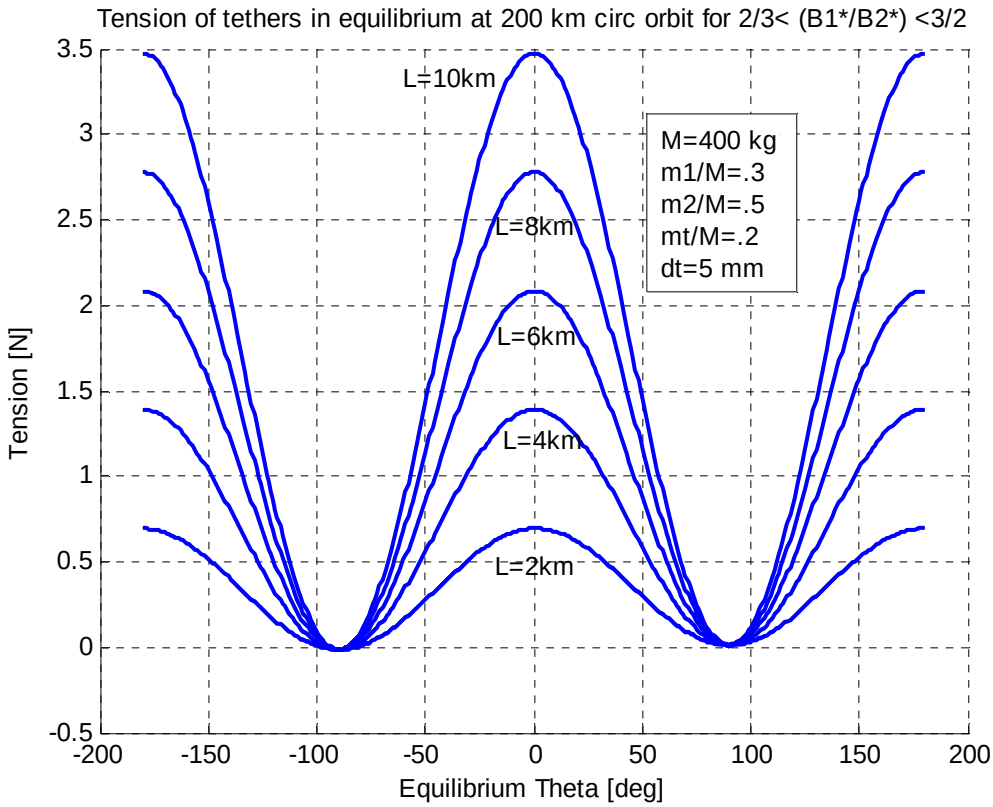
Tension of tethers in equilibrium at 200 km circ orbit for 2/3< (B1*/B2*) <3/2
L=10km
L=8km
L=6km
L=4km
L=2km
M=400 kg
m1/M=.3
m2/M=.5
mt/M=.2
dt=5 mm
Tension [N]
Equilibrium Theta [deg]
3.5
3
2.5
2
1.5
1
0.5
0
-0.5
-200
-150
-100
-50
0
50
100
150
200

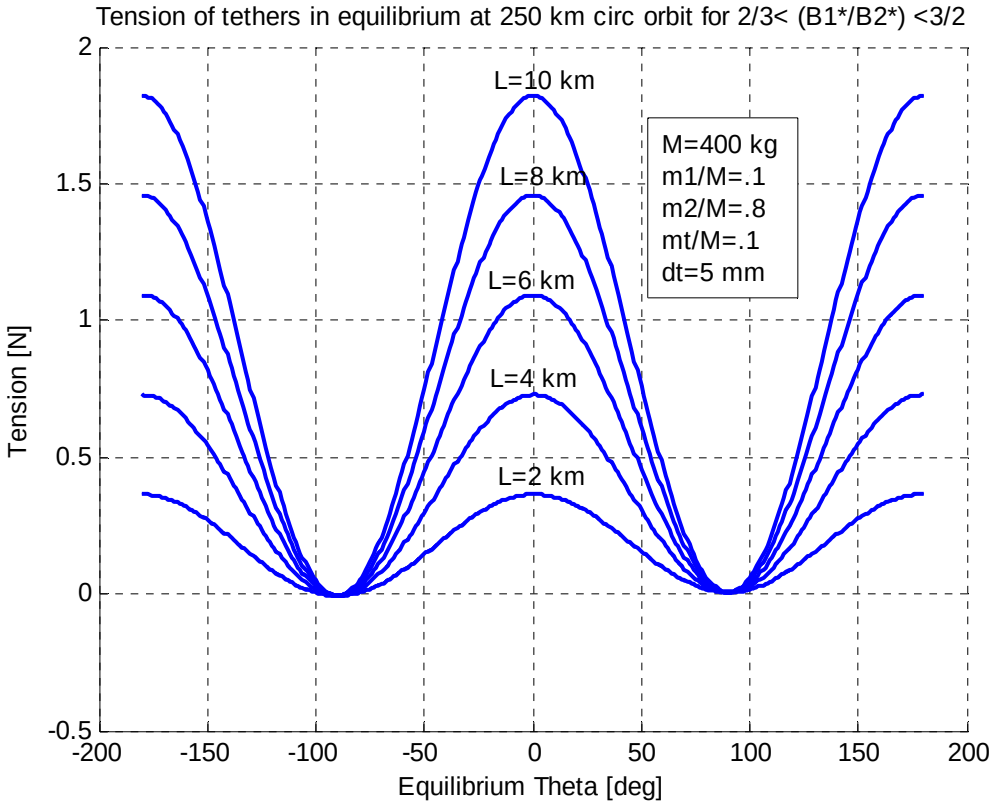
Tension of tethers in equilibrium at 250 km circ orbit for 2/3< (B1*/B2*) <3/2
L=10 km
L=8 km
L=6 km
L=4 km
L=2 km
M=400 kg
m1/M=.1
m2/M=.8
mt/M=.1
dt=5 mm
Tension [N]
Equilibrium Theta [deg]
2
1.5
1
0.5
0
-0.5
-200
-150
-100
-50
0
50
100
150
200

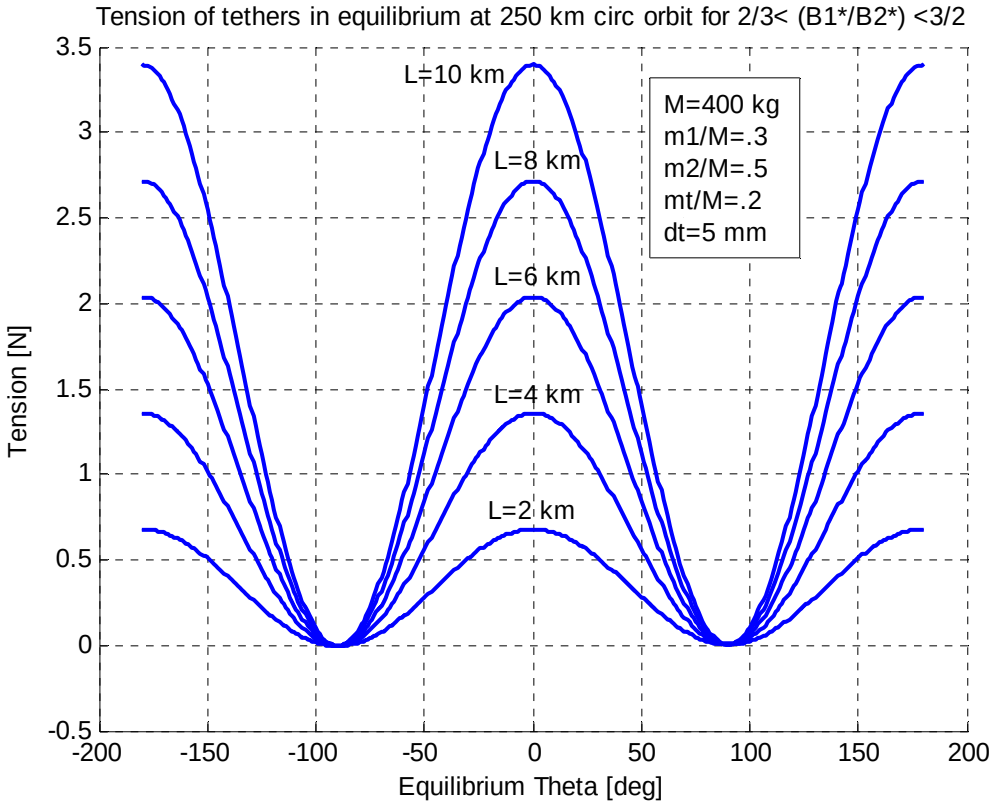
Tension of tethers in equilibrium at 250 km circ orbit for 2/3< (B1*/B2*) <3/2
L=10 km
L=8 km
L=6 km
L=4 km
L=2 km
M=400 kg
m1/M=.3
m2/M=.5
mt/M=.2
dt=5 mm
Tension [N]
Equilibrium Theta [deg]
3.5
3
2.5
2
1.5
1
0.5
0
-0.5
-200
-150
-100
-50
0
50
100
150
200

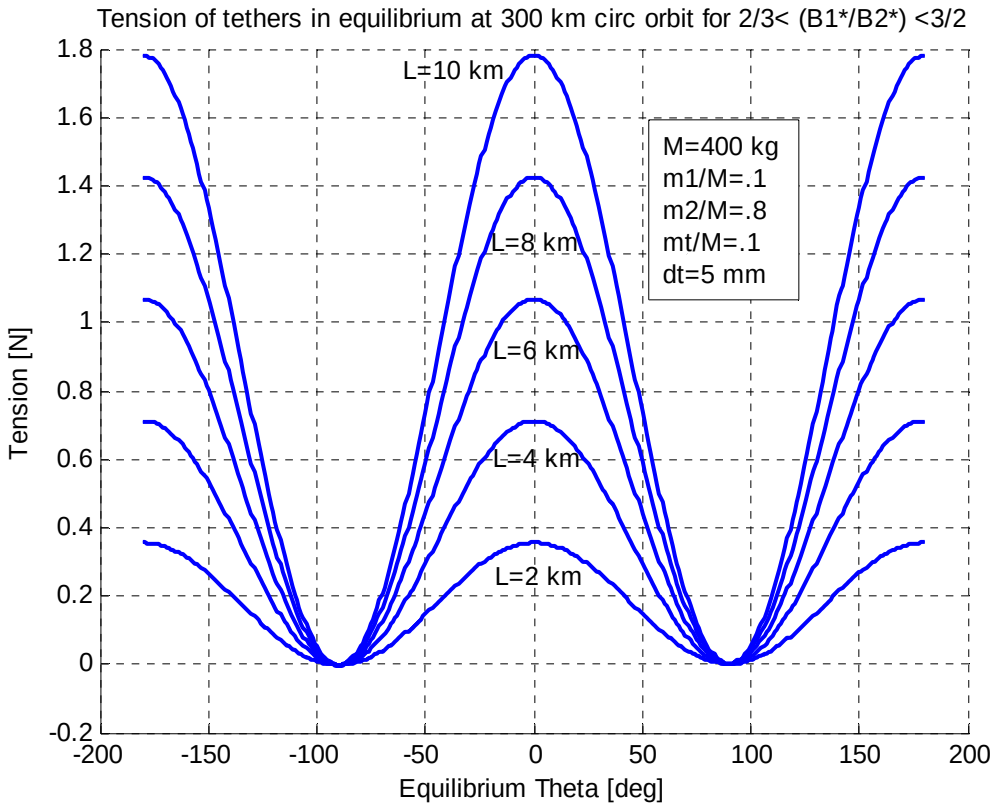
Tension of tethers in equilibrium at 300 km circ orbit for 2/3< (B1*/B2*) <3/2
L=10 km
L=8 km
L=6 km
L=4 km
L=2 km
M=400 kg
m1/M=.1
m2/M=.8
mt/M=.1
dt=5 mm
Tension [N]
Equilibrium Theta [deg]
1.8
1.6
1.4
1.2
1
0.8
0.6
0.4
0.2
0
-0.2
-200
-150
-100
-50
0
50
100
150
200

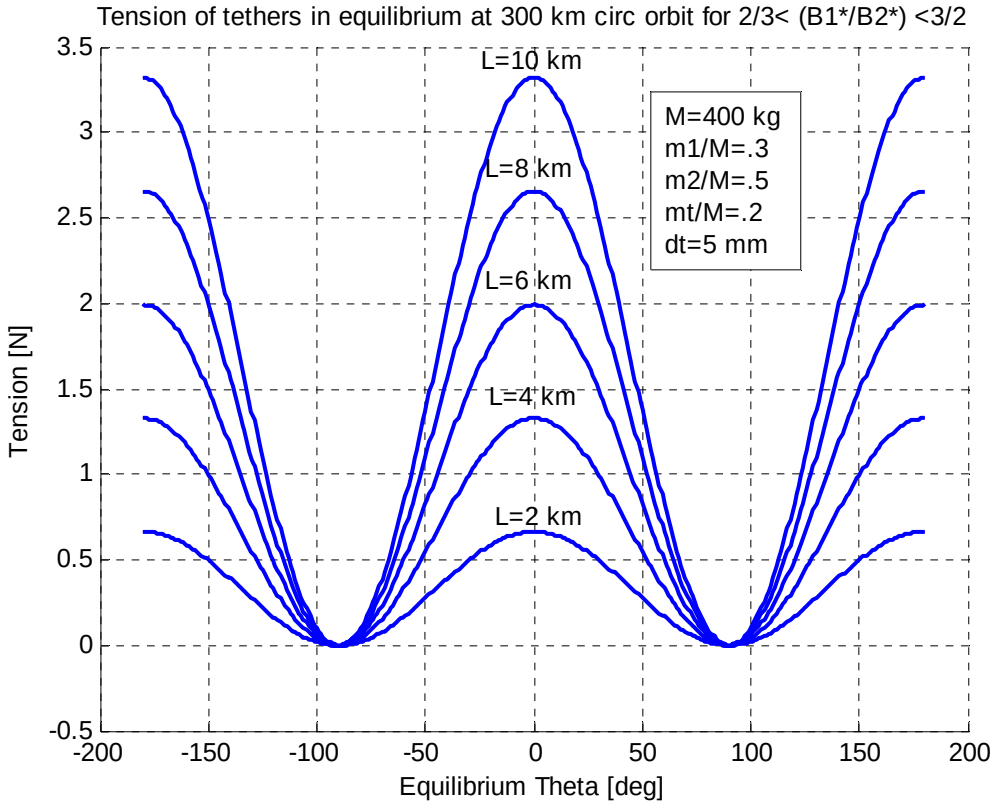
Tension of tethers in equilibrium at 300 km circ orbit for 2/3< (B1*/B2*) <3/2
L=10 km
L=8 km
L=6 km
L=4 km
L=2 km
M=400 kg
m1/M=.3
m2/M=.5
mt/M=.2
dt=5 mm
Tension [N]
Equilibrium Theta [deg]
3.5
3
2.5
2
1.5
1
0.5
0
-0.5
-200
-150
-100
-50
0
50
100
150
200

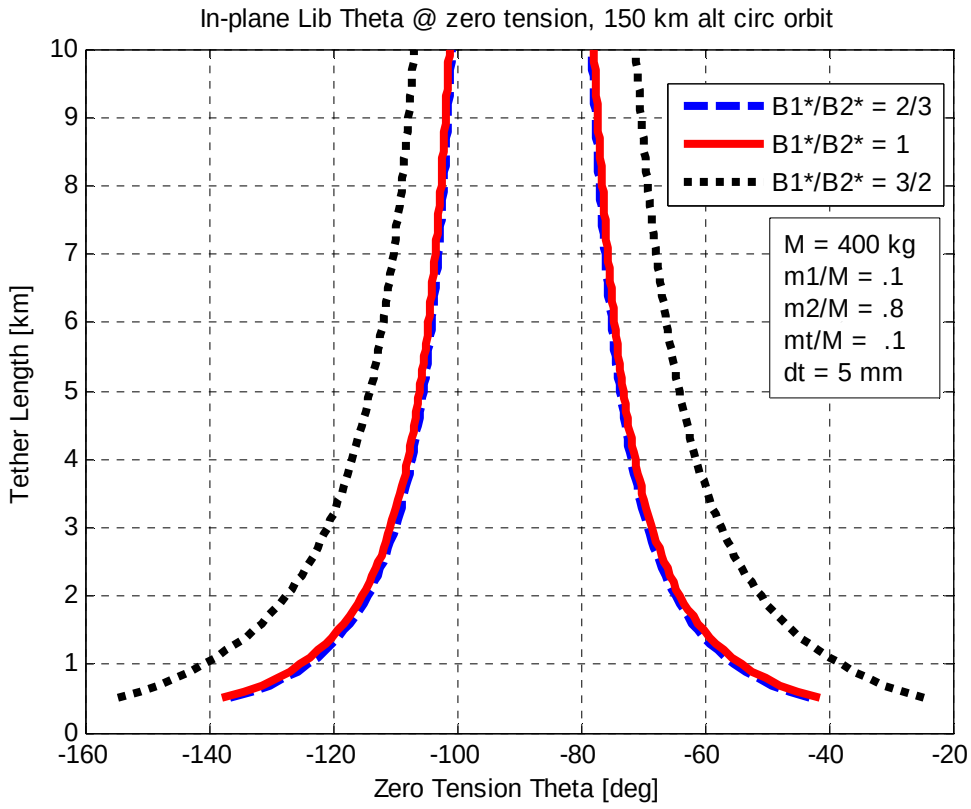
In-plane Lib Theta @ zero tension, 150 km alt circ orbit
B1*/B2* = 2/3
B1*/B2* = 1
B1*/B2* = 3/2
M = 400 kg
m1/M = .1
m2/M = .8
mt/M = .1
dt = 5 mm
Tether Length [km]
Zero Tension Theta [deg]
10
9
8
7
6
5
4
3
2
1
0
-160
-140
-120
-100
-80
-60
-40
-20

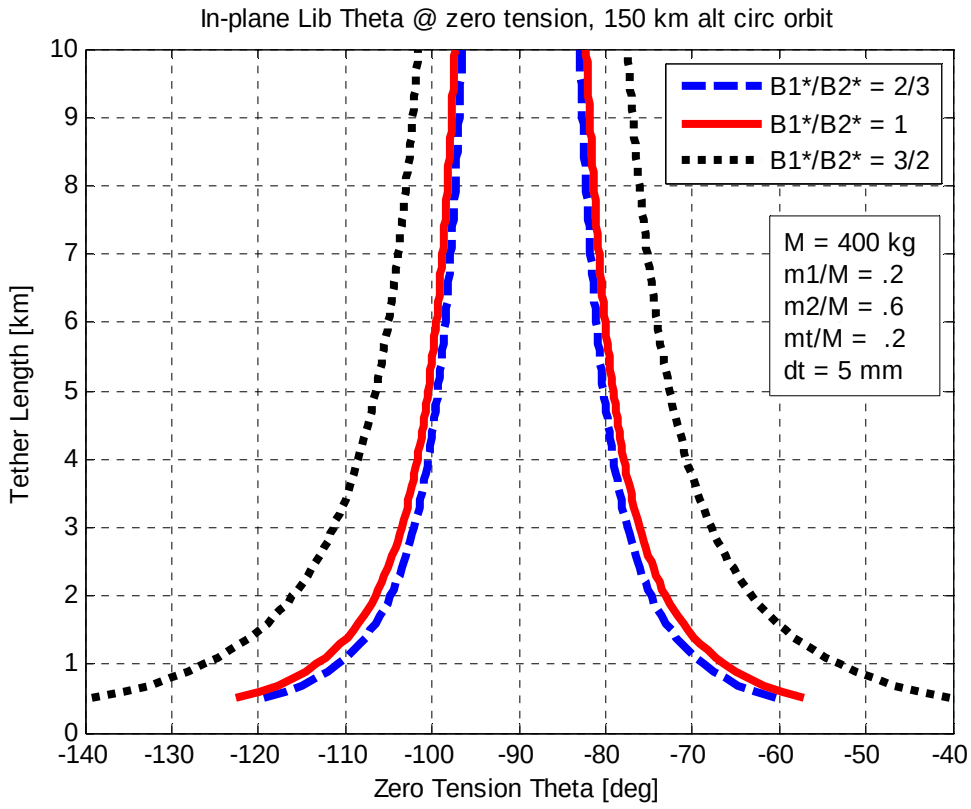
In-plane Lib Theta @ zero tension, 150 km alt circ orbit
B1*/B2* = 2/3
B1*/B2* = 1
B1*/B2* = 3/2
M = 400 kg
m1/M = .2
m2/M = .6
mt/M = .2
dt = 5 mm
Tether Length [km]
Zero Tension Theta [deg]
10
9
8
7
6
5
4
3
2
1
0
-140
-130
-120
-110
-100
-90
-80
-70
-60
-50
-40

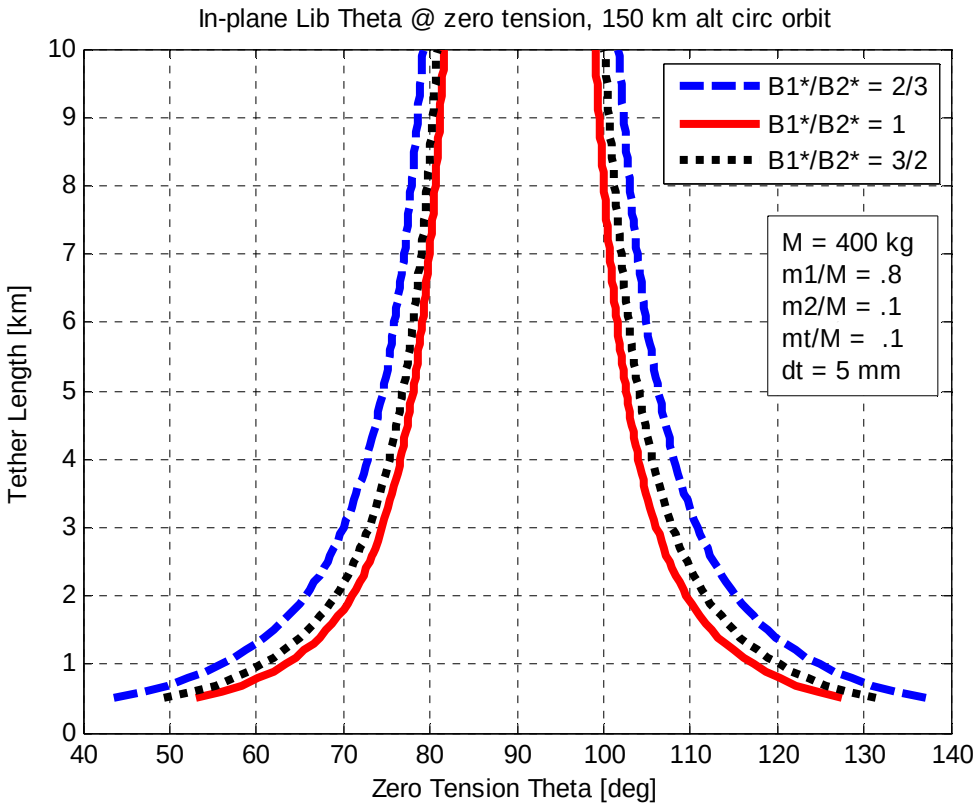
In-plane Lib Theta @ zero tension, 150 km alt circ orbit
B1*/B2* = 2/3
B1*/B2* = 1
B1*/B2* = 3/2
M = 400 kg
m1/M = .8
m2/M = .1
mt/M = .1
dt = 5 mm
Tether Length [km]
Zero Tension Theta [deg]
0
1
2
3
4
5
6
7
8
9
10
40
50
60
70
80
90
100
110
120
130
140

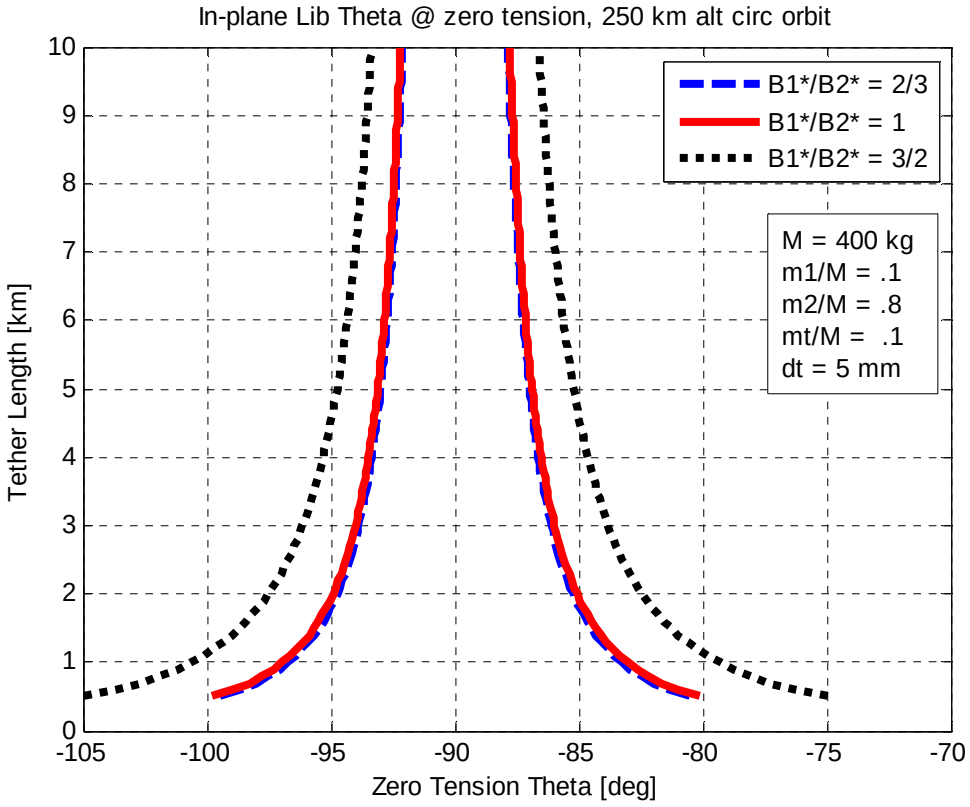
In-plane Lib Theta @ zero tension, 250 km alt circ orbit
B1*/B2* = 2/3
B1*/B2* = 1
B1*/B2* = 3/2
M = 400 kg
m1/M = .1
m2/M = .8
mt/M = .1
dt = 5 mm
Tether Length [km]
Zero Tension Theta [deg]
0
1
2
3
4
5
6
7
8
9
10
-105
-100
-95
-90
-85
-80
-75
-70

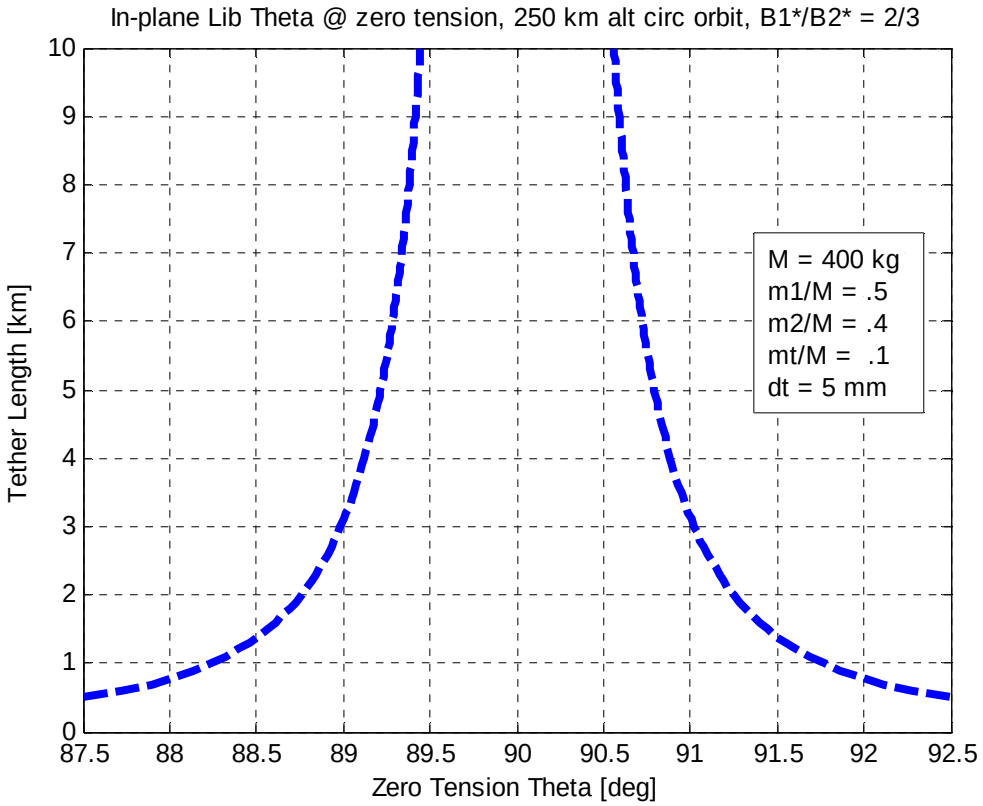
In-plane Lib Theta @ zero tension, 250 km alt circ orbit, B1*/B2* = 2/3
Tether Length [km]
Zero Tension Theta [deg]
M = 400 kg
m1/M = .5
m2/M = .4
mt/M = .1
dt = 5 mm

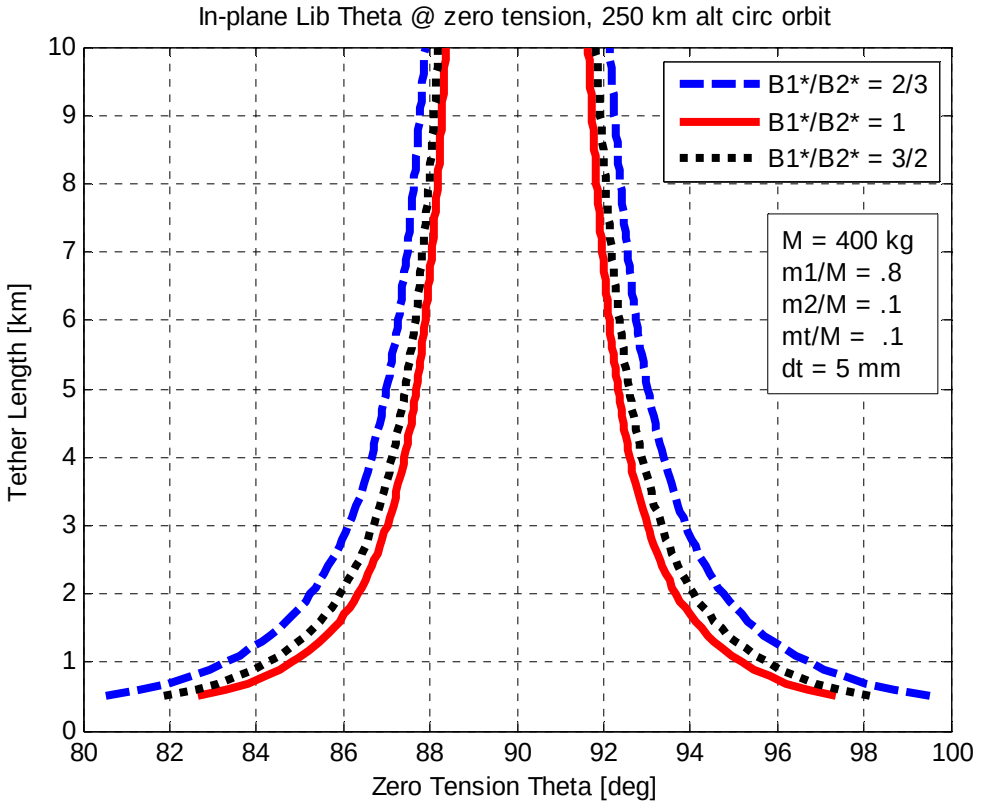
In-plane Lib Theta @ zero tension, 250 km alt circ orbit
Tether Length [km]
Zero Tension Theta [deg]
B1*/B2* = 2/3
B1*/B2* = 1
B1*/B2* = 3/2
M = 400 kg
m1/M = .8
m2/M = .1
mt/M = .1
dt = 5 mm

Appendix F: Scaling

Because of the nature of the optimal control problems posed in this paper, there are a number of states that can be very large or very small and ones that change over small and large time durations. Furthermore, it is important to scale the problem parameters, not only to assist in derivations of equations of motion, but also to condition a problem to achieve an accurate numerical solution. This appendix addresses the scaling that is required to achieve both goals. First, scaling the time variable to derive averaged state equations of motion, and second to scale all the problem parameters for well conditioned numerical solutions.

Scaling the Time Variable for Derivation of the Averaged State Equations of Motion

The control problems posed in this paper include states that undergo small rapid changes over short time scales, but on average change more significantly over long time scales. For maneuvers spanning long time scales, it is advantageous to average out the small fluctuations occurring over the short time scales and only consider the long term behavior of the average states. This is achieved through the method of averaging offered by perturbation theory. Averaging a state over a 2π period requires integration of the instantaneous state with respect to a time variable. It is important to recognize which terms change rapidly and must be integrated and which terms change so slowly that they may be considered constant over a single period. To assist in this clarification, two time scales are employed to identify parameters that change slowly and ones that change quickly.

The true anomaly, ν, is related to the clock time t through the equation

$$\nu = nt$$

where n is the mean motion of the orbit. This variable ν is be referred to as a "fast" time variable which changes rapidly on a "short" time scale, e.g. over a single orbit. On the other hand, the variable T is related to the clock time t by

$$T = \varepsilon t = \varepsilon \nu / n$$

where ε is a small parameter such that $\varepsilon \ll 1$. In this paper, a useful scaling factor is the non-dimensional electrodynamic torque defined in Eq. (43). The variable T captures the dynamics which vary slowly and is referred to as the "slow" time variable. Because T changes slowly with time, it represents the dynamics which take place on the "long" time scale, i.e. over many orbits. These variables may be treated as independent variables so long as $\varepsilon \ll 1$. Although two time scales are employed in this paper, multiple time scales may also be used in a similar fashion (e.g. including a rotating tilted magnetic dipole moment would introduce a medium time scale variable).

Scaling the OCP for Well-Conditioned Numerical Solutions

When solving an optimal control problem (OCP) using numerical methods, it is critical to condition the input parameters to achieve accurate results with faster CPU run times. Scaling is essential to writing a well conditioned problem for the computer. This section draws from discussions given in Ref 41, pg 31-36, and Ref 47 the salient points being repeated here for convenience. Recall the unscaled state and control vectors, $\mathbf{x}(T) = [a, h, k, i, z]^T$ and $\mathbf{u}(T) = [u_1, u_2, u_3, u_4, u_5]^T$ respectively. Numerically, it is advantageous to scale each element in the state and control vectors for computational efficiency, i.e.

$$\bar{\mathbf{x}}(T) = \left[\frac{a}{\bar{A}}, \frac{h}{\bar{H}}, \frac{k}{\bar{K}}, \frac{i}{\bar{I}}, \frac{z}{\bar{Z}}\right]^T = \left[\bar{a}, \bar{h}, \bar{k}, \bar{i}, \bar{z}\right]^T$$

$$\bar{\mathbf{u}}(T) = \left[\frac{u_1}{U_1}, \frac{u_2}{U_2}, \frac{u_3}{U_3}, \frac{u_4}{U_4}, \frac{u_5}{U_5}\right]^T = \left[\bar{u}_1, \bar{u}_2, \bar{u}_3, \bar{u}_4, \bar{u}_5\right]^T$$

where $\bar{A}, \bar{H}, \bar{K}, \bar{I}, \bar{Z}, U_1, U_2, U_3, U_4,$ and U_5 are arbitrary designer units. For the problems posed in this paper, designer units chosen to make the scaled states and controls roughly order one worked well. Time is scaled in a similar fashion expressed using a designer clock time unit, $\bar{t}_s$.

$$\bar{t} = \frac{t}{\bar{t}_s}$$

For the work presented here, the designer clock time unit was chosen such that $\bar{t}_f$ is order one. As an example, the OCP presented in Eq. (17) is rewritten in scaled form to input into the numerical optimizer.

Minimize Cost: $$J = \bar{t}_f \tag{73}$$

Subject to:

$$\begin{aligned}
&\dot{\bar{\mathbf{x}}}(T) = diag\left[\frac{\bar{t}_s}{\bar{A}}, \frac{\bar{t}_s}{\bar{H}}, \frac{\bar{t}_s}{\bar{K}}, \frac{\bar{t}_s}{\bar{I}}, \frac{\bar{t}_s}{\bar{Z}}\right]\mathbf{f}\left(\mathbf{x}(T), \mathbf{u}(T)\right) \\
&\bar{\mathbf{e}}_{\mathbf{0}}\left(\bar{\mathbf{x}}(T_0)\right) = \left[\bar{a}_0, \bar{e}_0, \bar{i}_0, \bar{z}_0\right]^T \\
&\bar{\mathbf{e}}_{\mathbf{f}}\left(\bar{\mathbf{x}}(T_f)\right) = \left[\bar{a}_f, \bar{i}_f, \bar{z}_f\right]^T \\
&g_1\left(\mathbf{u}(T)\right) = I_{rms}^2 - I_m^2 \le 0
\end{aligned}$$

where I_m is the maximum allowable rms control current. The scaled box constraints are enforced as well, i.e.

$$\begin{aligned}
&\bar{\mathbf{x}}_l \le \bar{\mathbf{x}}(\bar{t}) \le \bar{\mathbf{x}}_u \\
&\bar{\mathbf{u}}_l \le \bar{\mathbf{u}}(\bar{t}) \le \bar{\mathbf{u}}_u \\
&\bar{t}_{0l} \le \bar{t}_0 \le \bar{t}_{0u} \\
&\bar{t}_{fl} \le \bar{t}_f \le \bar{t}_{fu}
\end{aligned} \tag{74}$$

Note that the OCP presented here is mathematically identical to the unscaled one in Eq. (17). Also, recognize that the dynamic constraint vector $\mathbf{f}$ has elements containing unscaled states. The output, however, is scaled to be compatible with the other scaled constraints. Using the fact that a generic unscaled state and time are related to their scaled counterparts by $x = \bar{x}\bar{X}$ and $t = \bar{t}\bar{t}_s$, each individual time derivative is scaled as

$$\frac{d\bar{x}}{d\bar{t}} = \frac{dx}{dt}\frac{d\bar{x}}{dx}\frac{dt}{d\bar{t}} = \dot{x}\frac{\bar{t}_s}{\bar{X}}$$

The scaled OCP in the form of Eqs. (73) and (74) were used as the input for the optimizer (DIDO) that yielded the solutions in this paper.

Appendix G: Derivation of Averaged Orbital Element Equations of Motion

This appendix provides a derivation of secular equations of motion using a mixed set of classical and equinoctial coordinates and the method of averaging. To determine the secular change in a given state x_i, we start with the perturbation equations of motion given in Eq.(9) and use the approximation $dt \approx \frac{1}{n}(1-2e\cos\nu)\,d\nu$ then integrate over N periods as follows.

$$\Delta x_i = \int_{t_0}^{t_f} dx_i \approx \frac{1}{n}\int_0^{2\pi N} \frac{dx_i}{dt}(1-2e\cos\nu)d\nu$$

Because the orbits considered are nearly circular, eccentricity is very small and the argument of perigee is ill defined. Therefore two equinoctial coordinates defined as $h = e\sin\omega$ and $k = e\cos\omega$ are better suited for this orbit type. Thus, changes in semi-major axis, inclination and right ascension of the ascending node are approximated as

$$\Delta \mathrm{a} \approx 2Ca\cos i\left(\frac{1}{n}\right)\int_0^{2\pi N} I\left(1+2e\cos\nu\right)d\nu - \frac{2D}{n}\int_0^{2\pi N}\left(1+2e\cos\nu+\frac{ae\cos\nu}{h^*}\right)(1-2e\cos\nu)d\nu$$

$$\Delta i \approx -C\sin i\left(\frac{1}{n}\right)\int_0^{2\pi N} I\cos^2(\omega+\nu)d\nu = -C\sin i\left(\frac{1}{n}\right)\int_0^{2\pi N}\frac{I}{e^2}\left(k^2\cos^2\nu + h^2\sin^2\nu - hk\sin 2\nu\right)d\nu$$

$$\Delta\Omega \approx -\frac{C}{2}\left(\frac{1}{n}\right)\int_0^{2\pi N} I\sin(2\nu+2\omega)d\nu = -\frac{C}{2}\left(\frac{1}{n}\right)\int_0^{2\pi N}\frac{I}{e^2}\left(hk\cos 2\nu + \frac{1}{2}\left(k^2-h^2\right)\sin 2\nu\right)d\nu$$

where $C = \frac{L\gamma_m}{nma^4}$ represents the thrust per unit current and the drag rate is $D = \frac{B^*\mu\rho(a)}{2na}$. Note that $\frac{CI}{n}$ is dimensionless.

The only control that will yield non-zero solutions after integrating the above equations is a periodic current. The control current may be expressed as the sum of the periodic functions that produce secular changes to the states, therefore we use the first five terms of a Fourier series shown in Eq. (1). After integration we obtain the secular changes to three of the five states that change on a long time scale.

$$\Delta a \approx \left[2CI_m a\cos i\left(u_1+u_2 e\right)-2D\right]\frac{2\pi N}{n}$$
$$\Delta i \approx -CI_m \sin i\left(\frac{u_1}{2}+\frac{k^2-h^2}{4e^2}u_4-\frac{hk}{2e^2}u_5\right)\frac{2\pi N}{n} \tag{75}$$
$$\Delta\Omega \approx -CI_m\left(\frac{hk}{2e^2}u_4+\frac{k^2-h^2}{4e^2}u_5\right)\frac{2\pi N}{n}$$

The time derivatives of the equinoctial coordinates may be calculated as follows.

$$\begin{aligned}\dot{h} &= e\cos\omega\dot{\omega}+\dot{e}\sin\omega \\ &\approx CI\cos i\left[\cos\left(\nu+\omega\right)\left(h\cos\nu+k\sin\nu\right)\left(1+2e\cos\nu\right)\cos\omega+\left(2-e\cos\nu\right)\left(1+3e\cos\nu\right)\sin\nu\cos\omega\right. \\ &\quad \left.+\left(2\cos\nu+e\sin^2\nu\right)\left(1+3e\cos\nu\right)\sin\omega\right]-\frac{2D}{a}\left\{\frac{\sin\nu}{2e}\left(1+\left(1+\frac{a}{h^*}\right)e\cos\nu\right)\left(2-e\cos\nu\right)\cos\omega\right. \\ &\quad \left.+\left(\cos\nu+e+\left(1+\frac{a}{h^*}\right)e\cos^2\nu\right)\sin\omega\right\}\end{aligned} \tag{76}$$

Carrying out the multiplications, eliminating second and higher order eccentricity terms, then substituting in h and k, we write

$$\begin{aligned}\dot{h} &\approx CI\cos i\left\{\left[\left(\frac{k}{e}\cos\nu-\frac{h}{e}\sin\nu+2k\cos^2\nu-h\sin 2\nu\right)\left(h\cos\nu+k\sin\nu\right)+\left(2\sin\nu+\frac{5}{2}e\sin 2\nu\right)\right]\frac{k}{e}\right. \\ &\quad \left.+\frac{2h}{e}\cos\nu+h+5h\cos^2\nu\right\}-\frac{2D}{a}\left\{\left(\frac{\sin\nu}{e}+\frac{a}{2h^*}\sin 2\nu-\left(1+\frac{a}{h^*}\right)\frac{e}{2}\cos^2\nu\sin\nu\right)\frac{k}{e}\right. \\ &\quad \left.+\left(\cos\nu+e+\left(1+\frac{a}{h^*}\right)e\cos^2\nu\right)\frac{h}{e}\right\}\end{aligned} \tag{77}$$

recognizing that $\cos\left(\nu+\omega\right)=\cos\nu\cos\omega-\sin\nu\sin\omega=\frac{k}{e}\cos\nu-\frac{h}{e}\sin\nu$ and $e^2=h^2+k^2$.

Integrating with respect to the true anomaly from 0 to $2\pi N$, we find the change in the average h state.

$$\Delta h \approx \left\{CI_m\cos i\left[u_1\left(\frac{3h}{2}\right)+u_2\left(\frac{h}{e}\right)+u_3\left(\frac{k}{e}\right)+u_4\left(\frac{h}{4}+\frac{hk^2}{2e^2}\right)+u_5\left(\frac{k}{4}+\frac{\left(k^2-h^2\right)k}{4e^2}\right)\right]-\frac{D}{a}\left(1+\frac{a}{h^*}\right)h\right\}\frac{2\pi N}{n} \tag{78}$$

We obtain the k state dynamics in a similar manner.

$$
\begin{aligned}
\dot{k} &= -e\sin\omega\dot{\omega} + \dot{e}\cos\omega \\
&\approx CI\cos i\left[-\cos(\nu+\omega)(h\cos\nu + k\sin\nu)(1+2e\cos\nu)\sin\omega - (2-e\cos\nu)(1+3e\cos\nu)\sin\nu\sin\omega\right. \\
&\quad \left.+\left(2\cos\nu + e\sin^2\nu\right)(1+3e\cos\nu)\cos\omega\right] - \frac{2D}{a}\left\{\frac{-\sin\nu}{2e}\left(1+\left(1+\frac{a}{h^*}\right)e\cos\nu\right)(2-e\cos\nu)\sin\omega\right. \\
&\quad \left.+\left(\cos\nu + e + \left(1+\frac{a}{h^*}\right)e\cos^2\nu\right)\cos\omega\right\}
\end{aligned}
\tag{79}
$$

Rewriting Eq. (79) using definitions of h and k, we obtain

$$
\begin{aligned}
\dot{k} &\approx CI\cos i\left\{\left[-\left(\frac{k}{e}\cos\nu - \frac{h}{e}\sin\nu + 2k\cos^2\nu - h\sin 2\nu\right)(h\cos\nu + k\sin\nu) - \left(2\sin\nu + \frac{5}{2}e\sin 2\nu\right)\right]\frac{h}{e}\right. \\
&\quad \left.+\frac{2k}{e}\cos\nu + k + 5k\cos^2\nu\right\} - \frac{2D}{a}\left\{-\left(\frac{\sin\nu}{e} + \frac{a}{2h^*}\sin 2\nu - \left(1+\frac{a}{h^*}\right)\frac{e}{2}\cos^2\nu\sin\nu\right)\frac{h}{e}\right. \\
&\quad \left.+\left(\cos\nu + e + \left(1+\frac{a}{h^*}\right)e\cos^2\nu\right)\frac{k}{e}\right\}
\end{aligned}
$$

Integrating with respect to the true anomaly from 0 to $2\pi N$, we find the change in the k state.

$$
\Delta k \approx \left\{CI_m\cos i\left[u_1\left(\frac{3k}{2}\right) + u_2\left(\frac{k}{e}\right) + u_3\left(\frac{-h}{e}\right) + u_4\left(\frac{k}{4} - \frac{h^2k}{2e^2}\right) + u_5\left(-\frac{h}{4} + \frac{\left(h^2-k^2\right)h}{4e^2}\right)\right] - \frac{D}{a}\left(1+\frac{a}{h^*}\right)k\right\}\frac{2\pi N}{n}
\tag{80}
$$

Appendix H: Propagation of Libration

When propagating a variable such as libration that exhibits rapidly changing behavior on short time scales but also exhibits slowly changing behavior over longer time scales, it is necessary to use stiff ordinary differential equation (ode) solvers. These numerical solvers are subject to errors which can grow as solutions are propagated over a long interval. To test the ode solver in a problem relevant to this research, the following homogeneous ordinary differential equation was propagated.

$$\begin{aligned} &\ddot{\phi}(\nu) + 4\phi(\nu) = 0 \\ &\phi(0) = \phi_m, \ \dot{\phi}(0) = 0 \end{aligned} \tag{81}$$

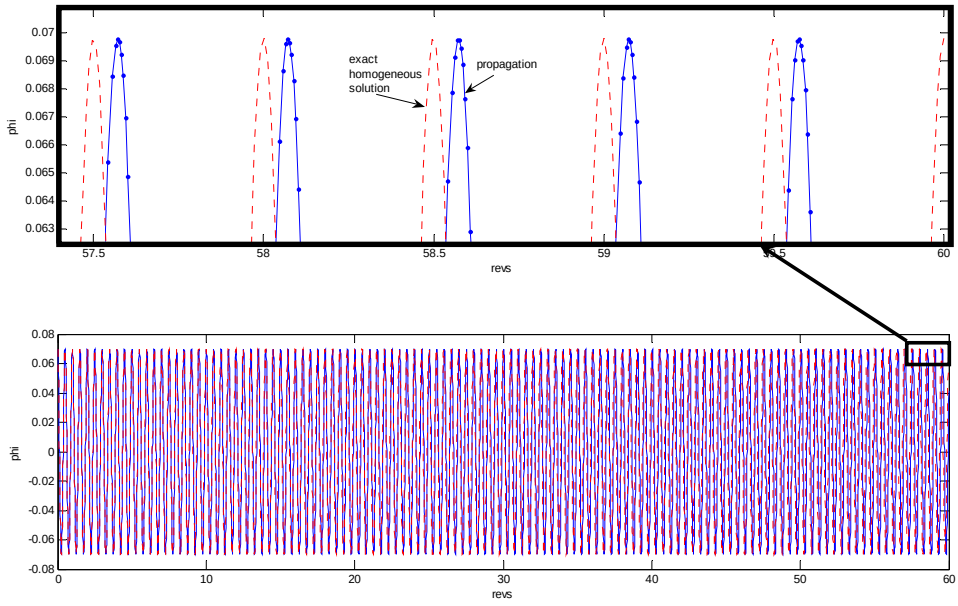

Figure 44. Matlab ode23 Solution to Homogeneous Equation vs. Exact Solution

The propagated solution to Eq. (81) is plotted in Figure 44 along with the exact solution to this equation using Matlab's ode23t (stiff solver). Notice that over the course of time the propagated solution's phase slowly drifts from the exact solution (i.e. $\phi = \phi_m \cos 2\nu$) where 1 rev = 2π rad. The shift is not due to real perturbations since this is an exact homogeneous solution, but rather due to numerical round off errors which must be addressed when propagating control solutions. When using a propagator to model a

nonlinear plant response to a control input, the controller could become out of phase with the propagated states due solely to numerical errors. To compensate for this small artificial phase shift when propagating control solutions, we provide the controller given by Eq. (1) with a slightly phase shifted true anomaly input, ν_c, at each instant. This correction has the effect of slightly raising or lowering the frequency of the periodic controller to match the frequency of the numerically propagated homogeneous solution. The modified true anomaly is designed to be in phase with the propagator to simulate a real plant that is unaffected by round off error and is defined by

$$\nu_c = \nu\left(1 - \frac{\Delta\nu_p}{\Delta\nu}\right) \tag{82}$$

where $\frac{\Delta\nu_p}{\Delta\nu}$ is the change in the propagated independent variable ν_p with respect to the change in the true independent variable ν. The easiest way to obtain $\Delta\nu_p$ is to determine the difference between the ν (in revs) corresponding to the final peak of the propagated homogeneous solution after $\Delta\nu = N$ revs, $\left(\nu_p\right)_{peak}$ and the peak of the exact solution (always corresponding to either whole or half revs). The difference $\Delta\nu_p$ is positive when the propagated peak lies to the right of the exact solution peak (i.e. lags the exact solution) and is negative when it lies to the left (i.e. leads exact solution), written as

$$\frac{\Delta\nu_p}{\Delta\nu} = \frac{\left(\nu_p\right)_{peak} - N}{N}$$

The value is non-dimensional and will shift the control input variable ν_c throughout the trajectory to maintain phase with the propagated phase ν_p (i.e. control frequency is matched with the "natural" frequency as determined by the numerical propagator). Note that at the final time after N revs the controller is in phase with the propagated trajectory, i.e.

$$\nu_c = N\left(1 - \frac{\Delta\nu_p}{N}\right) = N - \Delta\nu_p$$

The controller is then rewritten as

$$I = u_1(T) + u_2(T)\cos\nu_c + u_3(T)\sin\nu_c + u_4(T)\cos 2\nu_c + u_5(T)\sin 2\nu_c \tag{83}$$

It must be emphasized that this controller is only used for propagation to compensate for numerical errors to achieve more accurate comparisons. This scheme is not necessary when applied to a real world design, although some variation of this method would be useful for real perturbations originating from other sources.

Appendix I: Reference Synopses

Reference	Author	Title and Synopsis
JGCD Vol 26, #5 Sep-Oct 2003	Tragesser & San	Orbital Maneuvering with Electrodynamic Tethers Titlted Dipole Magnetic field. Perturbation equs (a,e,I,…) w/ expansion in e appx to get secular changes. Change shows how various current laws change a, e, I, etc. Ex I(nu) = cos(nu) changes e. EOM assumes tether aligned w/ vertical. Rigid rod model. Changes indep variable from t to nu. Maneuvers are NOT optimal.
JGCD Vol 28 #2	P Williams	Optimal Orbital Transfer with Electrodynamic Tether Change orbit by modulating current in wire. Takes into account librations, both in plane and out of plane. Compares w/ similar maneuvers using a hypothetical non-librating tether. Has useful reduced mass. No atmosphere considered. Example problem uses a 500 km orbit.
AIAA-2001-1139	West	Life Extension and Orbit Maneuvering Strategies for Small Satellites in LEO Using Electrodynamic Tethers. Has good sample parameters w/ which to frame the problem. Addresses micometeor problem and pourous tape. Shows graphs of responses to various tether configurations and conditions. No EOMs
AIAA-1999-2841-933	Gilchrist	Space Electrodynamic Tether Propulsion Technology: System Considerations and Future Plans Good plots of bare wire EDTs. ProSEDS and TSS-1R missions.
AIAA-2000-440-651	Estes	Performance and Dynamics of an Electrodynamic Tether Discusses advantages of a bare EDT in collecting electrons. Reviews boosting and deboosting applications. Gives system performance variation vs. key parameters. Discusses performance of bare EDTs for boost or de-boost applications
AIAA-2001-3980-120	Van Noord	Electrodynamic Tether Optimization for the STEP AIRSEDS mission Mostly about design, survivability and manufacture of EDT. No EOM
AIAA-2003-143-567	Santangelo	Evolution, Technology and Direction for the ASTOWSTEP AIRSEDS Electrodynamic Tether Mission Brief format, not paper
AIAA-2004-3501-989	Vaughn	Review of the PROSEDS Electrodynamic Tether Mission Development Mission never got off the ground, but good passdown for future EDT mission planners.
AIAA-2004-5309-275	Palaez	Self-Balanced Electrodynamic Tethers Inclined orbits produce instabilities on EDTs. Inert tethers are fine (for circular case). Zeroizing the Lorentz torque is addressed which eliminates instability. Mass distribution is critical, else damping or control is needed. Attitude dynamics and Mag field model. Rigid rod assumed.
AIAA-2004-5313-157	Watanabe	An Application of Input Shaping for Electrodynamic Tether Systems Input shaping to reduce vibrations and librations on an EDT being propelled. Mag field model includes massive flexible lumped mass tether. Considers one flexible mode of vibration. Uses Kanes equation (refs 4&7) although not supplied. Discusses how to do bang bang EDT thrust control by stepping in a controlled way that reduces vibes.

Reference	Author	Title and Synopsis
		Compares 3 different electron emission methods for different missions
AIAA-2005-4545-358	Bonometti	Free Reboost Electrodynamic Tether on the International Space Station Proposes tether flywheel design to reboost ISS. Has some charts w/ ISS data. Altitude history 1998-2004. No eom
AIAA 2002-4641	Tragesser	Orbital Design of Earth-Oriented Tethered Satellite Formations Looks at dynamics of multiple tethered satellites (3-D). Investigates stability. Flexible lumped mass tether. Starts w/ rigid model, then moves to flexible elastic one uses eoms and stability analysis from Hughes book. Example formation uses circular orbit.
AIAA 5479-983	Kumar	Review on Dynamics and Control of Non EDT Satellite Systems Light on equations but very thorough presentation of varius work in dynamics and control being done by different researchers. 275 refs!
AIAA 6473-285	Lorenzini	Libration control of EDTs in Inclined Orbit EOMS derived from Lagrangian
AIAA 6685-973	Pelaez	Dynamic Stability of EDTs in Inclined Elliptical Orbits Elliptic orbits yield periodic solutions not equilibrium positions. EDT control can be employed to manage the instability for small eccentricity orbits (e<.35). 3 stages. 1. Analyze stability of elliptical orbit inert tether. 2. Consider electrodynamic forces. 3. Compare w/ circular case.
AIAA 5077-785	Pelaez	Periodic Solutions in EDTs on Inclined Orbits Periodic solutions obtained using eigval of monodromy matrices compared with propagations based on Poincare method in both ep (mag to grav torque ratio) and then I (inclination). Even compares w/ linearized solution. Model is a rigid rod, dominant end mass, constant tehter current. Periodic solution exhibits frequency entrainment phenomenon (periodic sol'n has same period or integer multiple as forcing terms)
AIAA 17499-711	Williams	Libration Control of Tethered Satellites in Elliptical Orbits Non-EDTs. Control via tether tension (length variation). Stability analyzed via floquet theory.
AIAA 4992-661	Palaez	Two Bar Model for Dynamics and Stability of EDTs Looks at 2 rigid bar model for tether to analyze the impact of lateral dynamics on stability. Assumes Massive s/c, circ orbit, inclined, but only constant current, no control. 2 cases, 1. Continuous conductive wire, 2. Part discontinuous.
AIAA 1990-1197	Vadali	Feedback Control of Tethered Satellites Using Lyapunov Stability Theory (also hardcopy of Journal 0731-5090 Vol 14 #4 (729-735)) Has Dynamic Equations useful for stationkeeping, but mostly concentrates on deployment and retrieval of tethers. No atm drag. Lyapunav function provided for in plane theta and L eom. Coordinate xform is presented which partially decouples theta and phi dynamics.
AIAA 9166-681	Kojima	Non-linear Control of Librational Motion of Tethered Satellites in Elliptic Orbits Controls w/ thrusters at endmasses. Assumes no aerodrag, no elasticity of tether, only in-plane libration considered. Mother w/ 2 subsatellites connected w/ massless rigid rod tethers.
AIAA 2002 4045	Hoyt	Stabilization of EDTs Uses sensors to provide feedback control varying the current to stabilize the EDT. No eoms, but show output plots.
AIAA 2000-322	Lorenzini	An Overview of EDTs Good overview of actual deployed systems (TSS, ProSEDS, etc) their history, what we've learned, what we can do in future missions
AIAA 1990-656	Matteis	Dynamics of a Tethered Satellite Subjected to Aerodynamic Forces

		Includes aero forces on the subsatellite. Aerodynamic forces play a role in determining stability of system equilibrium. Circ orbit, equatorial plane, rotating atmosphere. 2 approaches 1. Linearize the eom. 2. Propagate non-linear equations. EOMS assume a dominant mass (shuttle), circ orbit, flexible tether. Contains excellent aero tether refs.
AIAA 1990-1198	Von Flotow	Insights and approximations in Dynamic Analysis of Spacecraft Tethers Discusses vibrational motion. Equilibrium shape of tether is slightly sagged from straight line. Includes stretch and flexibility in tether. Weak instabilities. Concludes passive damping has inconclusive effects.
AIAA 21768-992	Yu	Periodic Motion in the Tethered Satellite System Motion and control of Mother/daughter pair in circular orbit, then elliptical orbit. Control via length rate of tether. EOM include length rate and tension but in plane motion only. Below critical eccentricity (e<.3) motion is stable. Limit cycle.
AIAA 1991-532	Matteis	Dynamics of a Tethered Satellite in Elliptical, Non-Equatorial Orbits (also a JGCD article 0731-5090 1992 vol 15#3 (621-626). Depicts eoms with states expressed in Cartesian coords. 2 cases. 1. Equatorial eccentric orbits. 2. Inclined orbits. Includes aero forces and mentions peak natural freqs and driving aero force freq.
AIAA 10546-681	Sanyal	Stability and Stabilization of Relative Equilibria of Dumbell Bodies in Central Gravity Two identical masses, rigid rod, massless link. 5-DOF eom. Uses Lagrangian eom approach and then Routh reduction to eliminate a DOF.
AIAA 11822-945	Somenzi	Linear Stability Analysis of EDTs Assume circ orbit, inextensible tether 2 pt endmass. Electrodynamic forces cause coupling of cable oscillation. Constant current. Bending tether under current load included. Lat and long modes of vibration. Separates lateral modes of vib from librations.
AIAA 1990-1195	Modi	Dynamics and Control of a Tethered Spacecraft- A Brief Overview Has some history of the idea of EDTs and past missions (Gemini). Description of model and various control schemes, including tension control, offset control, etc. See also AIAA 1991-1002 below.
AIAA 1991-1002	Modi	On the Control of Tethered Satellite System Dynamics of tether. Three different LQR controllers (Thrusters, tension and offset control) for stationkeeping and retrieval. See also AIAA 1990-1195 prev entry.
AIAA-6934-481 JGCD 2005 vol28#3 541-545	Mankala	Equilibrium-to-Equilibrium Maneuvers of Rigid EDTs Note discusses a 2-D in plane libration stability of a varying resistance EDT. Tether modeled as rigid rod in equitorial circular orbit. Feedback linearization is used to provide the control history to move from one equilibrium position to another. Stability is not really addressed, but phase plot of the model used shows stable focus for a given set of tether params. Equilibrium points are expressed in terms of L and radial distance, r. Interesting.
AIAA 13956-480	Mankala	Equilibrium-to-Equilibrium Maneuvers of Flexible EDT in Equatorial Orbits Discusses shape of massless flexible EDT. Control resistor on a flexible massless EDTw/ dominant end mass in equatorial orbit (B field is perp to orbit and only er-et plane) Tether takes shape of an arc of circle and tether tension is constant. Equilibria are unstable w/o controller, but are stabilizable using either linear controller, non-linear controller or combo of both.
AIAA 2003-5781	Williams	Libration Control of Flexible Tethers Using Electromagnetic Forces and Movable Attachment See also JGCD v.27 n5 2004. Good ref list and what is in them. EOM included- rigid and flexible, no drag, mother satellite mass dominant, circular orbit..
AIAA 4057-325	Fujii	Nonlinear Dynamics of Tethered Subsatellite system During Stationkeeping Phase

		Poincare method used demonstrating chaotic behavior. Uses Lyaponov exponents and generates bifurcation maps. Models dominant mass w/ mt->0.
AIAA 2001-1141	Van Noord	EDT Tape Tether Performance in LEO Tether survivability w/ wider and shorter tethers. Reduce Drag, increase life. Includes twisting in model. Charts show decay time vs. tether width. Shows boosting by tether of various widths.
AIAA 2001-3980	Van Noord	EDT Optimization for STEP-AirSEDs Mission Design optimization considering survivability, drag, current collection, thrust produced, tether strength, thickness, etc. Has charts showing tether sever risk vs. width. Orbit transfer time vs. width.
AIAA 1759-102		Effect of Electromagnetic Forces on Orbital Dynamics of Tethered Satellites JGCD2005-G05-162
JGCD JGCD 1989 0731-5090 Vol 12#3 (431-433)	Misra	Breakwell Memorial Lecture- Dynamics and Control of Tethered Satellite Systems (Sept 29, 2003) Only owned by SISTI. OCLC#57023082. 54th international Astro Congress. Can't get my hands on this one.
book	Von Flotow	Some Approximations for the Dynamics of Spacecraft Tethers Explains why simple tether model is good enough. Walks through methodical approach to approximate dynamic modeling. Discusses curvature and stress, strain relations.
book	Misrah	Comments on "Some Approximations for the Dynamics of Spacecraft Tethers" Misrah took issue w/ some of the assumptions in Von Flotow's paper. A followon paper by Von Flotow takes issue with Misrah's issue. I'll stay out of it, but the issue only relates to deployment, not station-keeping dynamics.
JAS Vol 48#4 2000 p449-476		Effects of Atmospheric Density Gradient on Control of Tethered Subsatellites Need to obtain for longer tethers
JCGD v27 n5 2004	Beletsky	Dynamics of Space Tether Systems Advances in the Astronautical Sciences (An AAS publication), Vol 83. Checked out from Library.
	Penzo	Tethers in Space Handbook NASA report edited by Paul A. Penzo.
AIAA 3565-487 Journal of Spacecraft and Rockets, 2000, Vol37#2 187-196	Palaez	A New Kind of Dynamic Instability in Electrodynamic Tethers ED tether modeled as a rigid rod w/ point endmasses. Constant tether current causes constant energy being pumped into system causing instability w/ current on. There are no equilibrium positions (circ inclined orbit). Equations have periodic solutions. Does not consider variable current, tether flexibility or damping. Floquet theory used for periodic solutions and stability analysis.
JoVibeandAcoustics127_2_2005 Journal of Vibration and Acoustics, Col 127,#2pp144-156	Williams	Libration Control of Flesxible Tethers Using Electromagnetic Forces and Movable Attachment Good ref list and what is in them. EOM included- rigid and flexible, no drag, mother satellite mass dominant, circular orbit. See also AIAA 2003-5781
Eur Jour of Mech Vol 9, #2, 1990, pp207-224		Linear Stability Analysis of EDTs JGCD G05-109
AIAA-4147-252	Forward	Terminator Tether: A Spacecraft Deorbit Device

JGCD Vol 8, #1, Jan-Feb 1985	Mankala	Dynamic Modeling and sumulation of Satellite Tethered Systems Models tether shape dynamics.
AIAA-2947-955	Matteis	Equilibrium of a Tether-Subsatellite System Resonance due to aero gradient forces on subsatellite can cause instability. Sensitive to atm model. Assumptions- tether has no mass or aero forces on it, no bending. Alt ~110 km. Assuming relative constant atmosphere, no problem.
	Ketchichian	Trajectory Optimisation Using Non-Singular Elements and True Longitude Contains eom w/ states that avoid singularities
	Wiesel	Optimal Many-Revolution Orbit Transfer Multiple time-scale problem.
	Stevens	Preliminary Design of Earth-Mars Cyclers Using Solar Sails Optimal control methods for low thrust orbital maneuvering

References

[1] Williams, P., "Optimal Orbital Transfer with Electrodynamic Tether," Journal of Guidance, Control, and Dynamics, Vol. 28, No. 2, 2004, pp. 369-371.

[2] Tragesser, S. G., and San, H., "Orbital Maneuvering with Electrodynamic Tethers," Journal of Guidance, Control, and Dynamics, Vol. 26, No. 5, 2003, pp. 805-810

[3] De Matteis, G. and Socio, L., "Dynamics of Tethered Satellite Subjected to Aerodynamic Forces," Journal of Guidance, Control, and Dynamics, Vol. 14, No. 6, 1991, pp. 269-279.

[4] De Matteis, G., "Dynamics of a Tethered Satellite in Elliptical, Non-equatorial Orbits," Journal of Guidance, Control, and Dynamics, Vol. 15, No. 3, 1992, pp. 621-626.

[5] De Matteis, G, Socio, L., "Equilibrium of a Tether-Subsatellite System," European Journal of Mechanics, Vol. 9, No. 3, 1990, pp. 207-224

[6] Tragesser, S. G., and San, H., "Orbital Maneuvering with Electrodynamic Tethers," Journal of Guidance, Control, and Dynamics, Vol. 26, No. 5, 2003, pp. 805-810

[7] Williams, P., "Optimal Orbital Transfer with Electrodynamic Tether," Journal of Guidance, Control, and Dynamics, Vol. 28, No. 2, 2004, pp. 369-371

[8] Carroll, J., "Guidebook for Analysis of Tether Applications," Report for Martin Marietta Corp, Contract RH4-394049, March 1985, p 31.

[9] Pelaez, J. and Lorenzini, E. C., "Libration Control of Electrodynamic Tethers in Inclined Orbit," Journal of Guidance, Control, and Dynamics, Vol. 28, No. 2, Mar-Apr 2005, pp. 269-279

[10] Pelaez J., Lorenzini E. C., et. al., "A New Kind of Dynamic Instability in Electrodynamic Tethers," Journal of the Astronautical Sciences, Vol 48, No. 4, 2000, pp. 449-476

[11] Pelaez, J., Ruiz, M., Lopez, O., "Two Bar Model for Dynamics and Stability of Electrodynamic Tethers," Journal of Guidance, Control, and Dynamics, Vol. 25, No. 6, Nov-Dec, 2002

[12] Pelaez J., Lorenzini E. C., et. al., "A New Kind of Dynamic Instability in Electrodynamic Tethers," Journal of the Astronautical Sciences, Vol 48, No. 4, 2000, pp. 449-476

[13] Pelaez, J., "Self Balanced Electrodynamic Tethers," AIAA/AAS Astrodynamics Specialist Conference and Exhibit, 16-19 Aug, 2004, Providence, Rhode Island.

[14] Pelaez, J. and Andres, Y. N., "Dynamic Stability of Electrodynamic Tethers in Inclined Elliptical Orbits," Journal of Guidance, Control, and Dynamics, Vol. 28, No. 4, Jul-Aug 2005, pp. 1129-1135

[15] Hoyt, R., "Stabilization of Electrodynamic Tethers," AIAA Conference Paper, AIAA 2002-4045, 7-10 July, 2002, Indianapolis, IN

[16] Williams, P., "Libration Control of Tethered Satellites in Elliptical Orbits," Journal of Guidance, Control, and Dynamics, Vol. 43, No. 2, March–April 2006

[17] Yu, S., "Periodic Motion in the Tethered Satellite System," Journal of Guidance, Control, and Dynamics, Vol. 19, No. 5, pp 1195-1197

[18] Kojima, H., Masatake, I., Fujii, H., et. al., "Non-linear Control of Librational Motion of Tethered Satellites in Elliptic Orbits," Journal of Guidance, Control, and Dynamics, Vol. 27, No. 2, Mar-Apr 2004

[19] Modi, V., Lakshmanan, P., Misra, A., "On the Control of Tethered Satellite Systems," AIAA Conference Paper, AIAA-91-1002-CP, 1991

[20] Mankala, K., Agrawal, S., "Equilibrium-to-Equilibrium Maneuvers of Rigid Electrodynamic Tethers," Journal of Guidance, Control, and Dynamics, Vol. 28, No. 3, May-Jun 2005

[21] Mankala, K., Agrawal, S., "Equilibrium-to-Equilibrium Maneuvers of Flexible Electrodynamic Tethers in Equatorial Orbits," Journal of Guidance, Control, and Dynamics, Vol. 43, No. 3, May-Jun 2006

[22] Williams, P., Watanabe, T., et. al., "Libration Control of Flexible Tethers Using Electromagnetic Forces and Movable Attachment," Journal of Guidance, Control, and Dynamics, Vol. 27, No. 5, Sep-Oct 2004, pp. 882-896

[23] De Matteis, G., Socio, L., "Equilibrium of a Tether-Subsatellite System," European Journal of Mechanics, Vol. 9, No. 3, 1990, pp. 207-224

[24] Von Flotow, A. H. "Insights and Approximations in Dynamic Analysis of Spacecraft Tethers," AIAA Conference Paper, AIAA-90-1198-CP, 1990

[25] Watanabe, T., Singhose, W. "An Application of Input Shaping for Electrodynamic Tether Systems," AIAA Conference Paper, AIAA 2004-5313, 16-19 Aug 2004, Providence, RI

[26] Somenzi, L., Iess, L, Pelaez, J., "Linear Stability Analysis of Electrodynamic Tethers," Journal of Guidance, Control, and Dynamics, Vol. 28, No. 5, Sep-Oct 2005, pp. 843-849

[27] Watanabe, T., Singhose, W. "An Application of Input Shaping for Electrodynamic Tether Systems," AIAA Conference Paper, AIAA 2004-5313, 16-19 Aug 2004, Providence, RI

[28] Williams, P., Watanabe, T., et. al., "Libration Control of Flexible Tethers Using Electromagnetic Forces and Movable Attachment," Journal of Guidance, Control, and Dynamics, Vol. 27, No. 5, Sep-Oct 2004, pp. 882-896

[29] De Matteis, G., "Dynamics of a Tethered Satellite in Elliptical, Non-equatorial Orbits," Journal of Guidance, Control, and Dynamics, Vol. 15, No. 3, 1992, pp. 621-626

[30] Modi, V., "Dynamics and Control of a Tethered Spacecraft- A Brief Overview," AIAA Conference Paper, AIAA 1990-1195-CP, 1990

[31] Vadali, S., "Feedback Control of Tethered Satellites Using Lyapunov Stability Theory," AIAA Conference Paper, AIAA-90-1197-CP, 1990

[32] Gilchrist, B., "Space Electrodynamic Tether Propulsion Technology: System Considerations and Future Plans," AIAA Joint Propulsion Conference, A99-31507, 20-24 June 1999, Los Angeles, CA

[33] Estes, R.D., Lorenzini, E.C. "Performance and Dynamics of an Electrodynamic Tether," AIAA-2000-0440, 10-13 Jan 2000, Reno, NV

[34] West, B. and Gilchrist, B. "Life Extension and Orbit Maneuvering Strategies for Small Satellites in Low Earth Orbit Using Electrodynamic Tethers," AIAA Conference Paper, AIAA-2001-1139, 2001

[35] Van Noord, J., "Electrodynamic Tape Tether Performance with Varying Tether Widths at Low Earth Altitudes," AIAA Conference Paper, AIAA-2001-1141, 8-11 Jan 2000, Reno NV

[36] Van Noord, J., Sturmfels, R., "Electrodynamic Tether Optimization for STEP-AIRSEDs Mission," AIAA Conference Paper, AIAA-2001-3980, 8-11 Jul 2001, Salt Lake City, Utah

[37] Fuhrhop, K., Gilchrist, B., "Electrodynamic Tether System Analysis Comparing Various Mission Scenarios," AIAA Joint Propulsion Conference, AIAA 2005-4435, 10-13July 2005, Tucson, AZ

[38] Bonometti, J., Sorensen, K., "Free Reboost Electrodynamic Tether on the International Space Station," AIAA Joint Propulsion Conference, AIAA 2005-4545, 10-13July 2005, Tucson, AZ

[39] Estes, R., Lorenzini, E., Santangelo, A., "An Overview of Electrodynamic Tethers," AIAA Conference Paper, AIAA 2000-0322, 10-13 Jan 2000, Reno, NV

[40] Beletsky, V., Levin, E., *Dynamics of Space Tether Systems*, Advances in the Astronautical Sciences, Vol. 83, AAS Publication, San Diego CA, 1993

[41] Ross, I. M., *A Beginner's Guide to DIDO (Ver. 7.3)*, Document # TR-710, Elissar, LLC, Monterey, CA, 2007

[42] DIDO, A Matlab© Application Software Package for Solving Optimal Control Problems, Ver. 2003b, Elissar, Monterey, CA, *200*3.

[43] Wiesel., W., *Modern Astrodynamics*, Aphelion Press, Beavercreek, OH, 2003, pp. 147-151

[44] Meirovitch, L., Methods of Analytical Dynamics, Dover Publications, Inc., Mineola, New York, 1988, p. 129

[45] Levin, E., *Dynamic Analysis of Space Tether Missions*, Advances in the Astronautical Sciences, Vol. 126, AAS Publication, San Diego CA, 1993, pp. 115-116

[46] Ross, I. M., Fahroo, F., "Legendre Pseudospectral Approximations of Optimal Control Problems," Lecture Notes in Control and Information Sciences, Vol. 295, Springer-Verlag, New York, 2003, pp. 327-342

[47] Ross, I. M., Gong, Q., Sekhavat, P., "Low-Thrust, High-Accuracy Trajectory Optimization," *Journal of Guidance, Control, and Dynamics*, Vol. 30, No. 4, 2007, pp. 927-928.

[48] Gong, Q., Ross, IM., Kang, W., and Fahroo, F., "On the Pseudospectral Covector Mapping Theorem for Nonlinear Optimal Control", 45th IEEE Conference on Decision and Control, pp. 2679-2686, San Diego, CA, Dec. 2006.

[49] Slotine, J., Li, W., *Applied Nonlinear Control*, Prentice Hall International Inc., New Jersey, USA, 1991

[50] Bainum, P., Kumar, V., "Optimal Control of the Shuttle-Tethered System," *Acta Astronautica*, Vol. 7, No. 12, 1980, pp. 1333-1348

[51] Hughes, P., *Spacecraft Attitude Dynamics*, John Wiley & Sons, Inc., 1986

[52] Beletsky, V., Levin, E., *Dynamics of Space Tether Systems*, Advances in the Astronautical Sciences, Vol. 83, AAS Publication, San Diego CA, 1993, p. 209

[53] Meirovitch, L., *Methods of Analytical Dynamics*, Dover Publications, Inc., Mineola, New York, 1988, p. 129

[54] Von Flotow, A. H. "Insights and Approximations in Dynamic Analysis of Spacecraft Tethers," AIAA Conference Paper, AIAA-90-1198-CP, 1990

REPORT DOCUMENTATION PAGE

Form Approved
OMB No. 074-0188

PLEASE DO NOT RETURN YOUR FORM TO THE ABOVE ADDRESS.

1. REPORT DATE *(DD-MM-YYYY)*	**2. REPORT TYPE**	**3. DATES COVERED** *(From – To)*
10-07-2008	**Doctoral Dissertation**	Aug 2006 – Jul 2008

4. TITLE AND SUBTITLE

Optimal Control of Electrodynamic Tethers

5a. CONTRACT NUMBER

5b. GRANT NUMBER

5c. PROGRAM ELEMENT NUMBER

6. AUTHOR(S)

Stevens, Robert E., Commander, USN

5d. PROJECT NUMBER
na

5e. TASK NUMBER

5f. WORK UNIT NUMBER

7. PERFORMING ORGANIZATION NAMES(S) AND ADDRESS(S)
Air Force Institute of Technology
Graduate School of Engineering and Management (AFIT/EN)
2950 Hobson Way
WPAFB OH 45433-7765

8. PERFORMING ORGANIZATION REPORT NUMBER

AFIT/DS/ENY/08-13

9. SPONSORING/MONITORING AGENCY NAME(S) AND ADDRESS(ES)
United States Naval Academy (Aerospace Eng Dep)
590 Holloway Rd
Annapolis, MD
21402

10. SPONSOR/MONITOR'S ACRONYM(S) USNA

11. SPONSOR/MONITOR'S REPORT NUMBER(S) NA

12. DISTRIBUTION/AVAILABILITY STATEMENT
APPROVED FOR PUBLIC RELEASE; DISTRIBUTION UNLIMITED.

13. SUPPLEMENTARY NOTES

14. ABSTRACT

Low thrust propulsion systems offer a fuel-efficient means to maneuver satellites to new orbits, however they can only perform such maneuvers when they are continuously operated for a long time. Such long-term maneuvers occur over many orbital revolutions often rendering short time scale trajectory optimization methods ineffective. An approach to long time scale, multirevolution optimal control of an electrodynamic tether is investigated for a tethered satellite system in Low Earth Orbit with atmospheric drag. Optimal control problems are constructed in such a way as to maneuver the satellite to new orbits while minimizing a cost function subject to the constraints of the time-averaged equations of motion by controlling current in the tether. The method of averaging is employed to transform the optimal control problem from the time domain into a Fourier space where the complex problem is drastically reduced to a Zermelo type problem that is solved using a pseudospectral method. Optimal control solutions are determined that maneuver an electrodynamic tether to new orbits over long time scales while managing librational motion using only current in a wire. Results are simulated using a higher fidelity "truth" model to validate the controller performance.

15. SUBJECT TERMS
Orbiting Satellites, Optimization, Thrust Control, Perturbation Theory, Tethering, Control Theory, Electrodynamics, Lorentz Force, Spacecraft, Electromagnetic fields, Orbits, Electric Current, Dynamics

16. SECURITY CLASSIFICATION OF:			**17. LIMITATION OF ABSTRACT**	**18. NUMBER OF PAGES**	**19a. NAME OF RESPONSIBLE PERSON**
REPORT	**ABSTRACT**	**c. THIS PAGE**			William E. Wiesel (ENY)
U	**U**	**U**	**UU**	153	**19b. TELEPHONE NUMBER** *(Include area code)* (937) 255-6565, ext 4312; e-mail: William.Wiesel@afit.edu

Standard Form 298 (Rev: 8-98)
Prescribed by ANSI Std. Z39-18